

AD-A143 985

THE CONCENTRIC SPHERICAL CAVITY TE AND TM (TRANSVERSE
ELECTROMAGNETIC AND TRANSVERSE MAGNETIC) EIGENVALUES
(U) HARRY DIAMOND LABS ADELPHI MD L F LIBELO ET AL.

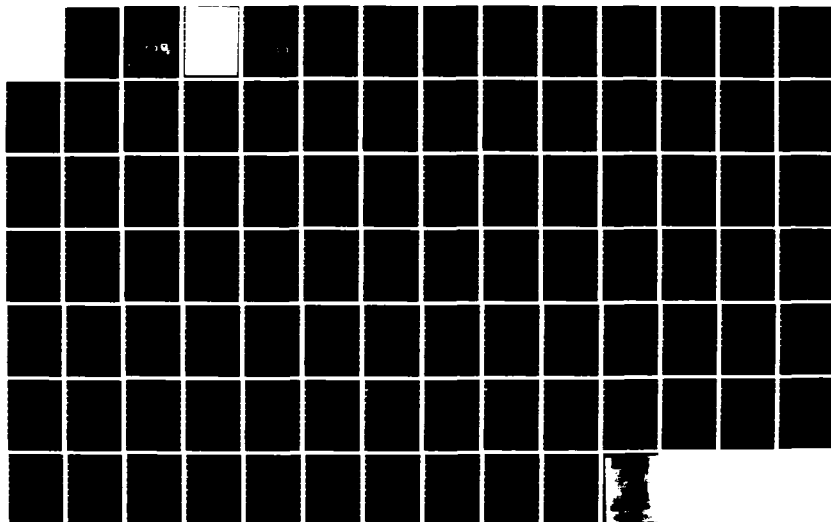
1/1

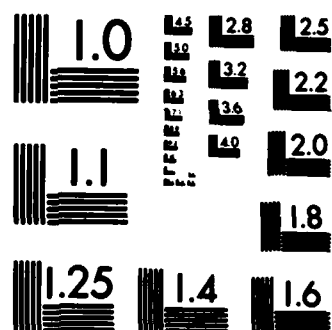
UNCLASSIFIED

JUL 84 HDL-TR-2038

F/G 20/3

NL





MICROCOPY RESOLUTION TEST CHART
NATIONAL BUREAU OF STANDARDS-1963-A

AD-A143 985

12

HDL-TR-2038

July 1984

The Concentric Spherical Cavity TE and TM Eigenvalues

by Louis F. Libelo
Morris Campi

DTIC
S
B

U.S. Army Electronics Research
and Development Command
Harry Diamond Laboratories
Adelphi, MD 20783

FILE COPY

Approved for public release; distribution unlimited.

84 08 08 077

UNCLASSIFIED

SECURITY CLASSIFICATION OF THIS PAGE (When Data Entered)

REPORT DOCUMENTATION PAGE		READ INSTRUCTIONS BEFORE COMPLETING FORM
1. REPORT NUMBER HDL-TR-2038	2. GOVT ACCESSION NO.	3. RECIPIENT'S CATALOG NUMBER
4. TITLE (and Subtitle) The Concentric Spherical Cavity TE and TM Eigenvalues		5. TYPE OF REPORT & PERIOD COVERED Technical Report
		6. PERFORMING ORG. REPORT NUMBER
7. AUTHOR(s) Louis F. Libelo Morris Campi		8. CONTRACT OR GRANT NUMBER(s) PRON: 1F3R0001011FA9
9. PERFORMING ORGANIZATION NAME AND ADDRESS Harry Diamond Laboratories 2800 Powder Mill Road Adelphi, MD 20783		10. PROGRAM ELEMENT, PROJECT, TASK AREA & WORK UNIT NUMBERS Program Ele: 61102A
11. CONTROLLING OFFICE NAME AND ADDRESS U.S. Army Materiel Development and Readiness Command Alexandria, VA 22333		12. REPORT DATE July 1984
		13. NUMBER OF PAGES 92
14. MONITORING AGENCY NAME & ADDRESS (if different from Controlling Office)		15. SECURITY CLASS. (of this report) UNCLASSIFIED
		15a. DECLASSIFICATION/DOWNGRADING SCHEDULE
16. DISTRIBUTION STATEMENT (of this Report) Approved for public release; distribution unlimited.		
17. DISTRIBUTION STATEMENT (of the abstract entered in Block 20, if different from Report)		
18. SUPPLEMENTARY NOTES HDL Project: A43312 DRCMS Code: 611102H440011 DA Project: 1L161102AH44		DTIC ELECTE S AUG 8 1984 D B
19. KEY WORDS (Continue on reverse side if necessary and identify by block number) Concentric cavity Modes Spherical Eigenvalues		
20. ABSTRACT (Continue on reverse side if necessary and identify by block number) <p>→ The eigenvalue problem for the concentric spherical cavity has been extensively investigated. This simple system is an important starting point for a number of important practical problems. In this report, the basic field theory for the eigenmodes and eigenvalues is formulated. We investigate the effect of a lossy dielectric on these properties and determine a large number of transverse electromagnetic and transverse magnetic (TE and TM) eigenvalues as a function of the cavity dimensions. The results given in tabular as well as graphical form reveal some rather unexpected properties.</p>		

DD FORM 1 JAN 73 1473 EDITION OF 1 NOV 65 IS OBSOLETE

UNCLASSIFIED

SECURITY CLASSIFICATION OF THIS PAGE (When Data Entered)

CONTENTS

	<u>Page</u>
1. INTRODUCTION	7
2. FORMAL SOLUTION FOR FIELDS WITHIN CAVITY	7
2.1 Basic Field Theory	7
2.2 The Eigenmodes	14
2.3 The Eigenvalues	21
2.4 Effect of Lossy Dielectric on Eigenvalues and Eigenmodes	22
3. ANALYTIC AND NUMERICAL DETERMINATION OF THE EIGENVALUES	25
3.1 General Range of the Eigenvalues	25
3.2 The TE Eigenvalues $\gamma_{np}^{(1)}$	26
3.2.1 The $\gamma_{1p}^{(1)}(R)$	26
3.2.2 The $\gamma_{2p}^{(1)}(R)$	32
3.2.3 The $\gamma_{3p}^{(1)}(R)$	38
3.2.4 The $\gamma_{4p}^{(1)}(R)$	43
3.2.5 TE, $n > 4$	46
3.3 The TM Eigenvalues $\gamma_{np}^{(2)}$	47
3.3.1 The $\gamma_{1p}^{(2)}(R)$	47
3.3.2 The $\gamma_{2p}^{(2)}(R)$	51
3.3.3 The $\gamma_{3p}^{(2)}(R)$	55
3.3.4 The $\gamma_{4p}^{(2)}(R)$	60
3.3.5 The $\gamma_{5p}^{(2)}(R)$	64
3.4 Summary Discussion of Eigenvalues	68
DISTRIBUTION	91

APPENDICES

A.--ORTHOGONALITY OF THE ELECTRIC FIELD EIGENVECTORS $E_{npm}^{(j, \delta)}(\vec{r})$	75
B.--COMPUTER PROGRAM FOR THE EIGENVALUES AND THEIR GENERATING FUNCTIONS	85

FIGURES

	<u>Page</u>
1. Geometry of concentric spherical cavity	8
2. Rational fraction function $f_1(R;x)$ used to find $n = 1$ TE Eigenvalues for values of ratio of inner to outer sphere radii $R_1 < R_2 < R_3$	28
3. Family of $\tan(1 - R)x$ for $R_1 < R_2$	29
4-12. Generating functions for the $\gamma_{1,p}^{(1)}$ with $R = 0.10$ to $R = 0.90$	30-31
13. Rational fraction function $f_2(R_0;x)$ for $R_1 < R_2 < R_0$	34
14. First crossing of $f_2(R_0;x)$ and $\tan(1 - R_0)x$ at $x_{21}^{(1)}(R_0)$	36
15-24. Generating functions for $\gamma_{2p}^{(1)}$ with $R = 0.05$ to $R = 0.90$	37-38
25. Generating functions for the $\gamma_{3p}^{(1)}$ with $R = 0.05$	40
26. Enlarged view of the generating functions for $\gamma_{3p}^{(1)}(0.05)$ near their first singularities	40
27. The generating functions for the $\gamma_{3p}^{(1)}$ with $R = 0.10$	40
28. Enlarged view of generating functions for $\gamma_{3p}^{(1)}(0.10)$ near their first singularities	40
29. Enlarged view of generating functions for $\gamma_{3p}^{(1)}(0.10)$ showing no intersections just beyond first singularities	40
30-37. Generating functions for $\gamma_{3p}^{(1)}$ with $R = 0.20$ to $R = 0.90$	41-42
38. Generating functions for $\gamma_{4p}^{(1)}$ with $R = 0.05$	45
39. Enlarged view of generating functions for $\gamma_{4p}^{(1)}(0.05)$ near their first singularities	45
40-47. Generating functions for the $\gamma_{4p}^{(1)}$ with $R = 0.10$ to $R = 0.80$	45-46
48-58. Generating functions for the $\gamma_{1p}^{(2)}$ with $R = 0.05$ to $R = 0.90$	49-51
59-71. Generating functions for the $\gamma_{2p}^{(2)}$ with $R = 0.05$ to $R = 0.90$	53-55
72-81. Generating functions for the $\gamma_{3p}^{(2)}$ with $R = 0.05$ to $R = 0.90$	58-59

FIGURES (Cont'd)

	<u>Page</u>
82-91. Generating functions for the $\gamma_{4p}^{(2)}$ with $R = 0.05$ to $R = 0.90$	61-63
92-101. Generating functions for the $\gamma_{5p}^{(2)}$ with $R = 0.05$ to $R = 0.90$	66-67
102. TM modes $\gamma_{np}^{(2)}(R)a$ for non-lossy concentric spherical cavity	69
103. TE modes $\gamma_{np}^{(1)}(R)a$ for non-lossy concentric spherical cavity	69
Table 1. Numerical Values of the Concentric Spherical Cavity Eigenvalues $\gamma_{np}^{(j)}(R)a \equiv x_{np}^{(j)}(R)$	70



Accession For	
NTIS GRA&I	<input checked="" type="checkbox"/>
DTIC TAB	<input type="checkbox"/>
Unannounced	<input type="checkbox"/>
Justification	
By	
Distribution/	
Availability Codes	
Dist	Avail and/or Special
A-1	

1. INTRODUCTION

We present the results of an extensive investigation of the electrical characteristics of the concentric spherical cavity. Although this system possesses a very simple geometry, to date, an analysis of this cavity has nevertheless been almost totally ignored. The only meaningful earlier work is a short note by Broc.¹ Broc's work confined itself to determining the Q of a silver-walled concentric cavity at a fixed frequency for each of two low order modes. This note is far from a complete solution of the concentric spherical cavity problem. Since this cavity serves as the starting point for the solution of a number of important practical electromagnetic problems, especially when considered in one asymptotic limit or another, it was necessary to carefully examine it in its simplest form. The results obtained in the initial stages of this study are rather interesting in themselves, since they give insight into electrical characteristics of many problems of a considerably more complex nature. Indeed, a series of subsequent reports will elaborate on a number of such important practical problems, ranging from coupling phenomena to antenna properties.

At the outset a bookkeeping problem presents itself. To deal with this situation, the results of our investigations will be discussed in a number of reports. Each report will be sufficiently restricted both in size and subject to render the whole manageable while at the same time retaining coherent meaning and connectivity of one to the others.

This particular report in the sequence, Part I, considers the geometric characteristics of the concentric spherical system. The formal vector field solution appropriate for the system appears in Part II. Part III contains the formal analysis for the eigenvalue solution for this boundary value problem, and Part IV gives the numerical solutions obtained for the eigenvalues and plots of their trajectories, along with a discussion of the results presented.

2. FORMAL SOLUTION FOR FIELDS WITHIN CAVITY

2.1 Basic Field Theory

We shall assume harmonic time dependence of the form $\exp(j\omega t)$. The explicit fields we seek are those appropriate to the concentric spherical cavity illustrated in figure 1. At the start we must establish some conventional notation; hence, we denote the radius of the outer sphere by $r = a$ and the radius of the inner sphere by $r = b$. We shall find it convenient to introduce a parameter, namely, the ratio of the inner to outer sphere radii, which we denote by $R = b/a$. We shall restrict our considerations in this report to the situation where there are no sources present within the cavity (except of course on the boundary walls) and to perfectly conducting walls. Also, we shall consider at this time only an isotropic, homogeneous, linear dielectric medium filling the cavity. At first we assume a non-lossy dielectric. In section 3, we shall extend our results to lossy dielectrics.

¹J. Broc, *Électromagnétisme, Académie des Sciences*, 230, *Comptes Rendus* (January 1950), 198-9.

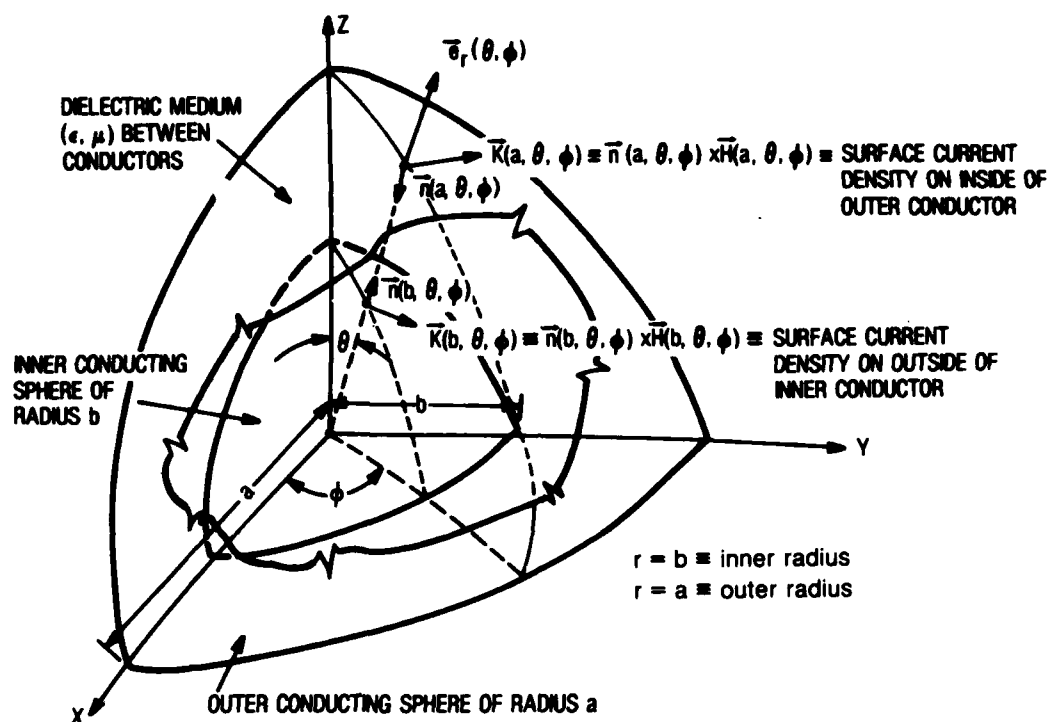


Figure 1. Geometry of concentric spherical cavity.

In our present problem the Maxwell equations are

$$\begin{aligned} \vec{\nabla} \times \vec{E} &= -j\omega\mu\vec{H} \quad , \quad \vec{\nabla} \cdot \vec{H} = 0 \\ \vec{\nabla} \times \vec{H} &= \vec{J} + j\omega\epsilon\vec{E} \quad , \quad \vec{\nabla} \cdot \vec{E} = \rho/\epsilon \end{aligned} \quad (1)$$

Since \vec{H} is solenoidal, we have then a vector potential \vec{A} such that

$$\vec{H}(\vec{r}) = \vec{\nabla} \times \vec{A}(\vec{r}) \quad , \quad (2)$$

which then yields

$$\vec{E}(\vec{r}) = -j\omega\mu\vec{A}(\vec{r}) - \vec{\nabla}\phi(\vec{r}) \quad , \quad (3)$$

where $\phi(\vec{r})$ is a scalar function. \vec{A} and $\phi(\vec{r})$ are connected via the relation

$$\vec{\nabla} \times \vec{\nabla} \times \vec{A} - \omega^2\mu\epsilon\vec{A} = \vec{J} - j\omega\epsilon\vec{\nabla}\phi \quad , \quad (4)$$

which we can write alternatively,

$$\nabla^2\vec{A} + \omega^2\mu\epsilon\vec{A} = -\vec{J} + \vec{\nabla}(\vec{\nabla} \cdot \vec{A}) + j\omega\epsilon\vec{\nabla}\phi \quad . \quad (5)$$

We can without loss of generality take the gauge condition

$$\vec{\nabla} \cdot \vec{A} = -j\omega\epsilon\phi \quad , \quad (6)$$

which then gives us the relation between the vector potential \vec{A} and the current sources \vec{J} , if there are any:

$$(\nabla^2 + \omega^2 \mu \epsilon) \vec{A} = -\vec{J} . \quad (7)$$

We may consider this vector potential $\vec{A}(\vec{r})$ as the generator of an electric and a magnetic field given by

$$\vec{E}_1(\vec{r}) = -j\omega\mu\vec{A}(\vec{r}) + \frac{1}{j\omega\epsilon} \vec{\nabla}[\vec{\nabla} \cdot \vec{A}(\vec{r})] \quad (8a)$$

$$\vec{H}_1(\vec{r}) = \vec{\nabla} \times \vec{A}(\vec{r}) \quad (8b)$$

Now in a source-free region, such as within our concentric spherical cavity, we have $\vec{\nabla} \cdot \vec{E} = 0$; hence, we can have, independent of the previous fields,

$$\vec{E} = -\vec{\nabla} \times \vec{F} , \quad (9)$$

where the vector potential \vec{F} gives rise to a solenoidal electric field. We then obtain from the Maxwell equations a corresponding magnetic field,

$$\vec{H}(\vec{r}) = -j\omega\epsilon\vec{F}(\vec{r}) - \vec{\nabla}\Psi(\vec{r}) , \quad (10)$$

where $\Psi(\vec{r})$ is a scalar potential. \vec{F} and Ψ are related through

$$\vec{\nabla} \times \vec{\nabla} \times \vec{F} - \omega^2 \mu \epsilon \vec{F} = -j\omega\mu\vec{\nabla}\Psi , \quad (11)$$

or alternatively through

$$(\nabla^2 + \omega^2 \mu \epsilon) \vec{F} = \vec{\nabla}(\vec{\nabla} \cdot \vec{F}) + j\omega\mu\vec{\nabla}\Psi . \quad (12)$$

Again without loss of generality we can fix the gauge by

$$\vec{\nabla} \cdot \vec{F} = -j\omega\mu\Psi , \quad (13)$$

and obtain for the vector potential \vec{F}

$$(\nabla^2 + \omega^2 \mu \epsilon) \vec{F} = 0 . \quad (14)$$

This vector potential generates an electric and a magnetic field within our source-free cavity given by

$$\vec{E}_2(\vec{r}) = -\vec{\nabla} \times \vec{F}(\vec{r}) \quad (15a)$$

$$\vec{H}_2(\vec{r}) = -j\omega\epsilon\vec{F}(\vec{r}) + \frac{1}{j\omega\mu} \vec{\nabla}[\vec{\nabla} \cdot \vec{F}(\vec{r})] . \quad (15b)$$

Since the fields generated by \vec{A} and by \vec{F} are independent, we have as the total fields in our source-free cavity the sum of the two contributions

$$\vec{E}(\vec{r}) = -\vec{\nabla} \times \vec{F}(\vec{r}) + \frac{1}{j\omega\epsilon} \vec{\nabla} \times \vec{\nabla} \times \vec{A} , \quad (16a)$$

and

$$\vec{H}(\vec{r}) = \vec{\nabla} \times \vec{A}(\vec{r}) + \frac{1}{j\omega\mu} \vec{\nabla} \times \vec{\nabla} \times \vec{F} . \quad (16b)$$

Now we can always decompose a vector field into a component transverse to the radial unit vector \vec{e}_r and a component along \vec{e}_r . We shall refer to the latter as the longitudinal component. Thus, the electric field at a point within our cavity can be formally decomposed in this fashion as follows:

$$\vec{E}(\vec{r}) = \vec{e}_r [\vec{e}_r \cdot \vec{E}(\vec{r})] - \vec{e}_r \times [\vec{e}_r \times \vec{E}(\vec{r})] . \quad (17)$$

We shall now proceed to construct the total electric and the total magnetic fields within the cavity as superpositions of just such transverse components and longitudinal components. This requires some arithmetic. Consider the specific vector functions

$$\vec{A}(\vec{r}) \equiv \vec{e}_r A_r(\vec{r}) , \quad \vec{F}(\vec{r}) \equiv \vec{e}_r F_r(\vec{r}) . \quad (18)$$

Note that it should not be expected that in general we can satisfy the relations

$$\vec{e}_r \cdot (\nabla^2 \vec{A}) = \nabla^2 (\vec{e}_r \cdot \vec{A}) \quad \text{or} \quad \vec{e}_r \cdot (\nabla^2 \vec{F}) = \nabla^2 (\vec{e}_r \cdot \vec{F}) ,$$

that is, A_r or F_r are solutions of the scalar Helmholtz equation. What we do have, in source-free regions, is

$$\vec{\nabla} \times \vec{\nabla} \times \vec{A} - \omega\mu\epsilon\vec{A} = -j\omega\epsilon\vec{\nabla}\phi , \quad (19a)$$

and

$$\vec{\nabla} \times \vec{\nabla} \times \vec{F} - \omega^2\mu\epsilon\vec{F} = -j\omega\mu\vec{\nabla}\psi . \quad (19b)$$

From these we can find the differential equations that $A_r(\vec{r})$ and $F_r(\vec{r})$ must satisfy. Let us work first with $\vec{A} = \vec{e}_r A_r$. Now some arithmetic exercises are necessary.

In spherical coordinates the gradient operator, we recall, is

$$\vec{\nabla} = \vec{e}_r \frac{\partial}{\partial r} + \frac{\vec{e}_\theta}{r} \frac{\partial}{\partial \theta} + \frac{\vec{e}_\phi}{r \sin \theta} \frac{\partial}{\partial \phi} . \quad (20)$$

Then from the following identities connecting the orthogonal unit vectors in cartesian coordinates and spherical coordinates,

$$\begin{aligned}\vec{e}_x &= \vec{e}_r \sin \theta \cos \phi + \vec{e}_\theta \cos \theta \cos \phi - \vec{e}_\phi \sin \phi , \\ \vec{e}_y &= \vec{e}_r \sin \theta \sin \phi + \vec{e}_\theta \cos \theta \sin \phi + \vec{e}_\phi \cos \phi , \\ \vec{e}_z &= \vec{e}_r \cos \theta - \vec{e}_\theta \sin \theta ,\end{aligned}\quad (21a)$$

$$\begin{aligned}\vec{e}_r &= \vec{e}_x \sin \theta \cos \phi + \vec{e}_y \sin \theta \sin \phi + \vec{e}_z \cos \theta , \\ \vec{e}_\theta &= \vec{e}_x \cos \theta \cos \phi + \vec{e}_y \cos \theta \sin \phi - \vec{e}_z \sin \theta , \\ \vec{e}_\phi &= -\vec{e}_x \sin \phi + \vec{e}_y \cos \phi ,\end{aligned}\quad (21b)$$

we find

$$\frac{\partial \vec{e}_r}{\partial r} = 0 , \quad \frac{\partial \vec{e}_r}{\partial \theta} = \vec{e}_\theta , \quad \frac{\partial \vec{e}_r}{\partial \phi} = \vec{e}_\phi \sin \theta , \quad (22a)$$

$$\frac{\partial \vec{e}_\theta}{\partial r} = 0 , \quad \frac{\partial \vec{e}_\theta}{\partial \theta} = -\vec{e}_r , \quad \frac{\partial \vec{e}_\theta}{\partial \phi} = \vec{e}_\phi \cos \theta , \quad (22b)$$

$$\frac{\partial \vec{e}_\phi}{\partial r} = 0 , \quad \frac{\partial \vec{e}_\phi}{\partial \theta} = 0 , \quad \frac{\partial \vec{e}_\phi}{\partial \phi} = -(\vec{e}_r \sin \theta + \vec{e}_\theta \cos \theta) . \quad (22c)$$

In turn we find

$$\vec{\nabla}(\vec{e}_r A_r) = \vec{e}_r \vec{e}_r \frac{\partial A_r}{\partial r} + \frac{\vec{e}_\theta \vec{e}_r}{r} \frac{\partial A_r}{\partial \theta} + \frac{\vec{e}_\phi \vec{e}_\theta}{r} A_r + \frac{\vec{e}_\phi \vec{e}_r}{r \sin \theta} \frac{\partial A_r}{\partial \phi} + \frac{\vec{e}_\phi \vec{e}_\phi}{r} A_r , \quad (23)$$

and then

$$\vec{\nabla} \times (\vec{e}_r A_r) = \frac{\vec{e}_\theta}{r \sin \theta} \frac{\partial A_r}{\partial \phi} - \frac{\vec{e}_\phi}{r} \frac{\partial A_r}{\partial \theta} , \quad (24)$$

which we note is transverse to \vec{e}_r . Continuing, we determine $\vec{\nabla}(\vec{\nabla} \times \vec{e}_r A_r)$, and finally,

$$\begin{aligned}\vec{\nabla} \times \vec{\nabla} \times (\vec{e}_r A_r) &= \vec{e}_r \left\{ -\left[\frac{1}{r^2 \sin \theta} \frac{\partial}{\partial \theta} \sin \theta \frac{\partial}{\partial \theta} + \frac{1}{r^2 \sin^2 \theta} \frac{\partial^2}{\partial \phi^2} \right] A_r(\vec{r}) \right\} \\ &+ \frac{\vec{e}_\theta}{r} \frac{\partial}{\partial \theta} \left(\frac{\partial A_r}{\partial r} \right) + \frac{\vec{e}_\phi}{r \sin \theta} \frac{\partial}{\partial \phi} \left(\frac{\partial A_r}{\partial r} \right) .\end{aligned}\quad (25)$$

We thus have for our choice of $\vec{A}(\vec{r})$ substituted into equation (19a); that is,

$$\vec{\nabla} \times \vec{\nabla} \times (\vec{e}_r A_r) - \omega^2 \mu \epsilon (\vec{e}_r A_r) = -j\omega \epsilon \vec{\nabla} \phi ,$$

or the more explicit relation, with $k^2 \equiv \omega^2 \mu \epsilon$

$$\begin{aligned} -e_r \left\{ \frac{1}{r^2} \left[\frac{1}{\sin \theta} \frac{\partial}{\partial \theta} \sin \theta \frac{\partial}{\partial \theta} + \frac{1}{\sin^2 \theta} \frac{\partial^2}{\partial \phi^2} + k^2 \right] A_r(\vec{r}) \right\} + \left(\frac{\vec{e}_\theta}{r} \frac{\partial}{\partial \theta} + \frac{\vec{e}_\phi}{r \sin \theta} \frac{\partial}{\partial \phi} \right) \\ \cdot \frac{\partial A_r(\vec{r})}{\partial r} = -j\omega \epsilon \left\{ \vec{e}_r \frac{\partial}{\partial r} \phi + \left[\frac{\vec{e}_\theta}{r} \frac{\partial}{\partial \theta} + \frac{\vec{e}_\phi}{r \sin \theta} \frac{\partial}{\partial \phi} \right] \phi(\vec{r}) \right\} \end{aligned} \quad (26)$$

Then if we choose, as we are free to,

$$-j\omega \epsilon \phi(\vec{r}) = \frac{\partial A_r(\vec{r})}{\partial r} , \quad (27)$$

this, indeed, follows from equation (6); we will obtain as the differential equation for A_r ,

$$\vec{e}_r \left[\frac{\partial^2 A_r}{\partial r^2} \frac{1}{r^2 \sin \theta} \frac{\partial}{\partial \theta} \left(\sin \theta \frac{\partial A_r}{\partial \theta} \right) + \frac{1}{r^2 \sin^2 \theta} \frac{\partial^2 A_r}{\partial \phi^2} + k^2 A_r \right] = 0 . \quad (28)$$

With the observation that

$$\frac{1}{r} \frac{\partial^2}{\partial r^2} \left[r \left(\frac{A_r}{r} \right) \right] = \frac{\partial^2}{\partial r^2} \left(\frac{A_r}{r} \right) + \frac{2}{r} \frac{\partial}{\partial r} \left(\frac{A_r}{r} \right) , \quad (29)$$

we can conveniently rewrite equation (28) as

$$(\nabla^2 + k^2) \frac{A_r(\vec{r})}{r} = 0 . \quad (30)$$

From equations (24) and (16b), we then conclude that A_r , the solution of the differential equation (30), will generate a magnetic field transverse to \vec{e}_r . This will be referred to as the TM field solution in the following discussions. In precisely the same manner, we can process $\vec{F}(\vec{r})$ of equation (18) and obtain

$$(\nabla^2 + k^2) F_r(\vec{r})/r = 0 \quad (31)$$

as the defining differential equation of the scalar function $F_r(\vec{r})$. Also we have as in equation (24),

$$\vec{\nabla} \times (\vec{e}_r F_r) = \frac{\vec{e}_\theta}{r \sin \theta} \frac{\partial F_r}{\partial \phi} - \frac{\vec{e}_\phi}{r} \frac{\partial F_r}{\partial \theta} , \quad (32)$$

which is transverse to \vec{e}_r .

Thus, F_r will generate an electric field within the cavity which is transverse to \hat{e}_r and which will be referred to as the TE field solution in what follows.

Once again we change notation by defining two scalar functions $\phi(\vec{r})$ and $\psi(\vec{r})$, such that

$$\vec{A}(\vec{r}) \equiv \vec{r}(A_r/r) = \vec{r}\psi(\vec{r}) \quad (33)$$

and

$$\vec{F}(\vec{r}) = \vec{r}(F_r/r) = \vec{r}\phi(\vec{r}) \quad (34)$$

The electric and magnetic fields in terms of these scalar functions are

$$\vec{E}(\vec{r}) = -\vec{\nabla} \times [\vec{r}\phi(\vec{r})] + \frac{1}{j\omega\epsilon} \vec{\nabla} \times \vec{\nabla} \times [\vec{r}\psi(\vec{r})] \quad (35)$$

and

$$\vec{H}(\vec{r}) = \vec{\nabla} \times [\vec{r}\psi(\vec{r})] + \frac{1}{j\omega\mu} \vec{\nabla} \times \vec{\nabla} \times [\vec{r}\phi(\vec{r})] \quad (36)$$

where the TM part of the fields is generated by the scalar function $\psi(\vec{r})$ and the TE part separately by $\phi(\vec{r})$, and of course we have

$$(\nabla^2 - \gamma^2) \psi(\vec{r}) = 0 \quad (37)$$

and

$$(\nabla^2 - \gamma^2) \phi(\vec{r}) = 0 \quad (38)$$

and where we choose to replace k by $j\gamma$.

It is useful to write out explicitly the field components in terms of the scalar functions $\psi(\vec{r})$ and $\phi(\vec{r})$. We have then from equations (35) and (36):

$$E_r(\vec{r}) = \frac{1}{j\omega\epsilon} \left[\frac{\partial^2}{\partial r^2} - \gamma^2 \right] [r\psi(\vec{r})] \quad (39)$$

$$E_\theta(\vec{r}) = -\frac{1}{r \sin \theta} \frac{\partial}{\partial \phi} [r\phi(\vec{r})] + \frac{1}{j\omega\epsilon} \frac{1}{r} \frac{\partial^2}{\partial r \partial \theta} [r\psi(\vec{r})] \quad (40)$$

$$E_\phi(\vec{r}) = \frac{1}{r} \frac{\partial}{\partial \theta} [r\phi(\vec{r})] + \frac{1}{j\omega\epsilon} \frac{1}{r \sin \theta} \frac{\partial^2}{\partial r \partial \phi} [r\psi(\vec{r})] \quad (41)$$

$$H_r(\vec{r}) = \frac{1}{j\omega\mu} \left[\frac{\partial^2}{\partial r^2} - \gamma^2 \right] [r\phi(\vec{r})] \quad (42)$$

$$H_\theta(\vec{r}) = \frac{1}{j\omega\mu} \frac{1}{r} \frac{\partial^2}{\partial r \partial \theta} [r\phi(\vec{r})] + \frac{1}{r \sin \theta} \frac{\partial}{\partial \phi} [r\psi(\vec{r})] \quad (43)$$

$$H_\phi(\vec{r}) = \frac{1}{j\omega\mu} \frac{1}{r \sin \theta} \frac{\partial^2}{\partial r \partial \phi} [r\phi(\vec{r})] - \frac{1}{r} \frac{\partial}{\partial \theta} [r\psi(\vec{r})] \quad (44)$$

2.2 The Eigenmodes

As usual we take the scalar functions as products of radial and angular function factors; that is,

$$\psi(\vec{r}) = \psi(r)Y(\theta, \phi) \quad (45a)$$

and

$$\phi(\vec{r}) = \phi(r)Y(\theta, \phi) \quad (45b)$$

From the forms of equations (37), (38), and (45), we find that we shall have solutions of the form

$$\psi_{nm}^{(e)}(\vec{r}) = \psi_n(r)P_{nm}(\cos \theta) \cos m\phi \quad , \quad (46)$$

$$\psi_{nm}^{(o)}(\vec{r}) = \psi_n(r)P_{nm}(\cos \theta) \sin m\phi \quad ,$$

and

$$\phi_{nm}^{(e)}(\vec{r}) = \phi_n(r)P_{nm}(\cos \theta) \cos m\phi \quad , \quad (47)$$

$$\phi_{nm}^{(o)}(\vec{r}) = \phi_n(r)P_{nm}(\cos \theta) \sin m\phi \quad ,$$

where n is a positive integer, m can run from 0 to n , and the functions P_{nm} are the familiar associated Legendre functions of the first kind.

The radial factors satisfy the differential equations

$$\frac{d^2}{dr^2} [r\psi_n(r)] - \left[\gamma^2 + \frac{n(n+1)}{r^2} \right] [r\psi_n(r)] = 0 \quad (48)$$

and

$$\frac{d^2}{dr^2} [r\phi_n(r)] - \left[\gamma^2 + \frac{n(n+1)}{r^2} \right] [r\phi_n(r)] = 0 \quad (49)$$

The formal fundamental solutions of equations (48) and (49) are the modified spherical Bessel functions $i_n(\gamma r)$ and $k_n(\gamma r)$, where the i_n are singular at $r = \infty$ and the k_n are singular at the origin. Complete information concerning the properties of these functions is available in the mathematics reference literature.²

In the concentric spherical cavity, the region of interest excludes the origin; hence, the radial factor must be a linear combination of the i_n and k_n functions, e.g.,

²A. Erdelyi, ed., Ch VII, *Higher Transcendental Functions*, California Institute of Technology, Bateman Manuscript Project, II, McGraw-Hill Book Co., Inc., NY (1953).

$$\psi_n(r) = \alpha_n i_n(\gamma r) + \beta_n k_n(\gamma r) ,$$

where α_n and β_n are independent of the radius r .

Furthermore, since the fields must satisfy boundary conditions at the cavity walls, solutions of equations (48) and (49) can exist only for certain values of γ , which we shall denote by γ_{np} and shall discuss in more detail momentarily. We then shall have solutions of the form

$$\psi_{npm}^{(e)}(\vec{r}) = \psi_{np} \left[\gamma_{np}^{(TM)} r \right] P_{nm}(\cos \theta) \cos m\phi , \quad (50a)$$

and

$$\psi_{npm}^{(o)}(\vec{r}) = \psi_{np} \left[\gamma_{np}^{(TM)} r \right] P_{nm}(\cos \theta) \sin m\phi , \quad (50b)$$

satisfying

$$\frac{d^2}{dr^2} \left[r \psi_{npm}^{(\cdot)}(\vec{r}) \right] - \left[\gamma_{np}^{2(TM)} + \frac{n(n+1)}{r^2} \right] \left[r \psi_{npm}^{(\cdot)}(\vec{r}) \right] = 0 \quad (51)$$

and

$$\phi_{npm}^{(e)}(\vec{r}) = \phi_{np} \left[\gamma_{np}^{(TE)} r \right] P_{nm}(\cos \theta) \cos m\phi , \quad (52a)$$

$$\phi_{npm}^{(o)}(\vec{r}) = \phi_{np} \left[\gamma_{np}^{(TE)} r \right] P_{nm}(\cos \theta) \sin m\phi , \quad (52b)$$

which satisfy

$$\frac{d^2}{dr^2} \left[r \phi_{npm}^{(\cdot)}(\vec{r}) \right] - \left[\gamma_{np}^{2(TE)} + \frac{n(n+1)}{r^2} \right] \left[r \phi_{npm}^{(\cdot)}(\vec{r}) \right] = 0 . \quad (53)$$

These scalar eigenfunctions generate, in turn, vector-field eigenmodes. Thus, we have

$$\vec{E}_{npm}^{(1,0)}(\vec{r}) \equiv -\vec{\nabla} \times \left[\vec{r} \phi_{npm}^{(0)}(\vec{r}) \right] \quad (54)$$

$$\vec{E}_{npm}^{(2,0)}(\vec{r}) \equiv \frac{1}{j\omega\epsilon} \vec{\nabla} \times \vec{\nabla} \times \left[\vec{r} \psi_{npm}^{(0)}(\vec{r}) \right] \quad (55)$$

$$\vec{H}_{npm}^{(1,0)}(\vec{r}) \equiv \frac{1}{j\omega\mu} \vec{\nabla} \times \vec{\nabla} \times \left[\vec{r} \phi_{npm}^{(0)}(\vec{r}) \right] \quad (56)$$

$$\vec{H}_{npm}^{(2,0)}(\vec{r}) \equiv \vec{\nabla} \times \left[\vec{r} \psi_{npm}^{(0)}(\vec{r}) \right] . \quad (57)$$

In the above we have made another attempt to condense the notation by defining for our vector field, $\vec{V}^{(j)}(\vec{r})$, the convention that $j = 1$ implies TE modes and $j = 2$ TM modes.

The vector field eigenmodes given in equations (54) and (55) form a complete orthogonal set for our cavity. The orthogonality is shown in appendix A. Any electric field within the cavity can be expanded in this set of eigenvectors. Thus, we may write

$$\vec{E}(\vec{r}) = \sum_{n=1}^{\infty} \sum_{p=1}^{\infty} \sum_{m=0}^n \sum_{j=1}^2 \left\{ A_{npm}^{(j,o)} \vec{E}_{npm}^{(j,o)}(\vec{r}) + A_{npm}^{(j,e)} \vec{E}_{npm}^{(j,e)}(\vec{r}) \right\} , \quad (58)$$

where, integrating over the cavity volume,

$$A_{npm}^{(j,e)} \equiv \iiint d\tau(\vec{r}) \vec{E}(\vec{r}) \cdot \vec{E}_{npm}^{(j,e)}(\vec{r}) \div \left[\Omega_{npm}^{(j,e)} \right]^2 , \quad (59a)$$

where

$$\left[\Omega_{npm}^{(j,e)} \right]^2 \equiv \iiint d\tau(\vec{r}) \vec{E}_{npm}^{(j,e)}(\vec{r}) \cdot \vec{E}_{npm}^{(j,e)}(\vec{r}) . \quad (59b)$$

We have, of course, the vector relations

$$\vec{\nabla} \times \vec{\nabla} \times \vec{E}_{npm}^{(j,e)}(\vec{r}) + \left[\gamma_{np}^{(j)} \right]^2 \vec{E}_{npm}^{(j,e)}(\vec{r}) = 0 , \quad (60)$$

$$\vec{\nabla} \times \vec{\nabla} \times \vec{H}_{npm}^{(j,o)}(\vec{r}) + \left[\gamma_{np}^{(j)} \right]^2 \vec{H}_{npm}^{(j,o)}(\vec{r}) = 0 ; \quad (61)$$

and we have, in addition, the relations between the electric and magnetic eigenvectors

$$\vec{H}_{npm}^{(j,o)}(\vec{r}) = \frac{1}{j[\gamma_{np}^{(j)}]} \vec{\nabla} \times \vec{E}_{npm}^{(j,e)}(\vec{r}) , \quad (62)$$

$$\vec{E}_{npm}^{(j,e)}(\vec{r}) = \frac{1}{j[\gamma_{np}^{(j)}]} \vec{\nabla} \times \vec{H}_{npm}^{(j,o)}(\vec{r}) . \quad (63)$$

Any magnetic field within the cavity similar to equation (58) can be written as an expansion in the complete set of magnetic field eigenmodes of equations (56) and (57). This in its turn can be written using equation (62) as

$$\vec{H}(\vec{r}) = \sum_{n=1}^{\infty} \sum_{p=1}^{\infty} \sum_{m=0}^n \sum_{j=1}^2 \left\{ B_{npm}^{(j,e)} \frac{\nabla \times \vec{E}_{npm}^{(j,e)}(\vec{r})}{j\gamma_{np}^{(j)}} + B_{npm}^{(j,o)} \frac{\vec{\nabla} \times \vec{E}_{npm}^{(j,o)}(\vec{r})}{j\gamma_{np}^{(j)}} \right\}, \quad (64)$$

where the expansion coefficients are given by

$$\begin{aligned} B_{npm}^{(j,o)} &= \Lambda_{npm}^{(j,o)-2} \iiint d\tau(\vec{r}) \vec{H}(\vec{r}) \cdot \vec{H}_{npm}^{(j,o)}(\vec{r}) \\ &= \frac{[\Lambda_{npm}^{(j,o)}]^{-2}}{j\gamma_{np}^{(j)}} \iiint d\tau(\vec{r}) \vec{H}(\vec{r}) \cdot \vec{\nabla} \times \vec{E}_{npm}^{(j,o)}(\vec{r}), \end{aligned} \quad (65a)$$

where

$$[\Lambda_{npm}^{(j,o)}]^2 = \iiint d\tau(\vec{r}) H_{npm}^{(j,o)}(\vec{r}) \cdot \vec{H}_{npm}^{(j,o)}(\vec{r}). \quad (65b)$$

We can quickly obtain a useful identity using equations (59) and (65a&b) which enables us to formally write

$$\begin{aligned} \vec{E}(\vec{r}) &= \iiint d\tau(\vec{r}') \sum_{n=1}^{\infty} \sum_{p=1}^{\infty} \sum_{m=0}^n \sum_{j=1}^2 \left\{ \frac{\vec{E}_{npm}^{(j,e)}(\vec{r}) \vec{E}_{npm}^{(j,e)}(\vec{r}')}{[\Omega_{npm}^{(j,e)}]^2} + \frac{\vec{E}_{npm}^{(j,o)}(\vec{r}) \vec{E}_{npm}^{(j,o)}(\vec{r}')}{[\Omega_{npm}^{(j,o)}]^2} \right\} \cdot \vec{E}(\vec{r}'), \end{aligned} \quad (65c)$$

$$\begin{aligned} \vec{H}(\vec{r}) &= \iiint d\tau(\vec{r}') \sum_{n=1}^{\infty} \sum_{p=1}^{\infty} \sum_{m=0}^n \sum_{j=1}^2 \left\{ \frac{\vec{H}_{npm}^{(j,e)}(\vec{r}) \vec{H}_{npm}^{(j,e)}(\vec{r}')}{[\Lambda_{npm}^{(j,e)}]^2} + \frac{\vec{H}_{npm}^{(j,o)}(\vec{r}) \vec{H}_{npm}^{(j,o)}(\vec{r}')}{[\Lambda_{npm}^{(j,o)}]^2} \right\} \cdot \vec{H}(\vec{r}'). \end{aligned} \quad (65d)$$

From these we obtain the statement of completeness

$$\sum_{n=1}^{\infty} \sum_{p=1}^{\infty} \sum_{m=0}^n \sum_{j=1}^2 \left\{ \frac{\vec{E}_{npm}^{(j,e)}(\vec{r}) \vec{E}_{npm}^{(j,e)}(\vec{r}')}{[\Omega_{npm}^{(j,e)}]^2} + \frac{\vec{E}_{npm}^{(j,o)}(\vec{r}) \vec{E}_{npm}^{(j,o)}(\vec{r}')}{[\Omega_{npm}^{(j,o)}]^2} \right\} \equiv \vec{I} \delta(\vec{r} - \vec{r}') \quad (66a)$$

and

$$\sum_{n=1}^{\infty} \sum_{p=1}^{\infty} \sum_{m=0}^n \sum_{j=1}^2 \left\{ \frac{\vec{H}_{npm}^{(j,e)}(\vec{r}) \vec{H}_{npm}^{(j,e)}(\vec{r}')}{[\Lambda_{npm}^{(j,e)}]^2} + \frac{\vec{H}_{npm}^{(j,o)}(\vec{r}) \vec{H}_{npm}^{(j,o)}(\vec{r}')}{[\Lambda_{npm}^{(j,o)}]^2} \right\} \equiv \vec{I} \delta(\vec{r} - \vec{r}') \quad (66b)$$

where \vec{I} is the unit dyad. We can show that

$$\Lambda_{npm}^{(j,e)} \equiv \Omega_{npm}^{(j,e)} \quad (67)$$

and we therefore need consider only one set of normalization constants, which we shall assume to be the $\Omega_{npm}^{(j,o)}$. The proof is straightforward using the vector identity

$$\vec{\nabla} \cdot (\vec{M} \times \vec{N}) = \vec{N} \cdot \vec{\nabla} \times \vec{M} - \vec{M} \cdot \vec{\nabla} \times \vec{N} \quad (68a)$$

and choosing

$$\vec{M} \equiv \vec{E}_{npm}^{(j,e)}(\vec{r}) \quad , \quad \vec{N} \equiv \vec{\nabla} \times \vec{E}_{npm}^{(j,e)}(\vec{r}) \quad (68b)$$

We get upon substitution into the identity and integrating over the volume of the concentric spherical cavity

$$\begin{aligned} & \iiint d\tau(\vec{r}) \vec{\nabla} \cdot [\vec{E}_{npm}^{(j,e)}(\vec{r}) \times \vec{\nabla} \times \vec{E}_{npm}^{(j,e)}(\vec{r})] \\ &= \iiint d\tau(\vec{r}) \vec{\nabla} \times \vec{E}_{npm}^{(j,e)}(\vec{r}) \cdot \vec{\nabla} \times \vec{E}_{npm}^{(j,e)}(\vec{r}) \\ &- \iiint d\tau(\vec{r}) [\vec{E}_{npm}^{(j,e)}(\vec{r}) \cdot \vec{\nabla} \times \vec{\nabla} \times \vec{E}_{npm}^{(j,e)}(\vec{r})] \quad (68c) \end{aligned}$$

Rearranging and applying Stokes theorem this becomes

$$\begin{aligned} & \iiint d\tau(\vec{r}) \vec{\nabla} \times \vec{E}_{npm}^{(j,e)}(\vec{r}) \cdot \vec{\nabla} \times \vec{E}_{npm}^{(j,e)}(\vec{r}) = \iint_{\substack{\text{cavity} \\ \text{walls}}} d\vec{f}(\vec{r}) \cdot \left\{ \vec{E}_{npm}^{(j,e)}(\vec{r}) \right. \\ & \left. \times \vec{\nabla} \times \vec{E}_{npm}^{(j,e)}(\vec{r}) \right\} - [\gamma_{np}^{(j)}]^2 \iiint d\tau(\vec{r}) \vec{E}_{npm}^{(j,e)}(\vec{r}) \cdot \vec{E}_{npm}^{(j,e)}(\vec{r}) \quad (68d) \end{aligned}$$

The surface integral vanished due to the vanishing of E_{tan} on the cavity walls. Then, by equation (62), we can rewrite this as

$$\begin{aligned} & -[\gamma_{np}^{(j)}]^2 \iiint d\tau(\vec{r}) \vec{H}_{npm}^{(j)}(\vec{r}) \cdot \vec{H}_{npm}^{(j)}(\vec{r}) \\ & = -[\gamma_{np}^{(j)}]^2 \iiint d\tau(\vec{r}) \vec{E}_{npm}^{(j)}(\vec{r}) \cdot \vec{E}_{npm}^{(j)}(\vec{r}) , \end{aligned} \quad (68e)$$

from which the identity in equation (67) follows.

Weyl³ demonstrated earlier that a dyadic Green's function exists for the geometry we are dealing with. This function is of considerable significance. For the electric field, the dyadic Green's function $\vec{G}_E(\vec{r}, \vec{r}')$, which satisfies

$$\vec{\nabla} \times \vec{\nabla} \times \vec{G}_E(\vec{r}, \vec{r}') + \gamma^2 \vec{G}_E(\vec{r}, \vec{r}') = -\vec{I} \delta(\vec{r} - \vec{r}') , \quad (69a)$$

is given by

$$\begin{aligned} \vec{G}_E(\vec{r}, \vec{r}') = & - \sum_{n=1}^{\infty} \sum_{p=1}^{\infty} \sum_{m=0}^n \sum_{j=1}^2 \left\{ \frac{\vec{E}_{npm}^{(j,e)}(\vec{r}') \vec{E}_{npm}^{(j,e)}(\vec{r}) [\Omega_{npm}^{(j,e)}]^{-2}}{\gamma^2 - (\gamma_{np}^{(j)})^2} \right. \\ & \left. + \frac{\vec{E}_{npm}^{(j,o)}(\vec{r}') \vec{E}_{npm}^{(j,o)}(\vec{r}) [\Omega_{npm}^{(j,o)}]^{-2}}{\gamma^2 - (\gamma_{np}^{(j)})^2} \right\} . \end{aligned} \quad (69b)$$

³H. Weyl, *Über die Randwertaufgabe der Strahlungstheorie und Asymptotische Spektralgesetze*, Z. Reine und Angewand. Math, 143 (1913), 177-202.

As a demonstration we show that

$$\begin{aligned}
& \iiint_{\text{conc. sphere. cavity}} d\tau(\vec{r}') \vec{E}(\vec{r}') \cdot \left\{ \vec{\nabla}_{\vec{r}} \times \vec{\nabla}_{\vec{r}'} \times \vec{G}_E(\vec{r}, \vec{r}') + \gamma^2 \vec{G}_E(\vec{r}, \vec{r}') + \vec{I} \delta(\vec{r} - \vec{r}') \right\} \\
&= \sum_{n=1}^{\infty} \sum_{p=1}^{\infty} \sum_{m=0}^n \sum_{j=1}^2 (\gamma_{np}^{(j)})^2 \left\{ \left[\iiint d\tau(\vec{r}') \vec{E}(\vec{r}') \cdot \vec{E}_{n\pm m}^{(j,e)}(\vec{r}') \right] \vec{E}_{n\pm m}^{(j,e)}(\vec{r}) \left[\Omega_{n\pm m}^{(j,e)} \right]^{-2} \right. \\
&+ \left[\iiint d\tau(\vec{r}') \vec{E}(\vec{r}') \cdot \vec{E}_{n\pm m}^{(j,o)}(\vec{r}') \right] \vec{E}_{n\pm m}^{(j,o)}(\vec{r}) \left[\Omega_{n\pm m}^{(j,o)} \right]^{-2} \left. + \left[\gamma^2 - (\gamma_{np}^{(j)})^2 \right] \right. \\
&- \gamma^2 \sum_{n=1}^{\infty} \sum_{p=1}^{\infty} \sum_{m=0}^n \sum_{j=1}^2 \left\{ \left[\iiint d\tau(\vec{r}') \vec{E}(\vec{r}') \cdot \vec{E}_{n\pm m}^{(j,e)}(\vec{r}') \right] \vec{E}_{n\pm m}^{(j,e)}(\vec{r}) \left[\Omega_{n\pm m}^{(j,e)} \right]^{-2} \right. \\
&+ \left[\iiint d\tau(\vec{r}') \vec{E}(\vec{r}') \cdot \vec{E}_{n\pm m}^{(j,o)}(\vec{r}') \right] \vec{E}_{n\pm m}^{(j,o)}(\vec{r}) \left[\Omega_{n\pm m}^{(j,o)} \right]^{-2} \left. + \left[\gamma^2 - (\gamma_{np}^{(j)})^2 \right] \right\} \quad (69c) \\
&+ \iiint d\tau(\vec{r}') \vec{E}(\vec{r}') \delta(\vec{r} - \vec{r}') \\
&= -\vec{E}(\vec{r}) + \vec{E}(\vec{r}) = 0 .
\end{aligned}$$

We note that the poles of the Green's function for the electric field given in equation (69) are the eigenvalues or resonances of our perfect cavity.

The magnetic field dyadic Green's function is given by

$$\begin{aligned}
\vec{G}_H(\vec{r}, \vec{r}') &= - \sum_{n=1}^{\infty} \sum_{p=1}^{\infty} \sum_{m=0}^n \sum_{j=1}^2 \left\{ \vec{H}_{n\pm m}^{(j,e)}(\vec{r}) \vec{H}_{n\pm m}^{(j,e)}(\vec{r}') \left[\Lambda_{n\pm m}^{(j,e)} \right]^{-2} \right. \\
&+ \left. \vec{H}_{n\pm m}^{(j,o)}(\vec{r}) \vec{H}_{n\pm m}^{(j,o)}(\vec{r}') \left[\Lambda_{n\pm m}^{(j,o)} \right]^{-2} \right\} + \left[\gamma^2 - (\gamma_{np}^{(j)})^2 \right] , \quad (70)
\end{aligned}$$

which satisfies

$$\vec{\nabla} \times \vec{\nabla} \times \vec{G}_H(\vec{r}, \vec{r}') + \gamma^2 \vec{G}_H(\vec{r}, \vec{r}') = -\vec{I} \delta(\vec{r} - \vec{r}') . \quad (71)$$

Having formally discussed the vector fields for the cavity, we proceed next to a formal discussion of the eigenvalues.

2.3 The Eigenvalues

We shall discuss only briefly the determination of the eigenvalues $\gamma_{np}^{(j)}$ which yield the eigenfunctions $\psi_{np}(r)$ and $\phi_{np}(r)$. It is somewhat simpler to consider the TE fields which involve the scalar functions $\phi_{np}(r)$. At the cavity walls, the boundary conditions that the electric fields are required to satisfy are

$$E_{\theta;nm}(r = a) \equiv 0 \equiv E_{\theta;nm}(r = b) , \quad (72a)$$

and

$$E_{\phi;nm}(r = a) \equiv 0 \equiv E_{\phi;nm}(r = b) . \quad (72b)$$

Equation (40) then requires that we have

$$\phi_n(a) = 0 , \quad (73a)$$

and

$$\phi_n(b) = 0 , \quad (73b)$$

which can be satisfied if we take $\phi_n(r)$ in the form

$$\phi_n(r) = i_n(\gamma r)k_n(\gamma b) - i_n(\gamma b)k_n(\gamma r) . \quad (74)$$

Clearly, equation (73b) is automatically satisfied. To satisfy equation (73a), we must find the roots or, equivalently, those values of γ for which

$$i_n(\gamma a)k_n(\gamma b) - i_n(\gamma b)k_n(\gamma a) = 0 . \quad (75)$$

In section 2.4 we shall go into great detail concerning the analytic procedure for solving this eigenvalue problem. We shall see at that time that there is a discrete, ordered infinite set of roots for each order n . These roots, which we denote by $\gamma = j\gamma_{np}^{(1)}$ for $p = 1, 2, \dots$, lie along the positive imaginary axis in the complex γ -plane. For each of these values we obtain a radial factor; i.e.,

$$\phi_{np}(r) \equiv i_n(j\gamma_{np}^{(1)} r)k_n(j\gamma_{np}^{(1)} b) - i_n(j\gamma_{np}^{(1)} b)k_n(j\gamma_{np}^{(1)} r) . \quad (76)$$

The functions given in equation (76) used in equation (52) will generate the corresponding TE vector eigenmode fields from equations (40) through (44).

For the TM modes, we need to determine the eigenfunctions $\psi_{np}(r)$ which satisfy the boundary conditions given in equation (72). From equations (41) and (46) we find we must have

$$\left\{ \frac{d}{dr} [r\psi_{np}(r)] \right\} = 0 \quad (77a)$$

at $r = a$,

$$\left\{ \frac{d}{dr} [r\psi_{np}(r)] \right\} = 0 \quad (77b)$$

at $r = b$.

These requirements can be met if we take $\psi_n(r)$ of the form

$$\psi_n(r) = i_n(\gamma r) [\gamma b k_n(\gamma b)]' - k_n(\gamma r) [\gamma b i_n(\gamma b)]' , \quad (78)$$

where $[XZ_n(X)]'$ means differentiate with respect to the variable X . We observe that equation (77a) is automatically satisfied. Equation (77a) requires that we have

$$[\gamma a i_n(\gamma a)]' [\gamma b k_n(\gamma b)]' - [\gamma a k_n(\gamma a)]' [\gamma b i_n(\gamma b)]' = 0 . \quad (79)$$

We shall see in the following section that this relation will be satisfied only for an ordered infinite discrete set of values $\gamma = \gamma_{np}^{(2)}$ for $p = 1, 2, \dots$, for each order n . The physically meaningful roots lie along the positive imaginary axis, just as for the TE case. Each such eigenvalue $\gamma_{np}^{(2)}$ gives rise to a radial factor function, i.e.,

$$\begin{aligned} \psi_{np}(r) \equiv & i_n(j\gamma_{np}^{(2)} r) \left[\gamma_{np}^{(2)} b k_n(j\gamma_{np}^{(2)} b) \right] \\ & - k_n(j\gamma_{np}^{(2)} r) \left[\gamma_{np}^{(2)} b i_n(j\gamma_{np}^{(2)} b) \right]' . \end{aligned} \quad (80)$$

Functions given in equation (80) used in equations (50) generate the corresponding TM vector eigenmode fields from equations (39) through (41) and (43) and (44).

Next, we briefly discuss the effect of a lossy dielectric on these eigenvalues and on the corresponding vector eigenmodes.

2.4 Effect of Lossy Dielectric on Eigenvalues and Eigenmodes

By allowing the dielectric to have a finite, isotropic, homogeneous, frequency independent, linear conductivity, we can account for the effects of a lossy dielectric filling the concentric spherical cavity. We now have

$$\vec{J}(\vec{r}, t) = \sigma \vec{E}(\vec{r}, t) . \quad (81)$$

The Faraday's Law and Ampere's Law equations can now be written

$$\vec{\nabla} \times \vec{E}(\vec{r}, t) = -\mu \frac{\partial \vec{H}(\vec{r}, t)}{\partial t} , \quad (82a)$$

$$\vec{\nabla} \times \vec{H}(\vec{r}, t) = \sigma \vec{E}(\vec{r}, t) + \epsilon \frac{\partial \vec{E}(\vec{r}, t)}{\partial t} , \quad (82b)$$

from which we obtain the relation

$$\mu \epsilon \frac{\partial^2 \vec{E}(\vec{r}, t)}{\partial t^2} + \sigma \mu \frac{\partial \vec{E}(\vec{r}, t)}{\partial t} + \vec{\nabla}_r \times \vec{\nabla}_r \times \vec{E}(\vec{r}, t) = 0 . \quad (83)$$

Since we have the same boundary conditions for $\vec{E}(\vec{r}, t)$ to satisfy, we can expand it in the same complete orthogonal set of electric eigenvectors given in equations (54) and (55). Equation (83), then, is equivalent to

$$\begin{aligned} & \sum_{n=1}^{\infty} \sum_{p=1}^{\infty} \sum_{m=0}^n \sum_{j=1}^2 \left[\mu \epsilon \iiint d\tau(\vec{r}') \frac{\partial^2 \vec{E}(\vec{r}', t)}{\partial t^2} \right. \\ & \cdot \left\{ \frac{\vec{E}_{npm}^{(j,e)}(\vec{r}') \cdot \vec{E}_{npm}^{(j,e)}(\vec{r})}{[\Omega_{npm}^{(j,e)}]^2} + \frac{\vec{E}_{npm}^{(j,o)}(\vec{r}') \cdot \vec{E}_{npm}^{(j,o)}(\vec{r})}{[\Omega_{npm}^{(j,o)}]^2} \right\} + \sigma \mu \iiint d\tau(\vec{r}') \frac{\partial \vec{E}(\vec{r}', t)}{\partial t} \\ & \cdot \left\{ \frac{\vec{E}_{npm}^{(j,e)}(\vec{r}') \cdot \vec{E}_{npm}^{(j,e)}(\vec{r})}{[\Omega_{npm}^{(j,e)}]^2} + \frac{\vec{E}_{npm}^{(j,o)}(\vec{r}') \cdot \vec{E}_{npm}^{(j,o)}(\vec{r})}{[\Omega_{npm}^{(j,o)}]^2} \right\} + \iiint d\tau(\vec{r}') \vec{E}(\vec{r}', t) \\ & \cdot \frac{\vec{E}_{npm}^{(j,e)}(\vec{r}') \cdot \vec{\nabla}_r \times \vec{\nabla}_r \times \vec{E}_{npm}^{(j,e)}(\vec{r})}{[\Omega_{npm}^{(j,e)}]^2} + \frac{\vec{E}_{npm}^{(j,o)}(\vec{r}') \cdot \vec{\nabla}_r \times \vec{\nabla}_r \times \vec{E}_{npm}^{(j,o)}(\vec{r})}{[\Omega_{npm}^{(j,o)}]^2} = 0 . \end{aligned}$$

If we dot through with, say, $\vec{E}_{n,p,m}^{(j,e)}(\vec{r})$ and integrate with respect to \vec{r} over the cavity, this reduces to

$$\begin{aligned} & \mu \epsilon \frac{\partial^2}{\partial t^2} \iiint d\tau(\vec{r}) \vec{E}(\vec{r}, t) \cdot \vec{E}_{npm}^{(j,e)}(\vec{r}) \\ & + \sigma \mu \frac{\partial}{\partial t} \iiint d\tau(\vec{r}) \vec{E}(\vec{r}, t) \cdot \vec{E}_{npm}^{(j,e)}(\vec{r}) \\ & - [\gamma_{o,np}^{(j)}]^2 \iiint d\tau(\vec{r}) \vec{E}(\vec{r}, t) \cdot \vec{E}_{npm}^{(j,e)}(\vec{r}) = 0 , \end{aligned} \quad (84)$$

where γ_o is the zero-conductivity value.

Assuming time dependence of the form $e^{j\omega t}$, where

$$\omega = \omega_1 + j\omega_2, \quad (85)$$

we can solve for the real and imaginary parts of the frequency. Equation (84) then becomes

$$\mu\epsilon\omega^2 - j\sigma\mu\omega + [\gamma_{o,np}^{(j)}]^2 = 0, \quad (86)$$

where

$$\gamma_{o,np}^{(j)} = j\omega_{o,np}\sqrt{\mu\epsilon}, \quad (87)$$

and $\omega_{o,np}$ is the eigenfrequency for $\sigma = 0$:

$$\omega_{np} = \omega_{o,np} \sqrt{1 - \left(\frac{\sigma}{2\omega_{o,np}\epsilon}\right)^2} + j \frac{\sigma}{2\epsilon}. \quad (88)$$

Adopting the conventional notation for the quality factor Q of the system, we define for the complex eigenfrequency, when $\sigma \neq 0$:

$$Q_{diel,np} \equiv \frac{\omega_{o,np}\epsilon}{\sigma}. \quad (89)$$

Then we rewrite the eigenfrequency for a simple lossy dielectric filling the cavity as

$$\omega_{np} = \omega_{o,np} \sqrt{1 - \frac{1}{(2Q_{diel,np})^2}} + j \frac{\omega_{o,np}}{2Q_{diel,np}}. \quad (90)$$

The imaginary part of the eigenfrequencies introduces a constant uniform damping factor over the entire cavity volume, namely $\exp(-\sigma t/2\epsilon)$, independent of frequency. This same damping is applied to every vector eigenmode. As the conductivity of the dielectric increases from zero we note that not only does the damping factor become stronger, but the frequency of oscillation decreases for each eigenmode until it eventually becomes zero at $\sigma = 2\epsilon\omega_{o,np}$ for the n , path mode.

The trajectory can be quite readily established for the eigenvalues ω_{np} in the complex plane as the conductivity increases from zero. Multiply equation (90) by $j/\omega_{o,np}$ to get

$$j\left(\frac{\omega_{n,p}}{\omega_{o,np}}\right) = j \sqrt{1 - \frac{1}{(2Q_{diel,np})^2}} - \frac{1}{2Q_{diel,np}}. \quad (91)$$

Define

$$x_{np} \equiv \frac{\omega_{o,np}}{2Q_{diel,np}} = \frac{\sigma}{2\epsilon} ,$$

and we can write equation (91) as

$$j\left(\frac{\omega_{np}}{\omega_{o,np}}\right) = j\sqrt{1 - \left(\frac{x_{np}}{\omega_{o,np}}\right)^2} - \left(\frac{x_{np}}{\omega_{o,np}}\right) ,$$

which we can rearrange to

$$j\left[\left(\frac{\omega_{np}}{\omega_{o,np}}\right) - j\left(\frac{x_{np}}{\omega_{o,np}}\right)\right] = j\sqrt{1 - \left(\frac{x_{np}}{\omega_{o,np}}\right)^2} . \quad (92)$$

From this relation we conclude that each eigenfrequency starts out on the positive imaginary axis at zero conductivity. As the conductivity increases, each eigenfrequency moves along a quadrant of its own circle in the complex plane with its center at the origin. At $\sigma = 2\epsilon\omega_{o,np}$, the eigenvalue reaches the negative real axis and all oscillatory temporal behavior ceases. All fields at this value of σ merely damp out exponentially with time.

Thus far we have considered only the effect of a simple lossy dielectric on the cavity modes. In a subsequent report we shall extend the discussion to include the more realistic case of finite conductivity for the boundary walls.

We now proceed to a detailed look into the method used to find the eigenvalues explicitly.

3. ANALYTIC AND NUMERICAL DETERMINATION OF THE EIGENVALUES

3.1 General Range of the Eigenvalues

We shall now present detailed analyses of the methods used to determine the numerical values of the eigenvalues $\gamma_{np}^{(j)}$ for a nonlossy dielectric within the cavity. The effect of a lossy dielectric has already been discussed. The analyses to be presented are quite tedious. Nevertheless, it is significant to discuss this in some depth, if only to put proper perspective on why the concentric spherical cavity problem has only now been resolved in detail. In our investigation of the eigenvalue problem, we evaluated all those γ 's such that $\gamma_{np}^{(j)} \leq 20$ for $n = 1$ through 4 in the TE case ($j = 1$) and for $n = 1$ through 5 in the TM case ($j = 2$). For the nonlossy dielectric the physically acceptable solutions for the eigenvalues lie along the positive imaginary axis in the complex γ plane. This will become evident as we proceed through the following discussions. The eigenvalues are determined as functions of R , i.e., the ratio of inner to outer radius.

3.2 The TE Eigenvalues $\gamma_{np}^{(1)}$

It is simpler to begin with the analysis for the determination of the TE eigenvalues. We indicated earlier that for $j = 1$ we need to find the roots for the functional relation in equation (75), which we repeat here:

$$i_n(\gamma a)k_n(\gamma b) - i_n(\gamma b)k_n(\gamma a) = 0 .$$

For convenience, we introduce the notation

$$jx \equiv \gamma a , \quad (93a)$$

$$jy \equiv \gamma b = \gamma R a = R jx , \quad (93b)$$

and hence what we seek are the values of x for each value of n such that

$$i_n(jx)k_n(jRx) - i_n(jRx)k_n(jx) = 0 . \quad (94)$$

Note that from the properties of the modified spherical Bessel functions, equation (75) will only possess roots along the imaginary axis in complex conjugate pairs. Only those on the positive half of this axis correspond to physically acceptable solutions for our cavity modes.

3.2.1 The $\gamma_{1p}^{(1)}(R)$

For $n = 1$ the explicit modified spherical Bessel functions are, for real x ,

$$i_1(jx) = \frac{\sinh(jx)}{(jx)^2} + \frac{\cosh(jx)}{jx} = j \left(\frac{\sin x}{x^2} - \frac{\cos x}{x} \right) , \quad (95)$$

$$k_1(jx) = e^{-jx} \left(\frac{1}{(jx)^2} + \frac{1}{(jx)} \right) = - \left(\frac{\cos x}{x^2} + \frac{\sin x}{x} \right) + j \left(\frac{\sin x}{x^2} - \frac{\cos x}{x} \right) . \quad (96)$$

Substituting these forms into equation (94) for $n = 1$ gives

$$j \left\{ \left(\frac{\cos x}{x^2} + \frac{\sin x}{x} \right) \left(\frac{\sin y}{y^2} - \frac{\cos y}{y} \right) - \left(\frac{\sin x}{x^2} - \frac{\cos x}{x} \right) \left(\frac{\cos y}{y^2} + \frac{\sin y}{y} \right) \right\} = 0 .$$

Note that the real part of the expression is identically zero. After some algebra, we can rearrange this to

$$\left(\frac{1}{xy} + \frac{1}{x^2 y^2} \right) \sin(x - y) - \left(\frac{1}{xy^2} - \frac{1}{x^2 y} \right) \cos(x - y) = 0 ,$$

or even more conveniently to

$$\tan[(1 - R)x] = (1 - R)x/[1 + Rx^2] \equiv f_1(R; x) . \quad (97)$$

It should be clear that our problem of determining the eigenvalues here reduces to finding the intersections, for given R , of the rational fraction $f_1(R;x)$ with the tangent function. We shall see that this will indeed be the case for all orders n . The intersections can be uniquely ordered in increasing value, i.e., $x_{1,1}^{(1)}(R)$, $x_{1,2}^{(1)}(R)$, $x_{1,3}^{(1)}(R)$,

We further observe that since

$$f_1'(R;x) = (1 - R)(1 - Rx^2)/(1 + Rx^2)^2, \quad (98a)$$

$$f_1'(R;0) = (1 - R), \quad (98b)$$

we have both the tangent function and its derivative, respectively, coincident with f_1 and its derivative at the origin. We further note that f_1 is never negative and, furthermore, goes to zero asymptotically with $x \rightarrow \infty$. The only zero of f_1 occurs at

$$x_0 = 1/\sqrt{R}. \quad (99a)$$

Since f_1 starts at the origin, goes positive, and ultimately goes to zero as $x \rightarrow \infty$, equation (99a) locates the one and only maximum for f_1 , where we have actually

$$f_1(R;x_0) = 1/2 \left(\frac{1}{\sqrt{R}} - \sqrt{R} \right) = 1/2 \frac{(1 - R)}{\sqrt{R}}. \quad (99b)$$

Also, we readily find for $R_2 > R_1$,

$$1/\sqrt{R_1} > 1/\sqrt{R_2}, \quad (100a)$$

$$\frac{f_1(R_1;x)}{f_1(R_2;x)} = \frac{(1 - R_1)}{(1 - R_2)} \frac{(1 + R_2x^2)}{(1 + R_1x^2)} > 1,$$

because $1 - R_2 < 1 - R_1$ and $1 + R_2x^2 > 1 + R_1x^2$. Thus, we see that as a function of R for fixed x we have

$$f_1(R_1;x) > f_1(R_2;x) > f_1(R_3;x) > \dots \text{ for } R_1 < R_2 < R_3, \quad (100b)$$

and the maximum value occurs earlier for the larger value of R . We illustrate this in figure 2. Note $(1 - R)$ is the initial slope at the origin. We now know all the essentials of the characteristics of the family of functions $f_1(R;x)$. Let us examine the family $\tan(1 - R)x$ in some detail. For a given R this function has singularities at

$$x_m(R) = (2m - 1) \frac{\pi}{2} \frac{1}{(1 - R)} \quad \text{for } m = 1, 2, \dots, \quad (101a)$$

and zeros at

$$x_q(R) = q\pi/(1 - R) \quad \text{for } q = 0, 1, 2, \dots. \quad (101b)$$

Since

$$\frac{1}{1 - R_1} < \frac{1}{1 - R_2} \quad \text{for } R_2 > R_1,$$

we find as usual that as R increases the singularities and poles move out along the x -axis. This behavior is illustrated in figure 3 for $x \geq 0$. Now we are familiar with the one-parameter family $\tan(1 - R)x$. The slope of $\tan(1 - R)x$ is $(1 - R) > 0$ at $x = 0$ and increases with x to become infinite as

$$x \rightarrow \frac{\pi}{2(1 - R)}.$$

On the other hand, $f_1' = 1 - R$ at $x = 0$ and decreases as x increases to become zero at $x_0 = 1/\sqrt{R}$. But to order x^3

$$\tan(1 - R)x \approx (1 - R)x + (1 - R)^3 \frac{x^3}{3}$$

$$f_1(R; x) \approx (1 - R)x - R(1 - R)x^3.$$

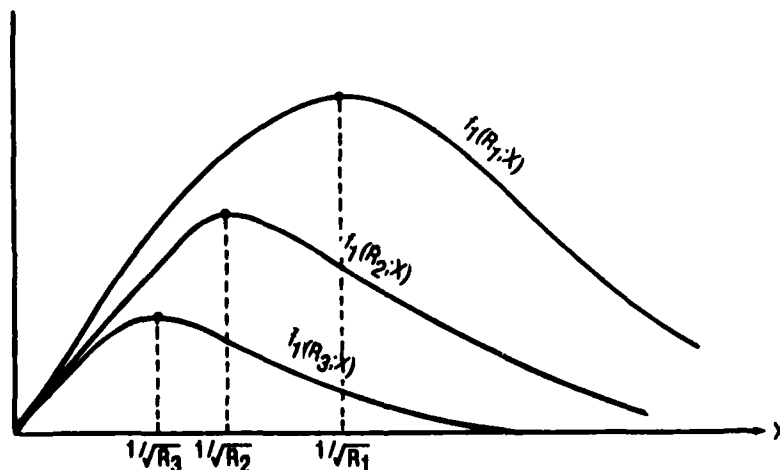


Figure 2. Rational fraction function $f_1(R; x)$ used to find $n = 1$ TE eigenvalues for values of ratio of inner to outer sphere radii $R_1 < R_2 < R_3$.

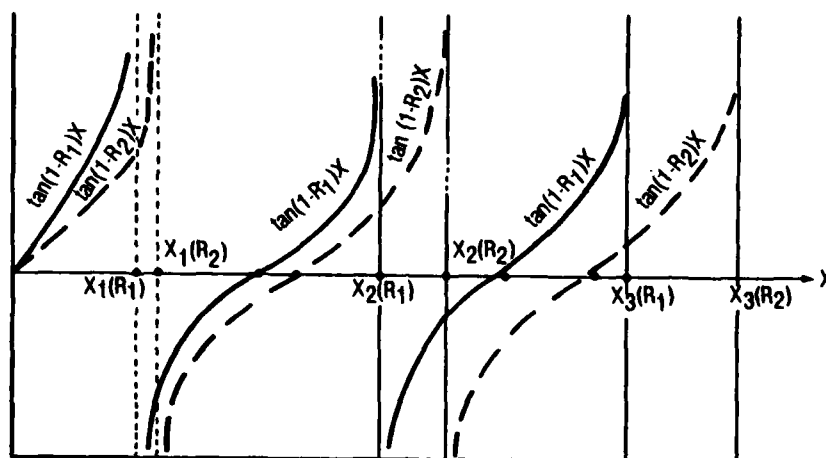


Figure 3. Family of $\tan(1 - R)x$ for $R_1 < R_2$.

Hence, for x just greater than zero, $f_1(R;x)$ lies below the $\tan(1 - R)x$ function. This is the relative position of the two functions as x increases out to the first singularity of the tangent function. Thus, we conclude that there will be no intersection of $\tan(1 - R)x$ and $f_1(R;x)$ for $x < \pi/2(1 - R)$; i.e., before the tangent attains its first singularity. Furthermore, the tangent function returns from $-\infty$ at

$$x = \frac{\pi}{2(1 - R)}$$

and remains negative as x increases until $x = \pi/(1 - R)$. The first crossing of $f_1(R;x)$ with the tangent then occurs at $x > \pi/(1 - R)$. Actually, $x_{11}^{(1)}(R)$ will occur between $x = \pi/(1 - R)$ and $x = 3\pi/2(1 - R)$, where the tangent is increasing with x from zero to $+\infty$. All further crossings will occur on the arcs of the tangent function where it is positive; i.e., $x_{1p}^{(1)}(R)$ will lie in the range $p\pi/(1 - R) < x < (2p + 1)\pi/2(1 - R)$ for $p = 1, 2, \dots$. For a given ratio R as p increases, the crossings are approximately periodic with the period of the tangent function. The larger the values of p , the closer this periodicity becomes. Since the tangent function essentially spreads out with higher values of R , the successive crossings occur at larger intervals. We have already noted that $f_1(R;x)$ flattens out as R increases. Then we conclude that the crossings will occur closer and closer to the zeros of the tangent

function with increasing R , which we have already noted are periodic in x with increasing period as R increases. The details of the behavior of the $x_{1p}^{(1)}(R)$ are rather nicely depicted in figures 4 through 12, which show the two functions for x out to 20 and for $0.1 \leq R \leq 0.9$ in steps of 0.1. Note that, for $R = 0.9$, $x_{11}^{(1)}(0.9)$ occurs beyond

$$x = \frac{\pi}{1 - R} = 10\pi > 20 ,$$

and also the tangent attains its first singular value at

$$x = \frac{\pi}{2(1 - R)} = 5\pi = 15.7080$$

(see fig. 12), which is the only singularity or zero in the range of x to which we have restricted our interest.

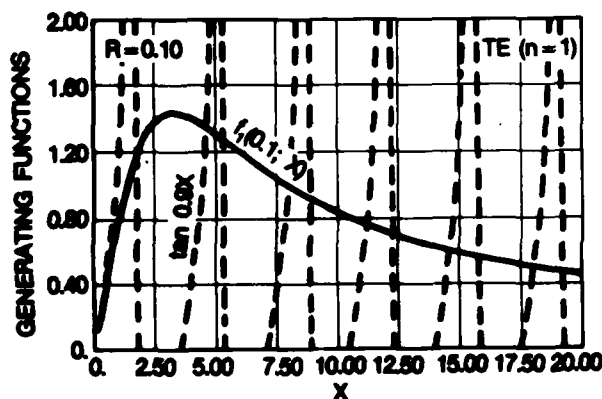


Figure 4. Generating functions for $\gamma_{1,p}^{(1)}$ with $R = 0.10$.

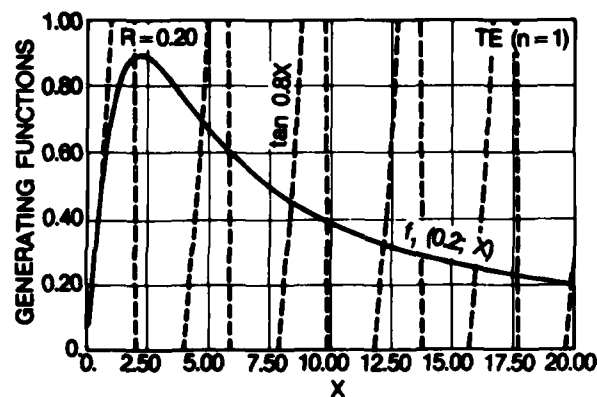


Figure 5. Generating functions for $\gamma_{1,p}^{(1)}$ with $R = 0.20$.

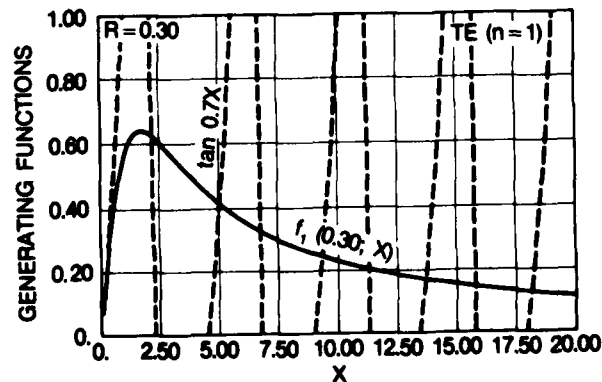


Figure 6. Generating functions for $\gamma_{1,p}^{(1)}$ with $R = 0.30$.

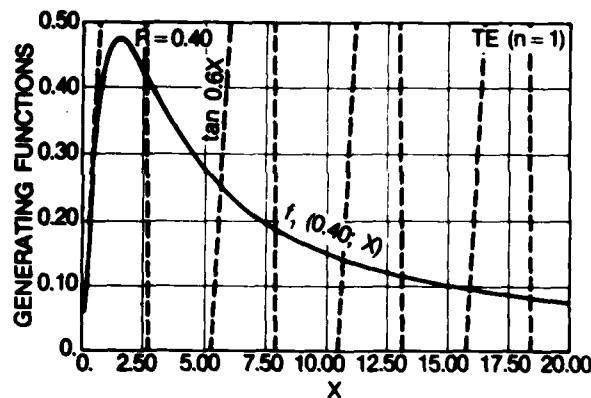


Figure 7. Generating functions for $Y_{1,p}^{(1)}$ with $R = 0.40$.

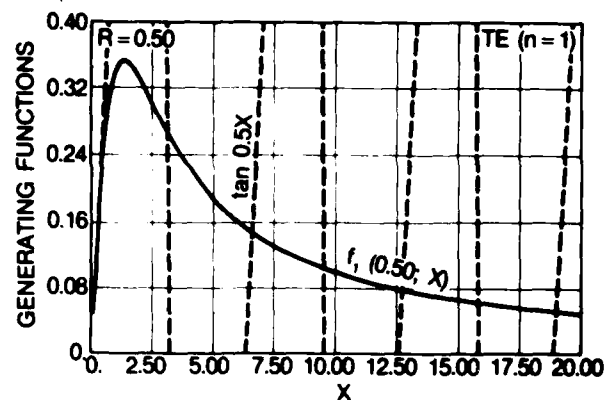


Figure 8. Generating functions for $Y_{1,p}^{(1)}$ with $R = 0.50$.

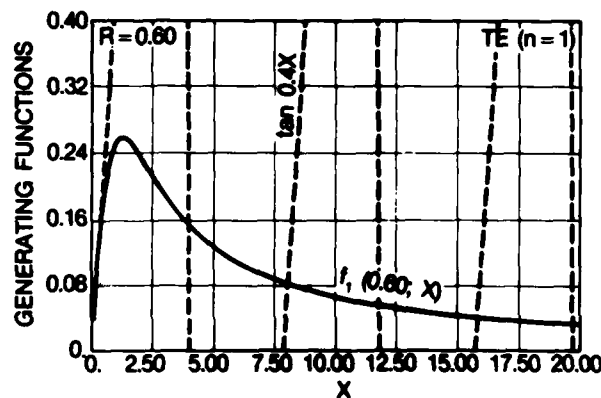


Figure 9. Generating functions for $Y_{1,p}^{(1)}$ with $R = 0.60$.

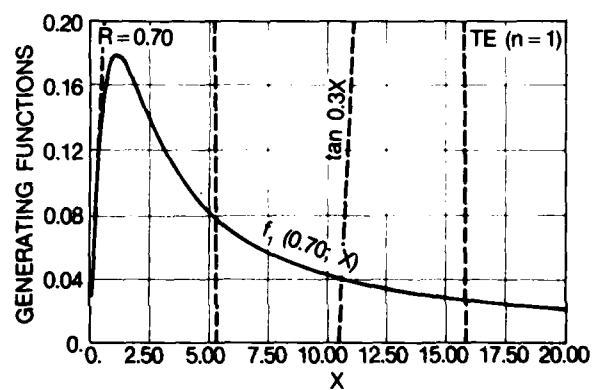


Figure 10. Generating functions for $Y_{1,p}^{(1)}$ with $R = 0.70$.

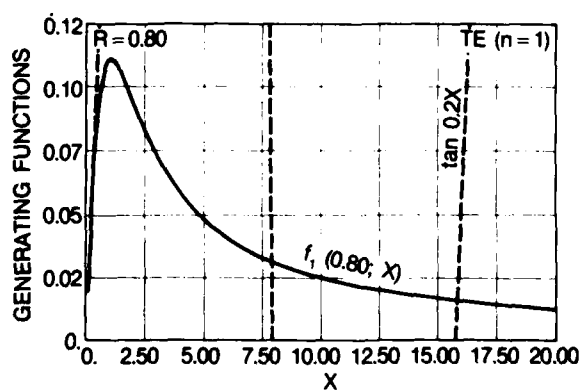


Figure 11. Generating functions for $Y_{1,p}^{(1)}$ with $R = 0.80$.

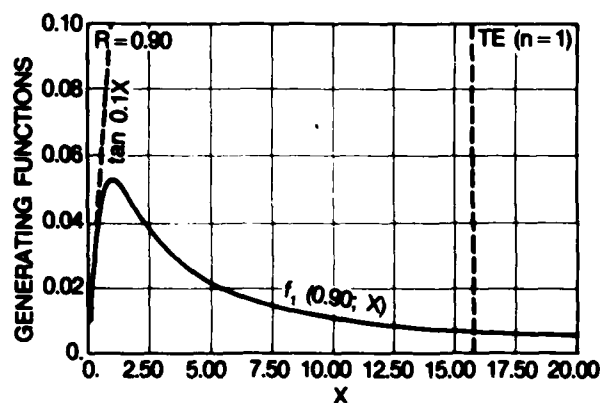


Figure 12. Generating functions for $Y_{1,p}^{(1)}$ with $R = 0.90$.

3.2.2 The $\gamma_{2p}^{(1)}(R)$

The modified spherical Bessel functions for $n = 2$ are

$$i_2(jx) \equiv \left[\frac{3}{(jx)^3} + \frac{1}{jx} \right] \sinh(jx) - \frac{3 \cosh(jx)}{(jx)^2} = \left[3 \frac{\cos x}{x^2} - \frac{3}{x^3} - \frac{1}{x} \sin x \right] , \quad (102)$$

$$k_2(jx) \equiv e^{-jx} \left[\frac{3}{(jx)^3} + \frac{3}{(jx)^2} + \frac{1}{jx} \right] = \left[\left(\frac{3}{x^3} - \frac{1}{x} \right) \sin x - \frac{3 \cos x}{x^2} \right] \\ + j \left[\frac{3 \sin x}{x^2} + \left(\frac{3}{x^3} - \frac{1}{x} \right) \cos x \right] , \quad (103)$$

which give for $n = 2$ in place of equation (94), upon substitution and simplification,

$$0 = j \left\{ \left[\frac{3 \cos x}{x^2} - \left(\frac{3}{x^3} - \frac{1}{x} \right) \sin x \right] \left[\frac{3}{y^2} \sin y + \left(\frac{3}{y^3} - \frac{1}{y} \right) \cos y \right] \right. \\ \left. - \left[\frac{3 \cos y}{y^2} - \left(\frac{3}{y^3} - \frac{1}{y} \right) \sin y \right] \left[\frac{3}{x^2} \sin x + \left(\frac{3}{x^2} - \frac{1}{x} \right) \cos x \right] \right\} . \quad (103a)$$

We note again that the real part of the expression is identically zero. With some algebraic exercising, this relation can be put in the form

$$\left[\left(\frac{3}{x^3} - \frac{1}{x} \right) \left(\frac{3}{y^3} - \frac{1}{y} \right) + \frac{9}{x^2 y^2} \right] \sin(x - y) \\ - \left[\frac{3}{x^2} \left(\frac{3}{y^3} - \frac{1}{y} \right) - \frac{3}{y^2} \left(\frac{3}{x^3} - \frac{1}{x} \right) \right] \cos(x - y) = 0 , \quad (103b)$$

or, in turn, into the more convenient form

$$\tan[(1 - R)x] = \frac{(1 - R)x \left(1 + \frac{R}{3} x^2 \right)}{1 - (R^2 - 3R + 1) \frac{x^2}{3} + \frac{R^2 x^4}{9}} \equiv f_2(R; x) . \quad (104)$$

Again, as for the previous case for $n = 1$, we have reduced our eigenvalue problem to determining the values of $x_{2p}^{(1)}(R)$, which now correspond to the intersections of the tangent function on the left-hand side of equation (104) with the rational fraction function $f_2(R; x)$. Consider the denominator of $f_2(R; x)$. We immediately see that

(a) For $R > R_0 = (3 - \sqrt{5})/2 = 0.381,966$, the denominator is positive for $x \geq 0$. In turn, $f_2(R;x)$ will be non-negative; starting at zero at the origin, it will at first increase with x . As $x \rightarrow \infty$, $f_2 \rightarrow 0$ asymptotically.

(b) For $R = R_0$ the denominator has a double real root at

$$x(R_0) = x_0 = \sqrt{3/R_0} = 2.802,517 \quad . \quad (105)$$

It then follows that $f_2(R_0;x)$ is non-negative starting at zero at $x = 0$, becomes infinite at x_0 , and also goes to zero asymptotically as $x \rightarrow \infty$.

(c) For $R < R_0$, the denominator has two distinct real positive roots at

$$x_-(R) = \sqrt{3(R^2 - 3R + 1)/2R^2} \left\{ 1 - \sqrt{1 - [2R/(R^2 - 3R + 1)]^2} \right\}^{1/2} \quad , \quad (106a)$$

$$x_+(R) = \sqrt{3(R^2 - 3R + 1)/2R^2} \left\{ 1 + \sqrt{1 - [2R/(R^2 - 3R + 1)]^2} \right\}^{1/2} \quad , \quad (106b)$$

where we should note that $x_-(R) < x_0 < x_+(R)$ and that as $R \rightarrow R_0$

$$x_+(R) - x_-(R) = 2 \sqrt{3(R^2 - 3R + 1)/2R^2} \sqrt{1 - [2R/(R^2 - 3R + 1)]^2} \rightarrow 0 \quad (107)$$

because the right-most factor vanishes in this limit. The function $f_2(R;x)$ starts out as zero at $x = 0$, becomes positive, and increases as x increases at first. $f_2 \rightarrow \infty$ as $x \rightarrow x_-$. It is negative between x_- and x_+ . As x increases from x_- , f_2 returns from $-\infty$, then again goes to $-\infty$ as $x \rightarrow x_+$. For $x > x_+$, f_2 returns from $+\infty$ to eventually go asymptotically to zero as $x \rightarrow \infty$. For $x > x_+$, $f_2 > 0$.

One further consideration is the case for $R \ll 1$. Here we find $x_- \approx \sqrt{3}$ and $x_+ \approx \sqrt{3}/R \gg 1$.

We have thus located all the zeros and singularities of $f_2(R;x)$. Additional information can be obtained from $f_2'(R;x)$, which is

$$\frac{1}{1-R} f_2'(R;x) = \frac{\{1 + (R^2 + 1)(x^2/3) - R(R^2 + 1)(x^2/3)^2 - R^3(x^2/3)^3\}}{\{1 - (R^2 - 3R + 1)(x^2/3) + R^2(x^2/3)^2\}^2} \quad . \quad (108)$$

Note that the denominator is never negative. For case (a), the denominator has no real roots. Upon simple test, the numerator which is a cubic in x^2 reveals that it can have at most one real positive root for x^2 . Since the function f_2 initially has a positive slope near $x = 0$ and a negative slope for large x , we conclude that there is one and only one real positive root for

$f_2(R;x)$ in case (a). Thus, for case (a), i.e., $R > R_0$, we see that $f_2(R;x)$ behaves essentially like $f_1(R;x)$, which we examined earlier. Now in case (b), the denominator of f_2 has a double root at $x = \sqrt{3/R_0}$. Consider then the numerator in equation (108). It also has only a single root which occurs at $x = \sqrt{3/R_0}$, and hence we can write

$$\begin{aligned} \frac{1}{1 - R_0} f_2'(R_0; x) &= \frac{\left\{ 1 + (R_0^2 + 1) \left(\frac{x^2}{3} \right) - R_0 (R_0^2 + 1) \left(\frac{x^2}{3} \right)^2 - R_0^3 \left(\frac{x^2}{3} \right)^3 \right\}}{\left[\frac{x^2}{3} - \frac{1}{R_0} \right]^4 (R_0)^4} \\ &= -R_0 \times \frac{\left(\frac{x^2}{3} - \frac{1}{R_0} \right) \left\{ \left(\frac{x^2}{3} \right)^2 + \left(\frac{R_0^2 + R_0 + 1}{R_0^2} \right) \left(\frac{x^2}{3} \right) + \frac{1}{R_0^2} \right\}}{\left(\frac{x^2}{3} - \frac{1}{R_0} \right) \left[\frac{x^2}{3} - \frac{1}{R_0} \right]^3} . \end{aligned}$$

We see that $f_2'(R_0; x)$ is singular at $x = \sqrt{3/R_0}$. Also for $x < x_0$, $f_2'(R_0; x) > 0$ and for $x > x_0$, $f_2'(R_0; x) < 0$. Since $f_2'(R_0; x)$ has no zeros for $x \neq x_0$, it is monotonic on either side of x_0 . Next we must give further effort to examine f_2' for case (c), where $R < R_0$. Again the numerator in equation (108) has at most a single real positive root. This must occur somewhere in the range $x_- \leq x < x_+$, where f_2' has to change from positive to negative to permit f_2 to behave properly there. In figure 13 we illustrate $f_2(R; x)$ for $R < R_0$.

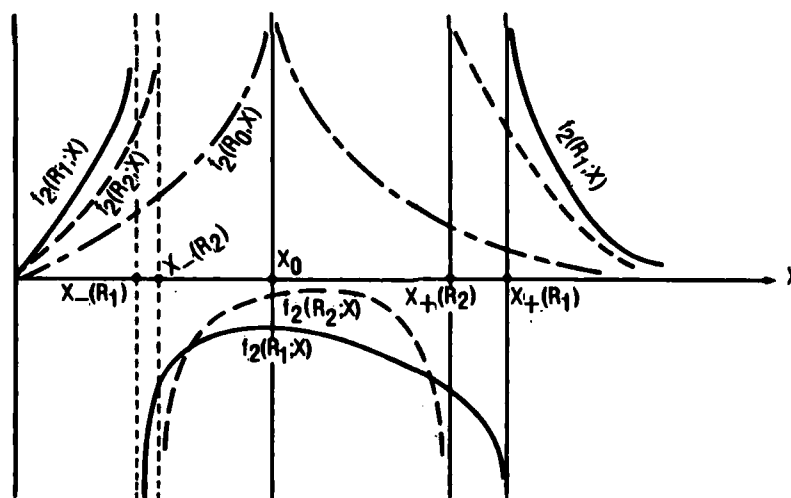


Figure 13. Rational fraction function $f_2(R_0; x)$ for $R_1 < R_2 < R_0$.

Next we consider the crossings of $f_2(R;x)$ and $\tan(1-R)x$. In the neighborhood of the origin, the terms to order x^5 of the series expansions of these functions are given by

$$f_2(R;x) \approx (1-R)x + (1-R)^3 \frac{x^3}{3} + 5\{(1-R)^5 - R(1-R)[R^2 + (1-R)]\} \frac{x^5}{45},$$

and

$$\tan(1-R)x \approx (1-R)x + (1-R)^3 \frac{x^3}{3} + \frac{6}{45} (1-R)^5 x^5.$$

Subtracting coefficients of the x^5 terms, we find for $R < 1$ that the difference is

$$\begin{aligned} & \frac{6}{45} (1-R)^5 - \frac{5}{45} \{(1-R)^5 - R(1-R)[R^2 + (1-R)]\} \\ &= \frac{(1-R)^5}{45} + \frac{1}{9} R(1-R)[R^2 + (1-R)] > 0. \end{aligned}$$

We conclude then that f_2 lies below the tangent function in the neighborhood of $x = 0$. For case (a), $R > R_0$, the story is essentially that for the TE, $n = 1$ case. In case (b), where $R = R_0$ we have

$$f_2(R_0;x) = (1-R_0)x \left(1 + \frac{R_0}{3} x^2\right) / \left(1 - \frac{R_0}{3} x^2\right)^2.$$

The first singularity of the tangent is at $x = \pi/2(1-R_0) = 2.541,602$, which occurs before $x_0(R_0) = 2.802,517$. The tangent, after x increases beyond this first singularity, is negative out to $\pi/(1-R_0) = 5.083,203$. Thereafter, it becomes positive and increases with x . Then in case (b), the first crossing occurs after $x = \pi/(1-R_0)$, where $f_2(R;x)$ is decreasing from $+\infty$ and the tangent is increasing from zero to its next singular value at $3\pi/2(1-R_0)$. This is illustrated in figure 14. The successive crossings will occur on the successive positive-going arcs of the tangent curve. The higher order ones, $x_{2p}^{(1)}(R_0)$, will occur at close to the period of the tangent curve.

Finally, we have a look at case (c), where $R < R_0$. Again, $f_2(R;x)$ and $\tan(1-R)x$ coincide and have the same derivatives at the origin. In the neighborhood of $x = 0$, we showed that $\tan(1-R)x$ sits above $f_2(R;x)$ and both functions are positive and increasing monotonically until they become singular at their respective singular points. Let us compare the series expansions of the two functions:

$$\frac{1}{1-R} \frac{d}{dx} \tan(1-R)x \approx 1 + (1-R)^2 x^2 + \frac{6}{9} (1-R)^4 x^4, \quad (109a)$$

and

$$\frac{1}{1-R} \frac{d}{dx} f_2(R;x) \approx 1 + (1-R)^2 x^2 + \frac{5}{9} \{ (1-R)^4 - R[R^2 + (1-R)] \} x^4. \quad (109b)$$

From these we observe that the tangent is increasing faster than f_2 and hence will continue to lie above f_2 until it reaches its first singular point, $\pi/2(1-R)$. It will then go negative and there will be no intersection out to $x = x_-(R)$. Over this range of x , $f_2(R;x)$ is positive and increasing until it goes to $+\infty$ at $x_-(R)$. For those values of $R \leq R_0$, such that $x_+(R) < 3\pi/2(1-R)$, there will be no intersection for $x \leq x_+(R)$. The first intersection $x_{21}^{(1)}(R)$ will occur just before $x = 3\pi/2(1-R)$, where both f_2 and $\tan(1-R)x$ are positive. Consecutive crossings $x_{2p}^{(1)}(R)$ will then occur on the positive-going arcs of the tangent curve with almost the periodicity of the tangent function itself. (Fig. 17, shown later, is a good illustration of this behavior.) For larger values of $R < R_0$, when $x_+(R)$ occurs for $x > 3\pi/2(1-R)$, the first crossing $x_{21}^{(1)}(R)$ will occur on the negative arc of the first branch of the tangent after its second singularity. Successive crossings will occur on successive negative arcs of the tangent out to $x_+(R)$, since $f_2(R;x)$ is negative between $x_-(R)$ and $x_+(R)$. Thereafter the curves will intersect on the positive-going branches of the tangent curve with nearly the periodicity of the tangent function. These intersections spread apart with increasing R , as is clearly illustrated in figures 15 and 16.

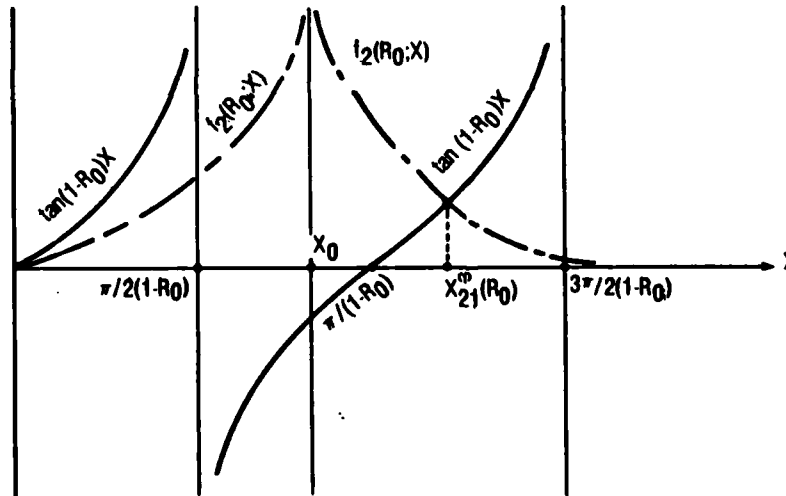


Figure 14. First crossing of $f_2(R_0;x)$ and $\tan(1-R_0)x$ at $x_{21}^{(1)}(R_0)$.

Figures 15 through 24 show the details of the $f_2(R;x)$, $\tan(1-R)x$ and the location of the eigenvalues $x_{2p}^{(1)}(R)$ for $x \leq 20$ for $R = 0.05$ and for $0.1 \leq R \leq 0.9$ in steps of 0.1. Although these illustrations only cover cases (a) and (c), the above discussions serve to round out the entire picture for determining the TE, $n = 2$, eigenvalues.

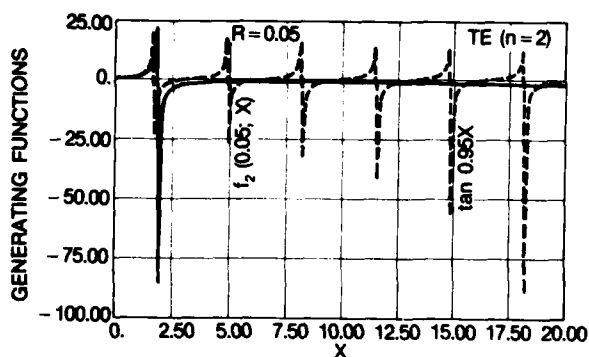


Figure 15. Generating functions for $Y_{2p}^{(1)}$ with $R = 0.05$.

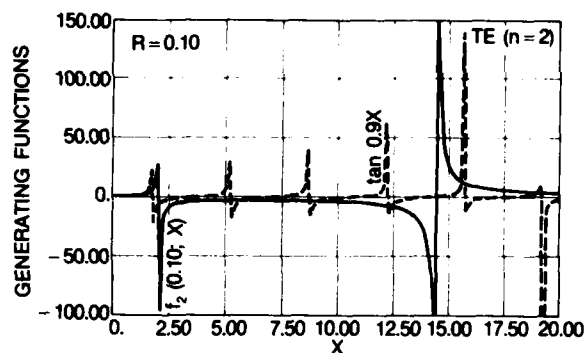


Figure 16. Generating functions for $Y_{2p}^{(2)}$ with $R = 0.10$.

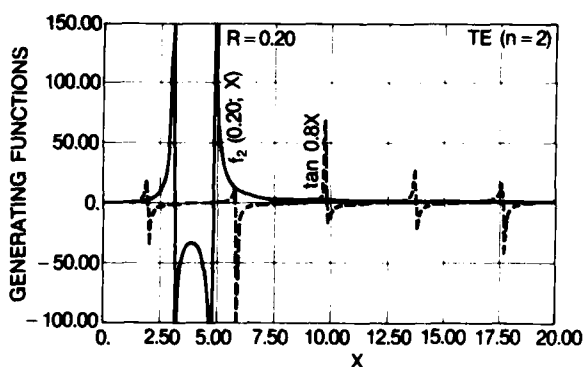


Figure 17. Generating functions for $Y_{2p}^{(1)}$ with $R = 0.20$.

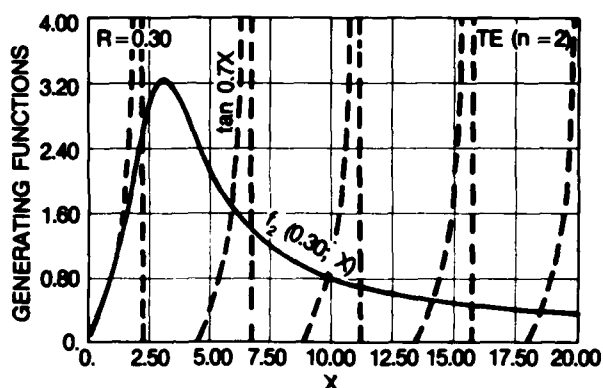


Figure 18. Generating functions for $Y_{2p}^{(1)}$ with $R = 0.30$.

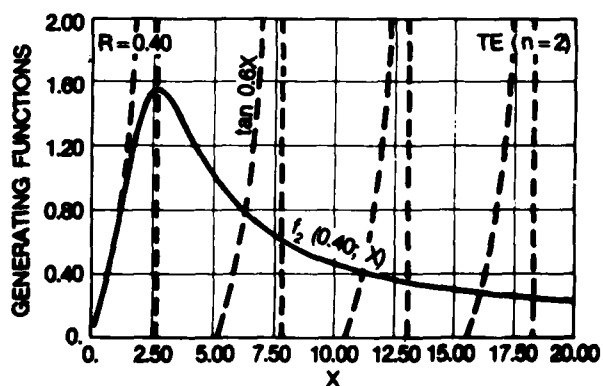


Figure 19. Generating functions for $Y_{2p}^{(1)}$ with $R = 0.40$.

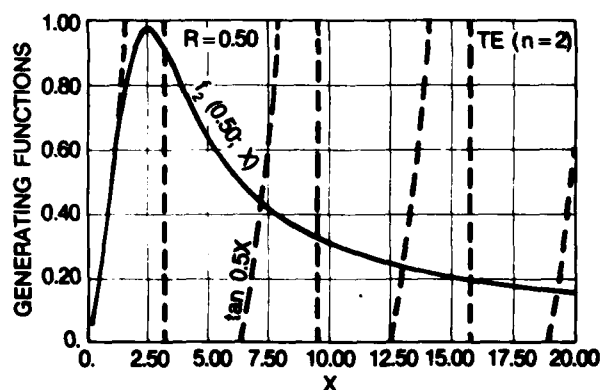


Figure 20. Generating functions for $Y_{2p}^{(1)}$ with $R = 0.50$.

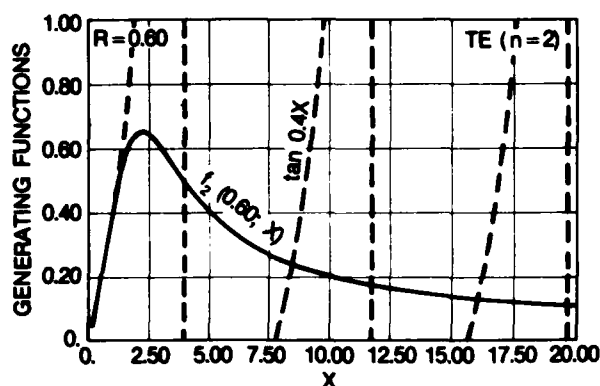


Figure 21. Generating functions for $\gamma_{2p}^{(1)}$ with $R = 0.60$.

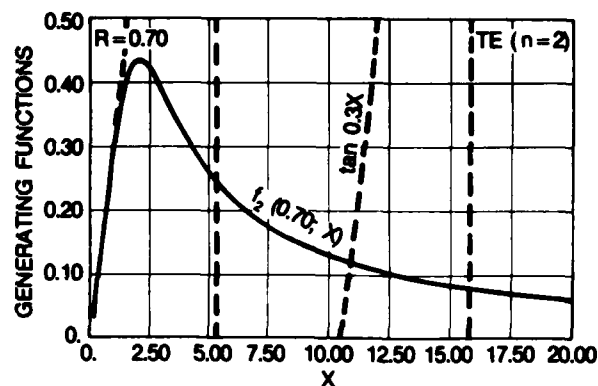


Figure 22. Generating functions for $\gamma_{2p}^{(1)}$ with $R = 0.70$.

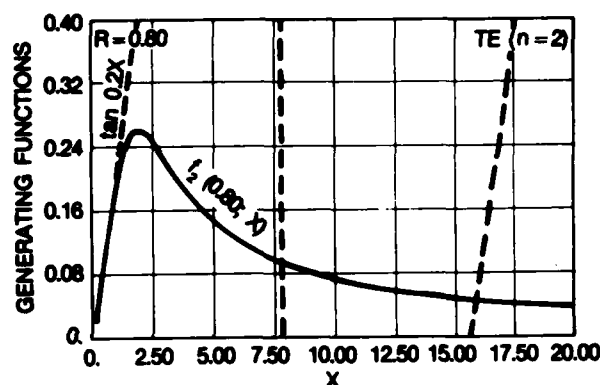


Figure 23. Generating functions for $\gamma_{2p}^{(1)}$ with $R = 0.80$.

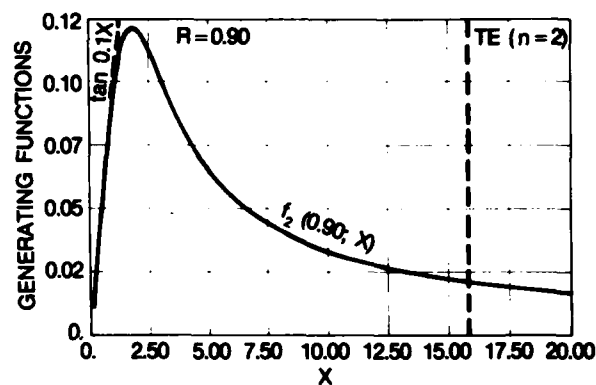


Figure 24. Generating functions for $\gamma_{2p}^{(1)}$ with $R = 0.90$.

3.2.3 The $\gamma_{3p}^{(1)}(R)$

The modified spherical Bessel functions for $n = 3$ are

$$\begin{aligned}
 i_3(jx) &= -\left[\frac{15}{(jx)^4} + \frac{6}{(jx)^2}\right] \sinh(jx) + \left[\frac{15}{(jx)^3} + \frac{1}{jx}\right] \cosh(jx) \\
 &\equiv -j \left\{ \left(\frac{15}{x^4} - \frac{6}{x^2}\right) \sin x - \left(\frac{15}{x^3} - \frac{1}{x}\right) \cos x \right\} , \\
 k_3(jx) &= e^{-jx} \left[\frac{15}{(jx)^4} + \frac{15}{(jx)^3} + \frac{6}{(jx)^2} + \frac{1}{jx} \right] = \left[\left(\frac{15}{x^4} - \frac{6}{x^2}\right) \cos x + \left(\frac{15}{x^3} - \frac{1}{x}\right) \right. \\
 &\quad \left. \times \sin x \right] - j \left[\left(\frac{15}{x^4} - \frac{6}{x^2}\right) \sin x - \left(\frac{15}{x^3} - \frac{1}{x}\right) \cos x \right] ,
 \end{aligned} \tag{110}$$

which give, upon substitution into equation (94), and some simplification,

$$0 = j \left\{ \left[\left(\frac{15}{x^4} - \frac{6}{x^2} \right) \sin x - \left(\frac{15}{x^3} - \frac{1}{x} \right) \cos x \right] \left[\left(\frac{15}{y^4} - \frac{6}{y^2} \right) \cos y + \left(\frac{15}{y^3} - \frac{1}{y} \right) \sin y \right] \right. \\ \left. - \left[\left(\frac{15}{y^4} - \frac{6}{y^2} \right) \sin y - \left(\frac{15}{y^3} - \frac{1}{y} \right) \cos y \right] \left[\left(\frac{15}{x^4} - \frac{6}{x^2} \right) \cos x + \left(\frac{15}{x^3} - \frac{1}{x} \right) \sin x \right] \right\} .$$

Again we see that the real part of the expression vanishes identically. As before, we perform some algebraic rearranging of this relation to the form

$$\left[\left(\frac{15}{x^4} - \frac{6}{x^2} \right) \left(\frac{15}{y^4} - \frac{6}{y^2} \right) + \left(\frac{15}{x^3} - \frac{1}{x} \right) \left(\frac{15}{y^3} - \frac{1}{y} \right) \right] \sin(x - y) - \left[\left(\frac{15}{x^3} - \frac{1}{x} \right) \left(\frac{15}{y^4} - \frac{6}{y^2} \right) \right. \\ \left. - \left(\frac{15}{x^4} - \frac{6}{x^2} \right) \left(\frac{15}{y^3} - \frac{1}{y} \right) \right] \cos(x - y) = 0 ,$$

or again to the preferred form,

$$\tan[(1 - R)x] = \left\{ x \left[\left(\frac{15 - x^2}{5 - 2x^2} \right) - R \left(\frac{15 - R^2 x^2}{5 - 2R^2 x^2} \right) \right] / 3 \left(1 + \frac{Rx^2}{9} \left[\frac{15 - x^2}{5 - 2x^2} \right] \left[\frac{15 - R^2 x^2}{5 - 2R^2 x^2} \right] \right) \right\} . \quad (111)$$

Once again the eigenvalue problem is reduced to determining the values $x_{3p}^{(1)}(R)$ at which intersection of the functions $\tan(1 - R)x$ and $f_3(R; x)$ occur.

We can write $f_3(R; x)$ as a ratio of two polynomials:

$$f_3(R; x) \equiv \frac{3(1 - R)x[75 - 5(1 - 5R + R^2)x^2 + 2R^2x^4]}{225 - 45(2 - 5R + 2R^2)x^2 - 3R(5 - 12R + 5R^2)x^4 + R^3x^6} . \quad (112)$$

The denominator considered as a polynomial in x^2 indicates that the maximum number of positive roots is two for x^2 . This in turn tells us that there can be at most two positive real roots, x_- and x_+ . For small values of R this is indeed the case. At these values x_{\pm} , f_3 becomes singular. Since the numerator and denominator are positive for small x and very large x , f_3 will also be positive for these ranges. Just as in the TE case where $n = 2$, as R increases, x_+ and x_- move toward one another and at some value $R = R_0$ we have a single real positive double root in the denominator. Thus, we will have a considerable amount of behavior of $n = 3$ that closely resembles that for $n = 2$. Here we have an additional characteristic, namely a numerator in equation (112) that can have at most two zeros for $x > 0$. This will somewhat

modify the $n = 2$ type of behavior. In figures 25 through 37 we illustrate the characteristics of $f_3(R;x)$, $\tan(1 - R)x$, and the intersections $x_{3p}^{(1)}(R) \leq 20$. Thus, figure 25 shows the behavior for the small value of $R = 0.05$. We can see in this illustration that $f_3(R = 0.05;x)$ has a zero $x_{-}(0.05)$ in the denominator below $x = 2$, and f_3 is very close to $\tan(1 - R)x$ all the way out to about $\pi/(1 - R)$.

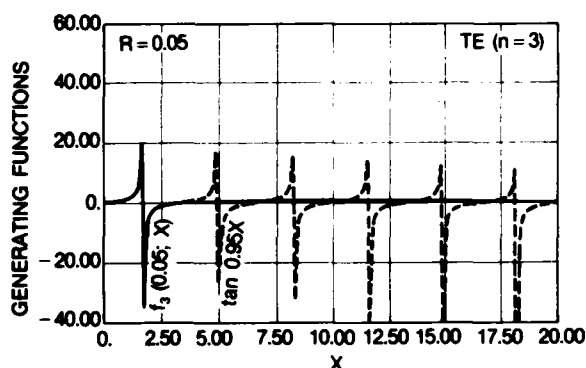


Figure 25. Generating functions for $\gamma_{3p}^{(1)}$ with $R = 0.05$.

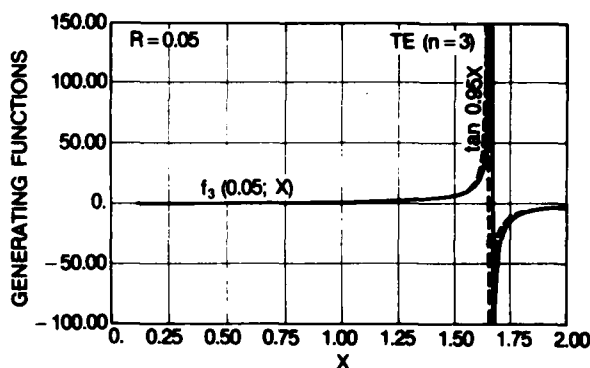


Figure 26. Enlarged view of generating functions for $\gamma_{3p}^{(1)}(0.05)$ near their first singularities.

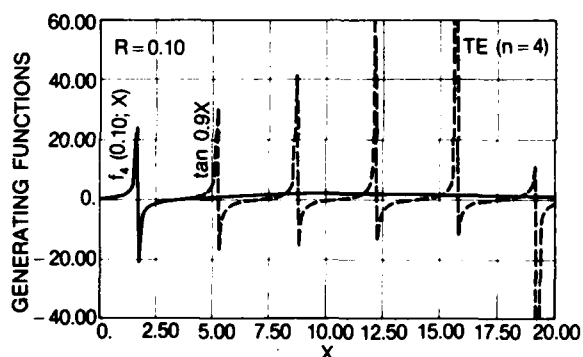


Figure 27. Generating functions for $\gamma_{3p}^{(1)}$ with $R = 0.10$.

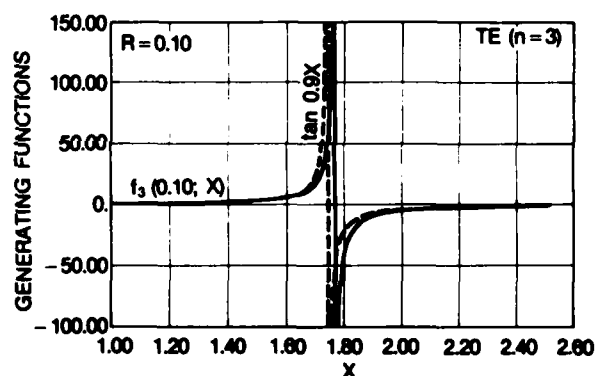


Figure 28. Enlarged view of generating functions for $\gamma_{3p}^{(1)}(0.10)$ near their first singularities.

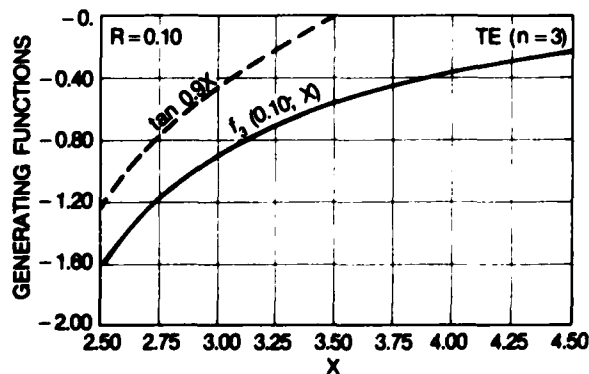


Figure 29. Enlarged view of generating functions for $\gamma_{3p}^{(1)}(0.10)$ showing no intersections just beyond first singularities.

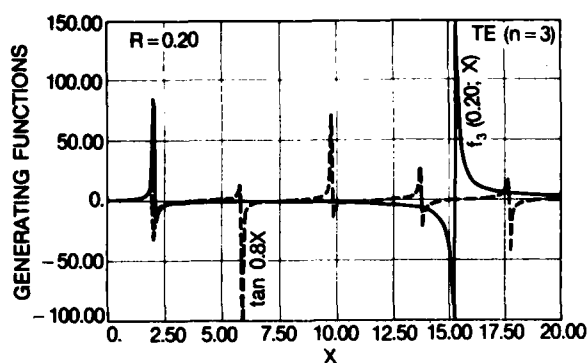


Figure 30. Generating functions for $\gamma_{3p}^{(1)}$ with $R = 0.20$.

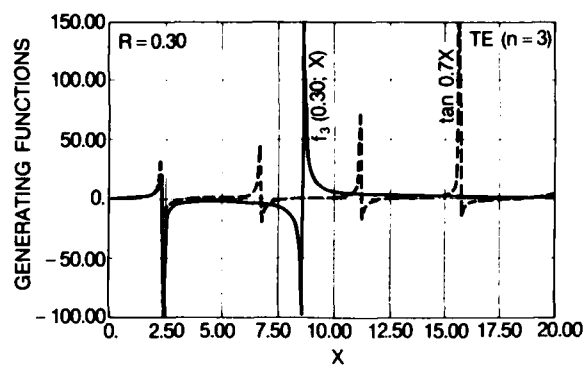


Figure 31. Generating functions for $\gamma_{3p}^{(1)}$ with $R = 0.30$.

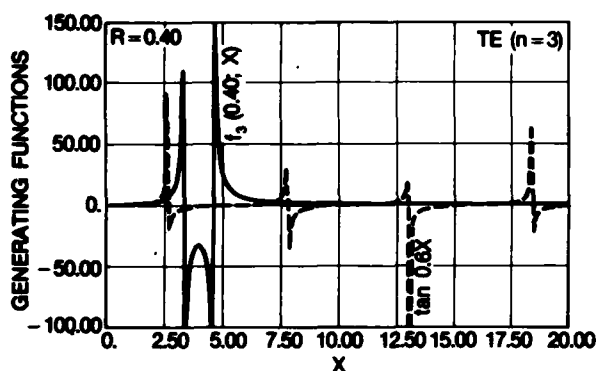


Figure 32. Generating functions for $\gamma_{3p}^{(1)}$ with $R = 0.40$.

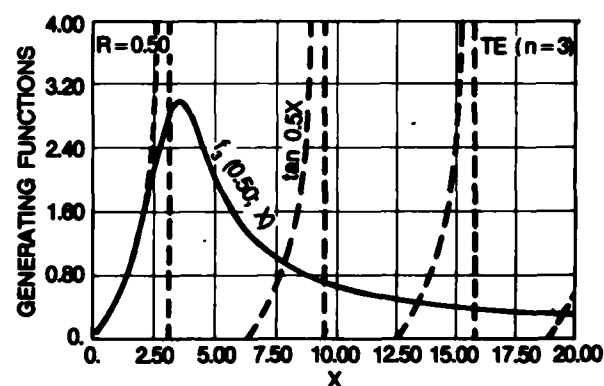


Figure 33. Generating functions for $\gamma_{3p}^{(1)}$ with $R = 0.50$.

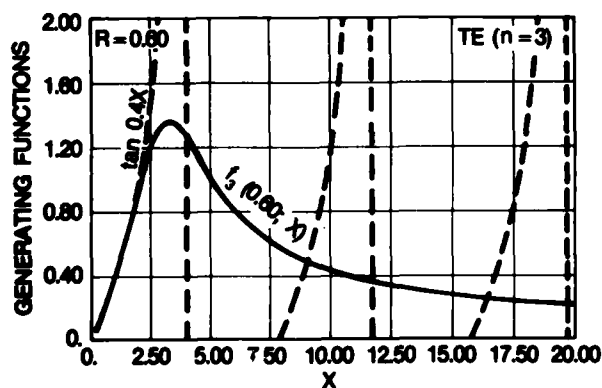


Figure 34. Generating functions for $\gamma_{3p}^{(1)}$ with $R = 0.60$.

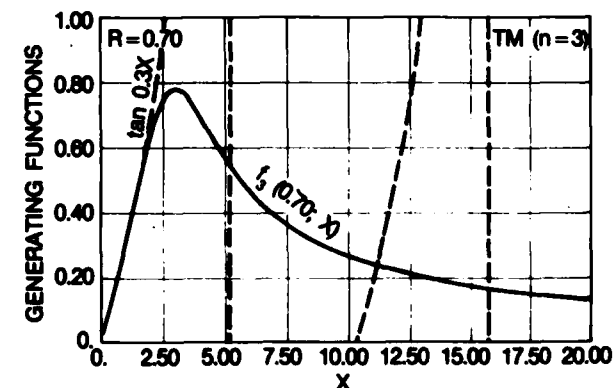


Figure 35. Generating functions for $\gamma_{3p}^{(1)}$ with $R = 0.70$.

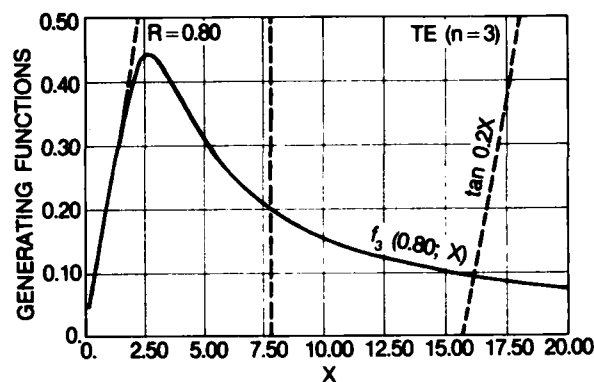


Figure 36. Generating functions for $\gamma_{3p}^{(1)}$ with $R = 0.80$.

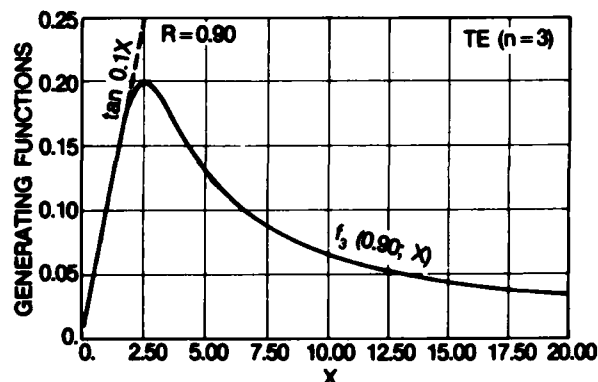


Figure 37. Generating functions for $\gamma_{3p}^{(1)}$ with $R = 0.90$.

In fact, if we expand $f_3(R; x)$ and $\tan(1 - R)x$ in a series in x about the origin, they agree exactly up to terms in x^5 . Figure 26 is an expanded look at the region $0 \leq x \leq 2.00$. We now see that $f_3(0.05; x)$ lies below $\tan 0.95x$ out to $x = \pi/2(0.95) \equiv$ the first singularity of the tangent; f_3 is positive over this range. The tangent goes singular first. Shortly thereafter, $f_3(0.05; x)$ goes singular to $+\infty$ at $x_-(0.05)$ (between 1.65 and 1.70). The two curves fail to intersect, as can be seen in figure 25, until the tangent is positive and going to ∞ beyond $2\pi/(1 - R) = 6.613$, where f_3 is also positive but decreasing. It is evident that the numerator of f_3 , and hence f_3 itself, has a root at x just below 5.0, and $f_3 > 0$ for $R = 0.05$, but is small all the way to $x = 20$. The succeeding intersections $x_{3p}^{(1)}(0.05)$ for $p = 2, 3$, and 4 occur on successive positive-going arcs of the tangent and again are almost periodic with the period of the tangent; i.e., $x_{3p+1}^{(1)}(0.05) - x_{3p}^{(1)}(0.05) \approx 3.3$. Figure 27 shows the properties for $R = 0.10$. Now we can just barely discern the two zeros in the numerator of f_3 which cause f_3 to vanish. These zeros occur at

$$x_{0-} = 6.784408 \quad , \quad \text{and} \quad x_{0+} = 9.026174 \quad .$$

Between these values of x , $f_3(0.1; x)$ is positive. As can be seen in figure 27 and the enlarged views of figures 28 and 29, the first intersection $x_{31}^{(1)}(0.1)$ does not occur until about 6.98, which is very close to $2\pi/0.9$, the third zero of the tangent in our range of x . The next three eigenvalues occur on the negative branches of the tangent just before the tangent passes through its zeros. Note in figure 28 just how close the two functions $f_3(0.1; x)$ and $\tan 0.9x$ are to each other.

As R increases further, the two zeros of the numerator move closer and eventually merge into a double root of $f_3(R; x)$. At the same time, the two roots of the denominator move toward one another. Further increasing R causes the numerator to become completely non-negative, as can be seen in figure 30 for $R = 0.20$. Between the two singularities of f_3 , the intersections occur on the negative branches of the tangent. For $R = 0.20$, we observe the first eigenvalue occurring before the tangent function crosses the horizontal axis the second time. The corresponding eigenvalue is slightly higher than that

for $R = 0.10$ since the tangent has been stretched out along x . After the second singularity in f_3 is passed, the intersections occur along the positive-going arcs of the tangent just before the tangent goes singular.

Increasing R still further causes the two singular points of $f_3(R;x)$ to move further toward each other, as can be clearly seen in figures 31 and 32. In the latter case, where $R = 0.40$, we note that the two roots of the denominator of $f_3(0.40)$ lie between the first two singularities of the tangent; hence, the first intersection occurs beyond the higher value of x where f_3 goes singular. The eigenvalues behave now in a familiar fashion.

Further increasing R eventually causes the two singularities of f_3 to merge into one. Thereafter, increasing R , as can be seen in figures 33 through 37, the singularities are gone from $f_3(R;x)$ and we again have the same characteristics that we found for $f_1(R;x)$ and for the eigenvalues in TE, for $n = 1$.

3.2.4 The $\gamma_{4p}^{(1)}(R)$

The last TE order we will consider explicitly (and thus only in a limited fashion) is that for $n = 4$. Here we have for the pertinent modified spherical Bessel functions,

$$\begin{aligned} i_4(jx) &= \left[\frac{105}{(jx)^5} + \frac{45}{(jx)^3} + \frac{1}{jx} \right] \sinh(jx) - \left[\frac{105}{(jx)^4} + \frac{10}{(jx)^2} \right] \cosh(jx) \\ &= \left(\frac{105}{x^5} - \frac{45}{x^3} + \frac{1}{x} \right) \sin x - \left(\frac{105}{x^4} - \frac{10}{x^2} \right) \cos x, \end{aligned} \quad (113)$$

and

$$\begin{aligned} k_4(jx) &= e^{-jx} \left[\frac{105}{(jx)^5} + \frac{105}{(jx)^4} + \frac{45}{(jx)^3} + \frac{10}{(jx)^2} + \frac{1}{jx} \right] \\ &= \left[\left(\frac{105}{x^4} - \frac{10}{x^2} \right) \cos x - \left(\frac{105}{x^5} - \frac{45}{x^3} + \frac{1}{x} \right) \sin x \right] \\ &\quad - j \left[\left(\frac{105}{x^5} - \frac{45}{x^3} + \frac{1}{x} \right) \cos x + \left(\frac{105}{x^4} - \frac{10}{x^2} \right) \sin x \right]. \end{aligned} \quad (114)$$

Substituting into equation (94) we get

$$\begin{aligned} 0 &= j \left[\left(\frac{105}{x^5} - \frac{45}{x^3} + \frac{1}{x} \right) \sin x - \left(\frac{105}{x^4} - \frac{10}{x^2} \right) \cos x \right] \left[\left(\frac{105}{y^5} - \frac{45}{y^3} + \frac{1}{y} \right) \cos y \right. \\ &\quad \left. + \left(\frac{105}{y^4} - \frac{10}{y^2} \right) \sin y \right] - \left[\left(\frac{105}{y^5} - \frac{45}{y^3} + \frac{1}{y} \right) \sin y - \left(\frac{105}{y^4} - \frac{10}{y^2} \right) \cos y \right] \\ &\quad \times \left[\left(\frac{105}{x^5} - \frac{45}{x^3} + \frac{1}{x} \right) \cos x + \left(\frac{105}{x^4} - \frac{10}{x^2} \right) \sin x \right]. \end{aligned}$$

Once more we observe that the real part vanishes identically. This can be rearranged to

$$\left[\left(\frac{105}{x^5} - \frac{45}{x^3} + \frac{1}{x} \right) \left(\frac{105}{y^5} - \frac{45}{y^3} + \frac{1}{y} \right) + \left(\frac{105}{x^4} - \frac{10}{x^2} \right) \left(\frac{105}{y^4} - \frac{10}{y^2} \right) \right] \sin(x - y) \\ - \left[\left(\frac{105}{x^4} - \frac{10}{x^2} \right) \left(\frac{105}{y^5} - \frac{45}{y^3} + \frac{1}{y} \right) - \left(\frac{105}{y^4} - \frac{10}{y^2} \right) \left(\frac{105}{x^5} - \frac{45}{x^3} + \frac{1}{x} \right) \right] \cos(x - y) = 0 ,$$

and this in turn can be brought into the form

$$\tan[(1 - R)x] = \left\{ x \left[\frac{105 - 10x^2}{105 - 45x^2 + x^4} \right] - R \left[\frac{105 - 10R^2x^2}{105 - 45R^2x^2 + R^4x^4} \right] \right. \\ \left. + \left[1 + Rx^2(105 - 10x^2)(105 - 10R^2x^2) + (105 - 45x^2 + x^4)(105 - 45R^2x^2 + R^4x^4) \right] \right\} \\ \equiv f_4(R; x) , \quad (115)$$

which upon simplification is a rational fraction whose numerator is a polynomial of degree 7 whose denominator is a polynomial of fourth degree in x^2 . The coefficients in these polynomials are of course functions (i.e., polynomials) of the ratio of inner to outer spherical radii R .

For small values of R , the denominator will have four real positive roots. If we examine figure 39 for $R = 0.05$ we can see the two smaller of these which correspond to singularities of $f_4(R; x)$. In addition, the numerator goes to zero at four real positive values of x . This occurs for $R < 0.05$. As R increases, the two zeros lying between the inner singularities of $f_4(R; x)$ merge, and by $R = 0.05$ they are gone, leaving only the innermost and outermost zeros of f_4 . The two functions $f_4(R; x)$ and $\tan(1 - R)x$ lie extremely close to one another for x values out to the first positive zero of f_4 as can be seen in figures 38 through 43. The latter of these is for $R = 0.40$. Figure 39 shows a magnified view in the neighborhood of the first singularities for both functions with $R = 0.05$, which shows rather dramatically how close the two functions are indeed. Fortunately, this figure also shows $f_4(0.05)$ lying below $\tan 0.95x$ as x increases from zero, the tangent going singular first and the relative positions of the two functions reversing as x increases beyond the singularities. Then, in figure 38, we can note that the first crossing $x_{41}^{(1)}(0.05)$ occurs beyond $x = 7.50$ just before the tangent goes to ∞ . The remaining eigenvalues for $x \leq 20$, $x_{4p}^{(1)}(0.05)$, occur one after the other on the negative-going arcs of the tangent, as can be very plainly seen in the figure.

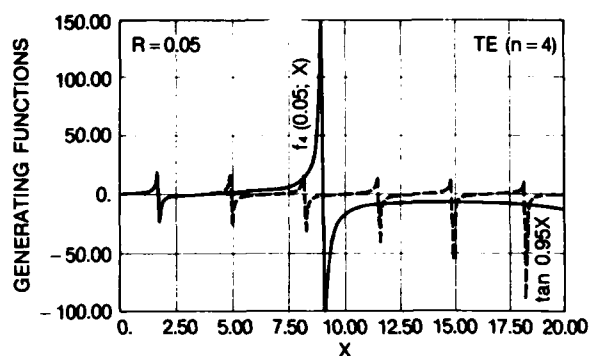


Figure 38. Generating functions for $\gamma_{4p}^{(1)}$ with $R = 0.05$.

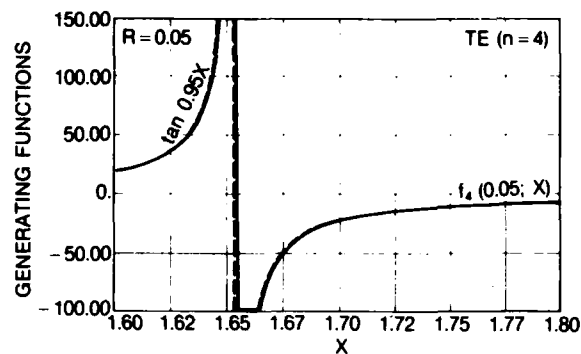


Figure 39. Enlarged view of generating functions for $\gamma_{4p}^{(1)}(0.05)$ near their first singularities.

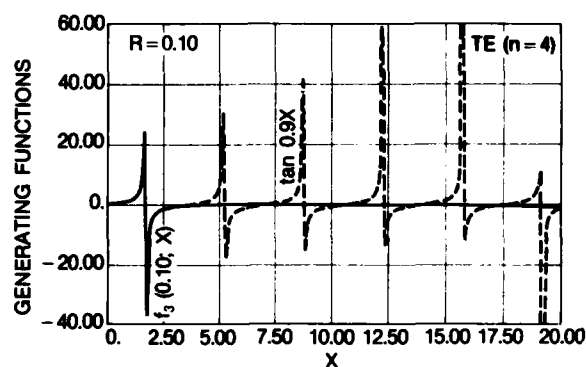


Figure 40. Generating functions for $\gamma_{4p}^{(1)}$ with $R = 0.10$.

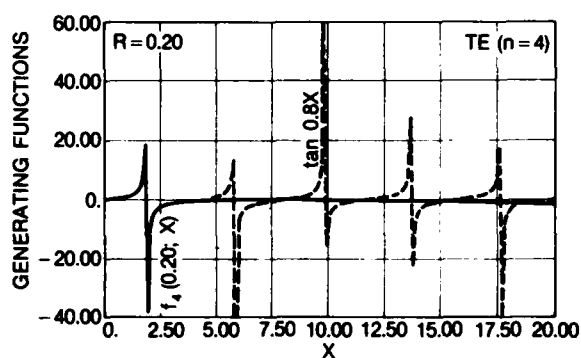


Figure 41. Generating functions for $\gamma_{4p}^{(1)}$ with $R = 0.20$.

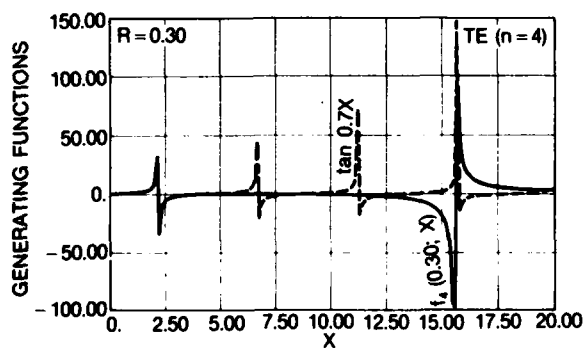


Figure 42. Generating functions for $\gamma_{4p}^{(1)}$ with $R = 0.30$.

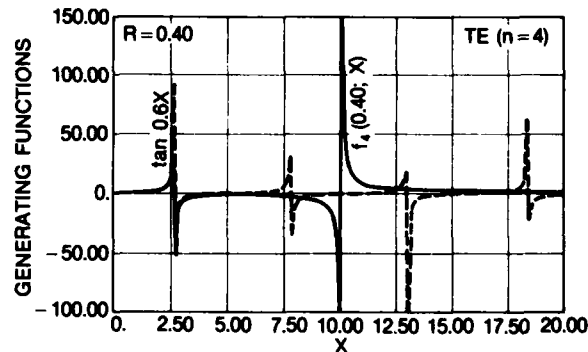


Figure 43. Generating functions for $\gamma_{4p}^{(1)}$ with $R = 0.40$.

As R increases, the outer pairs of singularities in f_4 merge into one another, which has already taken place by the time $R = 0.1$. Now we further find that $f_4(0.1; x)$ again has two zeros at positive values of x . This can be seen in figures 41 and 42 for $R = 0.2$ and $R = 0.3$.

Further increase in R merely reproduces the behavior we found for TE, $n = 3$. This can be readily observed by examining figures 43 through 47.

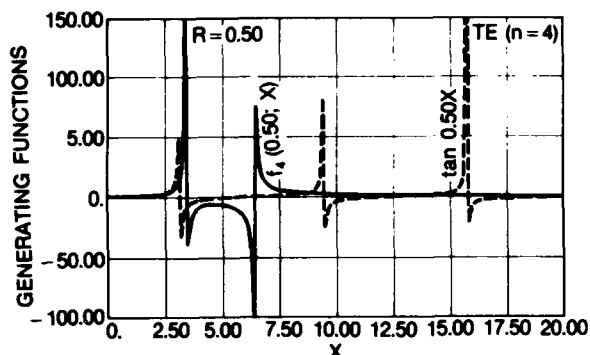


Figure 44. Generating functions for $\gamma_{4p}^{(1)}$ with $R = 0.50$.

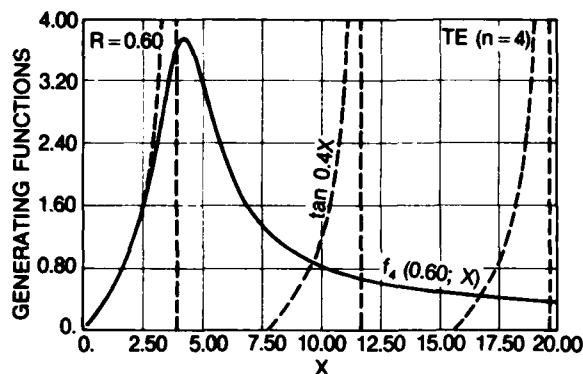


Figure 45. Generating functions for $\gamma_{4p}^{(1)}$ with $R = 0.60$.

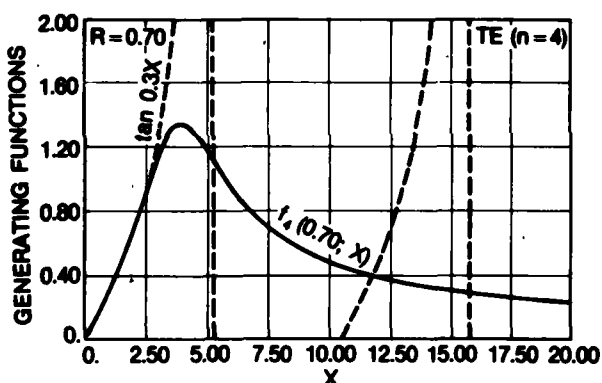


Figure 46. Generating functions for $\gamma_{4p}^{(1)}$ with $R = 0.70$.

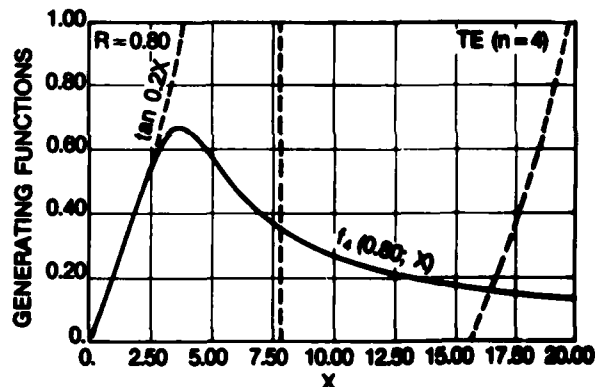


Figure 47. Generating functions for $\gamma_{4p}^{(1)}$ with $R = 0.80$.

3.2.5 TE, $n > 4$

Although we shall not go into any detail concerning $n > 4$, we can anticipate the additional complexities that will be incurred for these higher order TE mode eigenvalues. That is, additional pairs of singularities corresponding to a larger number of zeros of the denominator will enter and decrease in number as R increases. Similar behavior will occur in the $f_n(R; x)$ numerator. Nevertheless, f_n will always pass through the origin and have the same slope there as $\tan(1 - R)x$. The eigenvalues will always be such that they can be determined in the manner we have already seen from the roots of

$\tan(1 - R)x = f_n(R; x)$. Even though the formal algebraic analysis for the higher n can be quite formidable, it can be carried through by carefully going back and forth between computer calculations and graphics and formal derivations. In this manner all singularities and zeros of the $f_n(R; x)$ can be located, as well as the sign and behavior of the function itself over pertinent ranges of R and x . And, of course, the intersection with $\tan(1 - R)x$ can be determined definitively, and we thereby obtain the $\gamma_{np}^{(1)}(R)$ values. In fact, we have freely used this approach in the above considerations and in those below for the TM eigenvalues $\gamma_{np}^{(2)}(R)$ which we shall discuss next.

3.3 The TM Eigenvalues $\gamma_{np}^{(2)}$

We proceed to the analysis used in determining the TM eigenvalues. The roots of equation (79) have to be found. For convenience, we repeat the relation here,

$$[\gamma a i_n(\gamma a)]' [\gamma b k_n(\gamma b)]' - [\gamma b i_n(\gamma b)]' [\gamma a k_n(\gamma a)]' = 0 ,$$

and rewrite it

$$[j x i_n(j x)]' [j y k_n(j y)]' - [j y i_n(j y)]' [j x k_n(j x)]' = 0 . \quad (116)$$

As in the TE case, due to the nature of the modified spherical Bessel functions there will be roots only along the imaginary axis, and they will occur as complex conjugate pairs. Only those along the positive half of the imaginary axis will correspond to physically acceptable solutions for the modes of our concentric spherical cavity.

3.3.1 The $\gamma_{1p}^{(2)}(R)$

The derivatives that we shall need are

$$\begin{aligned} [\gamma a i_1(\gamma a)]'_{\gamma a=jx} &\equiv \left[1 + \frac{1}{(jx)^2} \right] \sinh(jx) - \frac{\cosh(jx)}{jx} \\ &= j \left[\left(1 - \frac{1}{x^2} \right) \sin x + \frac{\cos x}{x} \right] , \end{aligned} \quad (117)$$

$$\begin{aligned} [\gamma a k_1(\gamma a)]'_{\gamma a=jx} &\equiv -e^{-jx} \left[\frac{1}{(jx)^2} + \frac{1}{jx} + 1 \right] = \left[\left(\frac{1}{x^2} - 1 \right) \cos x + \frac{\sin x}{x} \right] \\ &\quad + j \left[\frac{\cos x}{x} - \left(\frac{1}{x^2} - 1 \right) \sin x \right] , \end{aligned} \quad (118)$$

which upon substitution in equation (116) gives us after some rearranging

$$0 = j \left\{ \left[\left(1 - \frac{1}{x^2}\right) \left(1 - \frac{1}{y^2}\right) + \frac{1}{xy} \right] \sin(x - y) - \left[\frac{1}{y} \left(1 - \frac{1}{x^2}\right) - \frac{1}{x} \left(1 - \frac{1}{y^2}\right) \right] \cos(x - y) \right\} , \quad (119)$$

or, equivalently,

$$\tan[(1 - R)x] = \frac{(1 - R)x(1 + Rx^2)}{[1 - (1 - R + R^2)x^2 + R^2x^4]} \equiv g_1(R; x) .$$

Clearly this function, $g_1(R; x)$, is of the same form as $f_2(R; x)$ that we found for the TE, $n = 2$ case. We have two zeros in the denominator and hence two distinct singularities for $g_1(R; x)$ for $R < R_0 = (3 - \sqrt{5})/2 = 0.381966$. These singularities occur at

$$x_{\pm}(R) = \sqrt{\frac{1 - R + R^2}{2R^2}} \pm \sqrt{\frac{1 - R + R^2}{2R^2} - \frac{1}{R^2}} .$$

Also in this case g_1 is non-negative for $0 \leq x \leq x_-$; it is negative for $x_- < x < x_+$ and positive thereafter, going to zero asymptotically as x becomes infinitely large. For $R = R_0$, the two singularities merge into one and $g_1(R_0; x)$ starts at zero for $x = 0$ and increases monotonically without bound as x goes to the double root at $x = \sqrt{3 + \sqrt{5}}/2$ of the denominator. On the other side of this double root, $g_1(R_0; x)$ decreases monotonically from $+\infty$ to zero as x increases. Finally, for $R > R_0$ the coefficient of x in the denominator of $g_1(R; x)$ is positive and hence $g_1(R; x)$ is well-behaved starting at zero at the origin, increasing smoothly to a maximum, and thereafter decreasing smoothly to vanish at infinity, remaining non-negative all along the positive side of the x -axis.

For $R < R_0$, the function $g_1(R; x)$ lies above the tangent function initially and goes singular first. Then it is negative while the tangent is still positive and increasing. Thus, $g_1(R; x)$ rises from $-\infty$ earlier than the tangent, after $x = \pi/2(1 - R)$, and still lies above the tangent curve for a while. Since the tangent will go positive at $x = \pi/(1 - R)$, the two functions will cross before $\tan(1 - R)x = 0$. This behavior will persist until the second singularity of $g_1(R; x)$ occurs before $x = \pi/2(1 - R)$. We see this in figures 48 through 51 for $R = 0.05, 0.1, 0.15, 0.20$, and 0.30 . In figure 52,

for $R = 0.35$, the second singularity occurs before $\pi/2(1 - R)$ and hence the first intersection, $x_{11}^{(2)}(0.35)$, now occurs while the tangent is going to its first singularity and g_1 is returning from its second singularity. In figures 48 through 51, the earlier intersections occur on the negative arcs of the tangent curve that lie between the singularities of $g_1(R; x)$. The later intersections must then lie on the positive increasing arcs of the tangent, as can be seen in these same figures. Since the two singularities collapse into one at $R = R_0$ for $x < \pi/2(1 - R_0)$, we can see in figures 52 through 58 that for $R \geq R_0$ intersections or eigenvalues occur on each successive positive-going branch of the tangent curve. As R increases, the successive eigenvalues move farther apart as $\tan(1 - R)x$ spreads out along x . In the TM, $n = 1$ case, we have included results for R at intermediate values to our more or less standard interval of 0.1 to show finer detailed behavior of the indicator function $g_1(R; x)$.

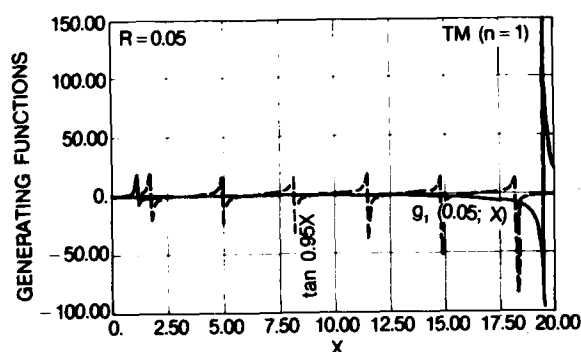


Figure 48. Generating functions for $\gamma_{1p}^{(2)}$ with $R = 0.05$.

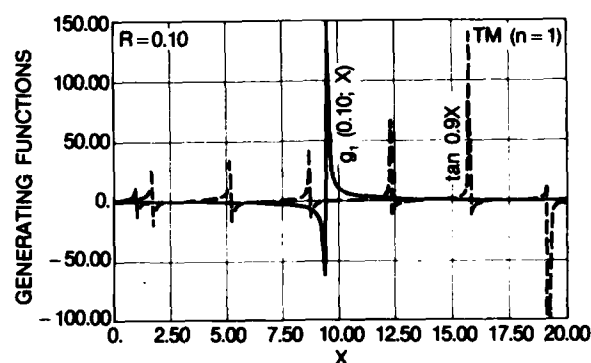


Figure 49. Generating functions for $\gamma_{1p}^{(2)}$ with $R = 0.10$.

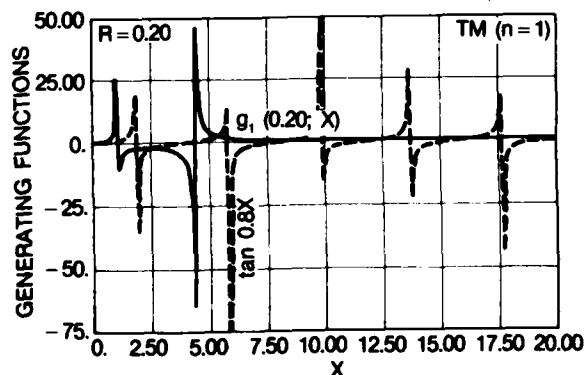


Figure 50. Generating functions for $\gamma_{1p}^{(2)}$ with $R = 0.20$.

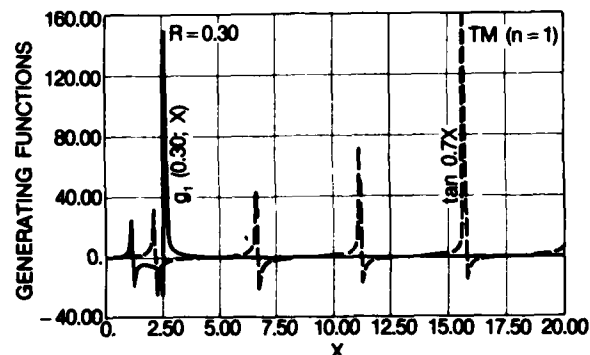


Figure 51. Generating functions for $\gamma_{1p}^{(2)}$ with $R = 0.30$.

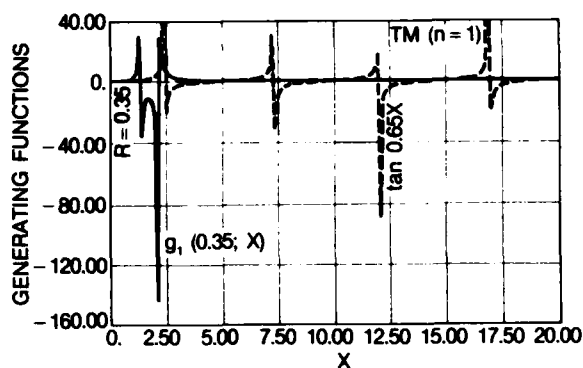


Figure 52. Generating functions for $Y_{1p}^{(2)}$ with $R = 0.35$.

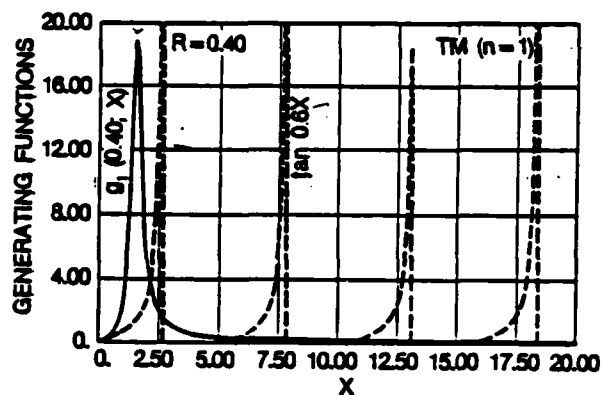


Figure 53. Generating functions for $Y_{1p}^{(2)}$ with $R = 0.40$.

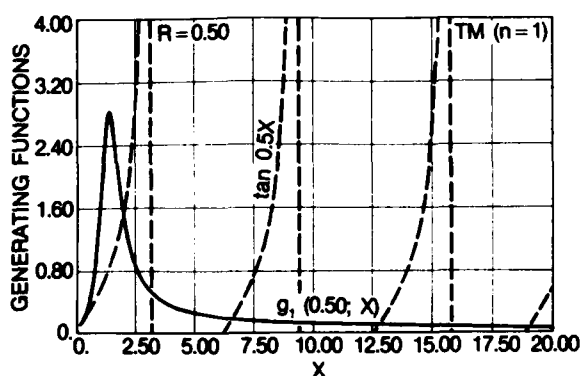


Figure 54. Generating functions for $Y_{1p}^{(2)}$ with $R = 0.50$.

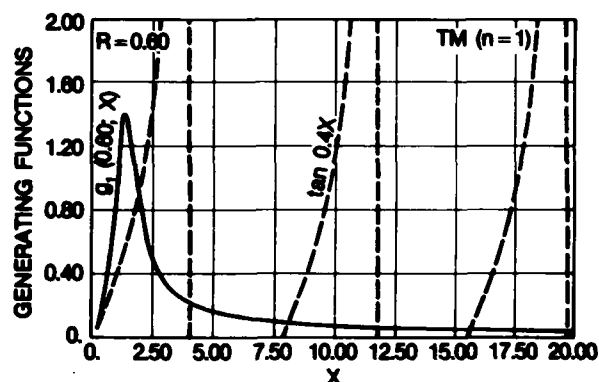


Figure 55. Generating functions for $Y_{1p}^{(2)}$ with $R = 0.60$.

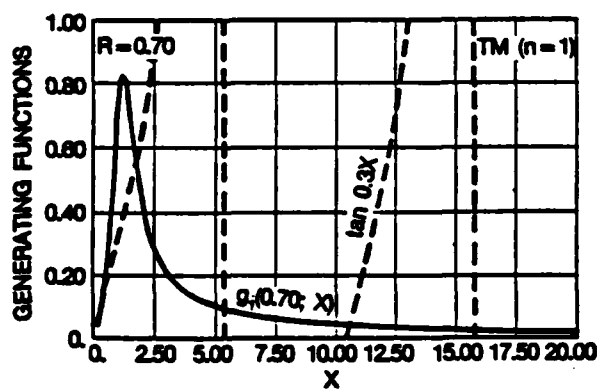


Figure 56. Generating functions for $Y_{1p}^{(2)}$ with $R = 0.70$.

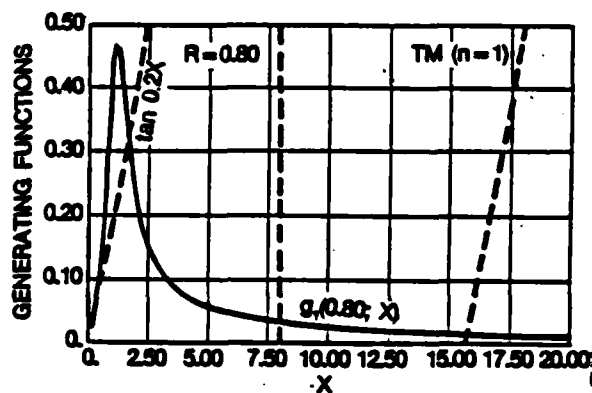


Figure 57. Generating functions for $Y_{1p}^{(2)}$ with $R = 0.80$.

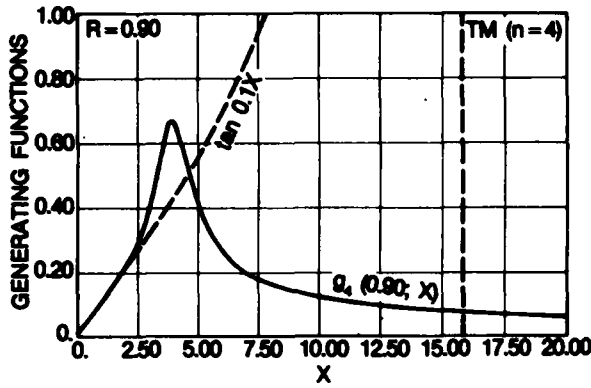


Figure 58. Generating functions for $Y_{1p}^{(2)}$ with $R = 0.90$.

3.3.2 The $\gamma_{2p}^{(2)}(R)$

We need the derivatives of the products

$$\begin{aligned} [\gamma_{a1_2}(\gamma_a)]'_{\gamma_a=jx} &\equiv -\left[\frac{6}{(jx)^3} + \frac{3}{jx}\right] \sinh(jx) + \left[\frac{6}{(jx)^2} + 1\right] \cosh(jx) \\ &= \left(\frac{6}{x^3} - \frac{3}{x}\right) \sin x + \left(1 - \frac{6}{x^2}\right) \cos x, \end{aligned} \quad (120)$$

and

$$\begin{aligned} [\gamma_{a2_2}(\gamma_a)]'_{\gamma_a=jx} &\equiv -e^{-jx} \left[\frac{6}{(jx)^3} + \frac{6}{(jx)^2} + \frac{3}{jx} + 1 \right] \\ &= \left[\left(\frac{6}{x^2} - 1 \right) \cos x - \left(\frac{6}{x^3} - \frac{3}{x} \right) \sin x \right] - j \left[\left(\frac{6}{x^2} - 1 \right) \sin x + \left(\frac{6}{x^3} - \frac{3}{x} \right) \cos x \right]. \end{aligned} \quad (121)$$

Substituting these two relations into equation (116) and rearranging, we get

$$\begin{aligned} 0 = j \left\{ \left[\left(\frac{6}{x^3} - \frac{3}{x} \right) \left(\frac{6}{y^3} - \frac{3}{y} \right) + \left(\frac{6}{x^2} - 1 \right) \left(\frac{6}{y^2} - 1 \right) \right] \sin(x-y) \right. \\ \left. - \left[\left(\frac{6}{x^2} - 1 \right) \left(\frac{6}{y^3} - \frac{3}{y} \right) - \left(\frac{6}{y^2} - 1 \right) \left(\frac{6}{x^3} - \frac{3}{x} \right) \right] \cos(x-y) \right\}; \end{aligned}$$

or, with some further rearranging, we bring this to the desired form:

$$\tan[(1 - R)x] = \frac{3x[(6 - x^2)(2 - R^2x^2) - R(6 - R^2x^2)(2 - x^2)]}{9(2 - x^2)(2 - R^2x^2) + Rx^2(6 - R^2x^2)} \equiv g_2(R; x) \quad (122)$$

We note that this function $g_2(R; x)$ is the ratio of a fourth-degree polynomial to a sixth-degree polynomial, just as we saw earlier for the TE, $n = 3$, case. Actually, the denominator of $g_2(R; x)$ is a cubic in x^2 . Thus, we can rewrite g_2 as

$$g_2(R; x) = \frac{3(1 - R)x[12 - 2(1 - R)^2x^2 + R^2x^4]}{36 - 18(1 - R)^2x^2 - 3R[2(1 - R)^2 + R]x^4 + R^3x^6} \quad (123)$$

Examining the denominator we see that the maximum number of positive roots for x^2 will be two, and in turn the maximum number of positive roots for x will be two, $x_-(R)$ and $x_+(R)$. Now let us look at the numerator. For $R = R_0 = (1 + \sqrt{3}) - \sqrt{\sqrt{3} + 2\sqrt{3}} = 0.189,591$, there will be only one root for the numerator at $x_0 = x(R_0) = (1 - R_0)/R_0 = 4.274,512$. For $R < R_0$, the numerator will have two roots and hence g_2 will vanish at $x = x_{0,\pm}(R)$, where

$$x_{0,\pm}(R) = \frac{1 - R}{R} \left\{ 1 \pm \sqrt{1 - [12R^2/(1 - R)^4]} \right\} ,$$

and

$$x_{0,-}(R) < x_0 < x_{0,+}(R) \quad .$$

Thus we see that as R increases, $x_{0,-}$ and $x_{0,+}$ move together and coincide at x_0 where $R \rightarrow R_0$. For $R > R_0$, the numerator becomes positive definite.

If we expand $g_2(R; x)$ around $x = 0$ in a power series, we find that, to order x^5 , $g_2(R; x) > \tan(1 - R)x$ near the origin. Of course g_2 and the tangents both pass through the origin with the same slope. As x increases from zero, g_2 will have a larger slope than the tangent. For small R , the function $g_2(R; x)$ goes singular before the tangent just as in the TM, $n = 1$, case. As a consequence of this behavior, $g_2(R; x)$ and $\tan(1 - R)x$ will not intersect for x less than $\pi/(1 - R)$. This property persists until R is sufficiently large for $g_2(R; x)$ to have no roots other than at the origin or infinity; i.e., for R to exceed R_0 . These characteristics can be seen in figures 59 through 62. Although explicit analysis can be carried out to determine when and where, as a function of R , the denominator of $g_2(R; x)$ vanishes and, hence, g_2 becomes singular, we shall not do so here. Examination of figures 59 through 67 reveals quite readily that, as R increases, there are two singular values of x , $0 < x_-(R) < x_+(R)$ which move toward each other as R increases

through $R = 0.58$ and which coalesce into one singularity at the double root of the denominator. By $R = 0.60$ this singular behavior is gone and as we see in figures 67 through 71 we have a familiar behavior for $g_2(R;x)$. For those values of R for which there are two singularities, $g_2(R;x)$ is a monotonic increasing function greater than zero and increasing with x increasing to $x_-(R)$. As x increases further, $g_2(R;x)$ returns from $-\infty$ toward a maximum value (which for $R > R_0$ is negative) and then again goes monotonically to $-\infty$ as x increases toward $x_+(R)$. It then jumps to $+\infty$ and decreases monotonically to go asymptotically to zero as x goes to infinity. In between x_- and x_+ the intersections are on the positive-going arcs of the tangent for $g_2 > 0$ and on the negative branches for $g_2 < 0$. For $x > x_+$ the intersections always occur on the positive arcs of the tangent function and are very close to being periodic with the period of the tangent itself. For $R \geq 0.58$, the first crossing of the two curves, $x_{21}^{(2)}(R)$, occurs on the first positive arc of the tangent (see fig. 67).

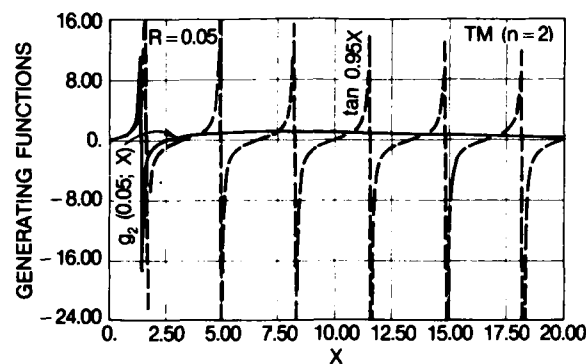


Figure 59. Generating functions for $\gamma_{2p}^{(2)}$ with $R = 0.05$.

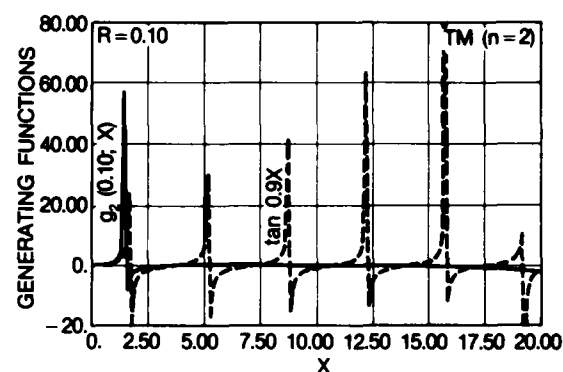


Figure 60. Generating functions for $\gamma_{2p}^{(2)}$ with $R = 0.10$.

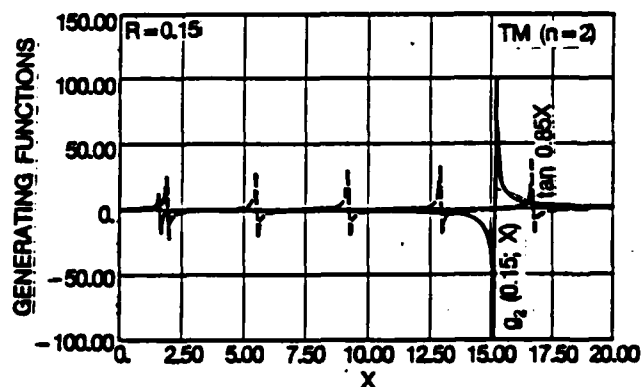


Figure 61. Generating functions for $\gamma_{2p}^{(2)}$ with $R = 0.15$.

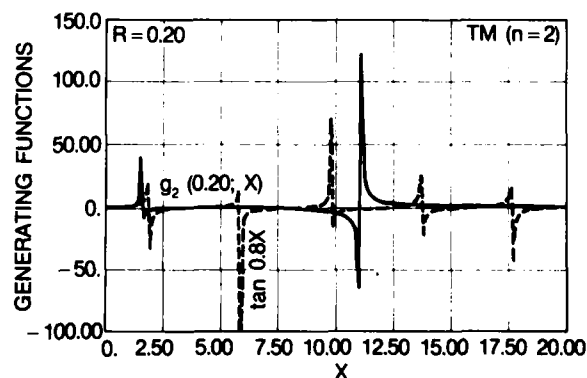


Figure 62. Generating functions for $\gamma_{2p}^{(2)}$ with $R = 0.20$.

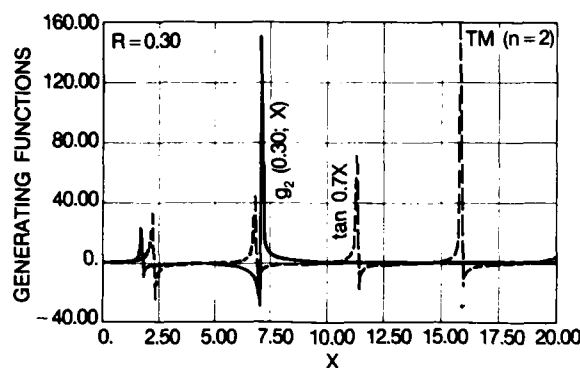


Figure 63. Generating functions for $Y_{2p}^{(2)}$ with $R = 0.30$.

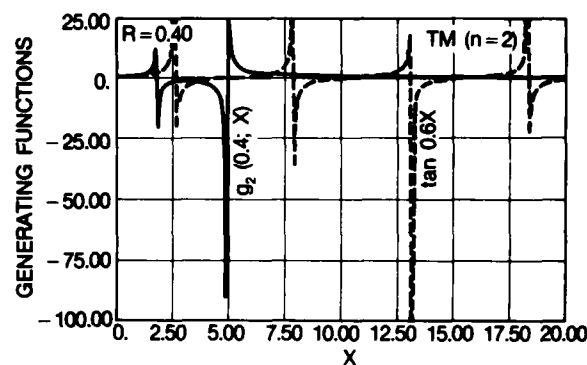


Figure 64. Generating functions for $Y_{2p}^{(2)}$ with $R = 0.40$.

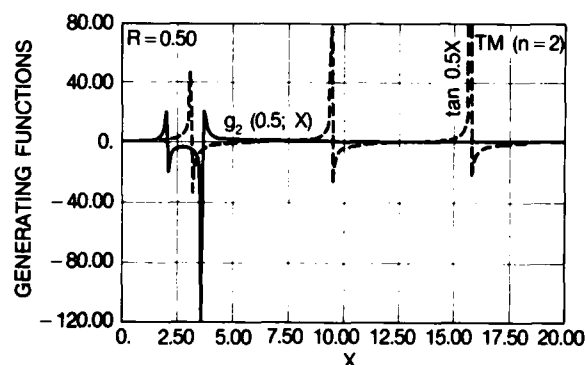


Figure 65. Generating functions for $Y_{2p}^{(2)}$ with $R = 0.50$.

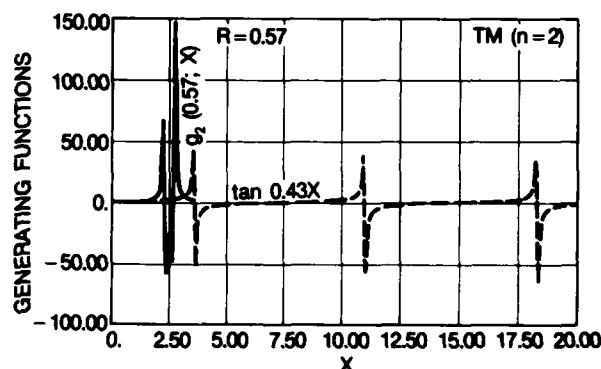


Figure 66. Generating functions for $Y_{2p}^{(2)}$ with $R = 0.57$.

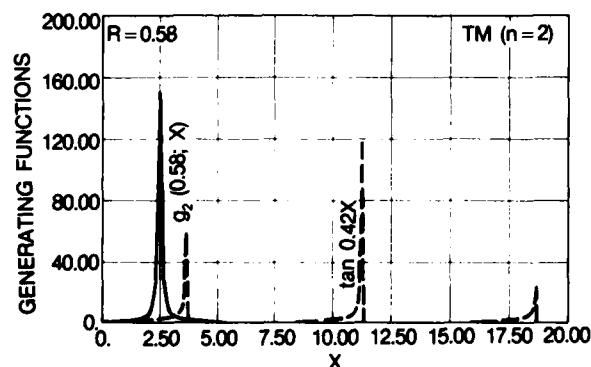


Figure 67. Generating functions for $Y_{2p}^{(2)}$ with $R = 0.58$.

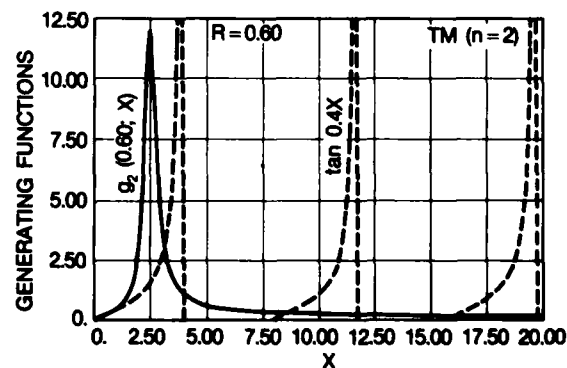


Figure 68. Generating functions for $Y_{2p}^{(2)}$ with $R = 0.60$.

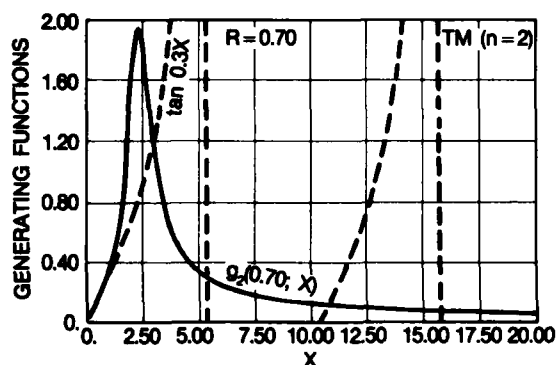


Figure 69. Generating functions for $\gamma_{2p}^{(2)}$ with $R = 0.70$.

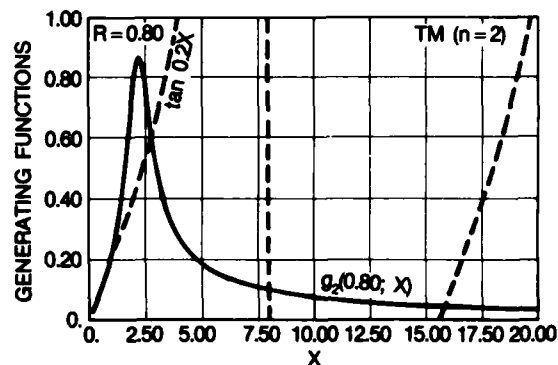


Figure 70. Generating functions for $\gamma_{2p}^{(2)}$ with $R = 0.80$.

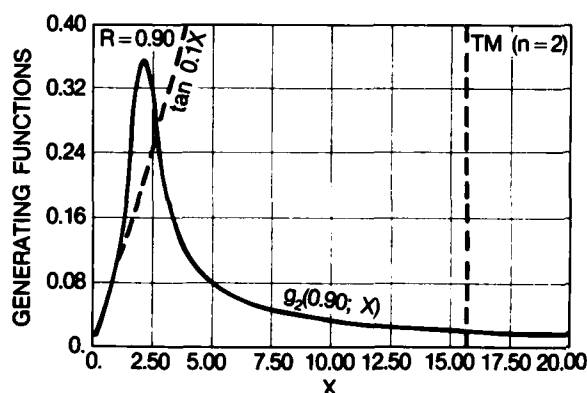


Figure 71. Generating functions for $\gamma_{2p}^{(2)}$ with $R = 0.90$.

We note now that, unlike the TE eigenvalues, $\gamma_{np}^{(1)}(R)$, which increase with R , the TM eigenvalues $\gamma_{21}^{(2)}(R)$ decrease slightly as R increases, and the $\gamma_{2p}^{(2)}(R)$ for $p > 1$ decrease initially and then increase as R increases. This was also true for $n = 1$.

3.3.3 The $\gamma_{3p}^{(2)}(R)$

The starting point here is

$$\begin{aligned} [\gamma a i_3(\gamma a)]'_{\gamma a = jx} &\equiv \left[\frac{45}{(jx)^4} + \frac{21}{(jx)^2} + 1 \right] \sinh(jx) - \left[\frac{45}{(jx)^3} + \frac{6}{jx} \right] \cosh(jx) \\ &\equiv j \left[\left(\frac{45}{x^4} - \frac{21}{x^2} + 1 \right) \sin x - \left(\frac{45}{x^3} - \frac{6}{x} \right) \cos x \right], \end{aligned} \quad (124)$$

and

$$\begin{aligned}
 [\gamma_{ak_3}(\gamma_a)]'_{\gamma_a \equiv jx} &\equiv -e^{-jx} \left[\frac{45}{(jx)^4} + \frac{45}{(jx)^3} + \frac{21}{(jx)^2} + \frac{6}{jx} + 1 \right] \\
 &= - \left\{ \left[\left(\frac{45}{x^4} - \frac{21}{x^2} + 1 \right) \cos x + \left(\frac{45}{x^3} - \frac{6}{x} \right) \sin x \right] + j \left[\left(\frac{45}{x^3} - \frac{6}{x} \right) \cos x \right. \right. \\
 &\quad \left. \left. - \left(\frac{45}{x^4} - \frac{21}{x^2} + 1 \right) \right] \sin(x - y) \right\} , \quad .
 \end{aligned}
 \tag{125}$$

which when substituted into equation (116) gives, after some rearranging,

$$\begin{aligned}
 0 &= j \left\{ \left[\left(\frac{45}{x^4} - \frac{21}{x^2} + 1 \right) \left(\frac{45}{y^4} - \frac{21}{y^2} + 1 \right) + \left(\frac{45}{x^3} - \frac{6}{x} \right) \left(\frac{45}{y^3} - \frac{6}{y} \right) \right] \sin(x - y) \right. \\
 &\quad \left. - \left[\left(\frac{45}{x^4} - \frac{21}{x^2} + 1 \right) \left(\frac{45}{y^3} - \frac{6}{y} \right) - \left(\frac{45}{x^3} - \frac{6}{x} \right) \left(\frac{45}{y^4} - \frac{21}{y^2} + 1 \right) \right] \cos(x - y) \right\} ,
 \end{aligned}$$

and in turn this can be put in the desired form for determining the eigenvalues from the intersections of two curves, namely,

$$\begin{aligned}
 \tan(1 - R)x &= 3x \left[\frac{15 - 2x^2}{45 - 21x^2 + x^4} - R \left(\frac{15 - 2R^2x^2}{45 - 21R^2x^2 + R^4x^4} \right) \right] \\
 &+ \left\{ 1 + 9Rx^2 \left[\frac{(15 - 2x^2)(15 - 2R^2x^2)}{(45 - 21x^2 + x^4)(45 - 21R^2x^2 + R^4x^4)} \right] \right\} \equiv g_3(R; x) .
 \end{aligned}
 \tag{126}$$

We point out that the denominator of $g_3(R; x)$ is a quartic in x^2 , just as we observed for the polynomial denominator of $f_4(R; x)$ in the TE, $n = 4$, case. Then we can anticipate a rapid increase in the complexity of the extensive analysis that accompanies $g_3(R; x)$. Only a small portion of this analysis is included here. Thus, for the behavior near $x = 0$, we have

$$\begin{aligned}
 g_3(R; x) &\equiv 3(1 - R)x [2R^3x^6 - 3R(5R^2 - 9R + 5)x^4 - 45(2R^2 - 5R + 2)x^2 + 675] \\
 &+ [R^4x^8 - 3R^2(7R^2 - 12R + 7)x^6 + 9(5R^4 - 30R^3 + 49R^2 - 30R + 5)x^4 \\
 &\quad - 145(7R^2 - 15R + 7)x^2 + 2025] .
 \end{aligned}
 \tag{127}$$

Expanding in a power series around $x = 0$, we find to order x^5 ,

$$g_3(R;x) \approx (1 - R)x + \frac{(1 - R)^3 x^3}{3} + \frac{2(1 - R)^5 x^5}{15} ,$$

but to the same order,

$$\tan(1 - R)x \approx (1 - R)x + \frac{(1 - R)^3 x^3}{3} + \frac{2(1 - R)^5 x^5}{15} .$$

Thus we see that just as in the TE, $n = 3$, case, both the tangent and g_3 coincide to order x^5 . This is reflected in the two curves being nearly indistinguishable for an appreciable range in x for the smaller values of R of figures 72 through 80. In figure 72, for $R = 0.05$, in fact, the two functions are extremely close together even beyond the first singularity of $g_3(R;x)$ and the first pole of $\tan(1 - R)x$. Next, if we examine the coefficient in the denominator, we observe that for small R there are at most four real positive roots or equivalently at most four singularities in $g_3(R;x)$ for positive x . The same type of consideration shows that the numerator has, at most, two roots for small R . In figure 72, for $R = 0.05$, we see one of the zeros of $g_3(0.05;x)$ and also two of the singularities. For x beyond the range shown in this figure, the pattern is repeated, but in reverse order; i.e., as x increases beyond 20 we find $g_3(0.05;x)$ negative and going to $-\infty$, then jumping to $+\infty$ and decreasing as x increases, going through zero at a specific value of x and then going to $-\infty$ again as x increases further. Next, g_3 jumps to $+\infty$ and then goes asymptotically to zero as $x \rightarrow \infty$. As R increases, the singularities move toward each other, with the inner pair closing together more rapidly. This can be seen in figure 73 for $R = 0.10$. Further increasing R causes the two innermost singularities to coincide and then disappear altogether. When this occurs, $g_3(R;x)$ has two zeros between the remaining singularities. Figures 74 and 75 show this rather clearly. Also, we note that the outer singularities move inward quite rapidly toward the slowly changing innermost singularity. With further increase in R , the two roots of $g_3(R;x)$ move together, coalesce, and then disappear altogether, as can be seen in figures 76, 77, and 78 for $R = 0.40$, 0.50 , and 0.60 , respectively. Now g_2 is less than zero in between the singularities and positive outside. As R increases even further, the two remaining singularities move together, coalesce, and vanish. The final state of affairs is represented by figure 79 for $R = 0.70$. Further growth in the size of R as usual results in the peak of $g_3(R;x)$ dropping and shifting down in x . All the features of $g_3(R;x)$ found here for TM, $n = 3$, are now familiar properties.

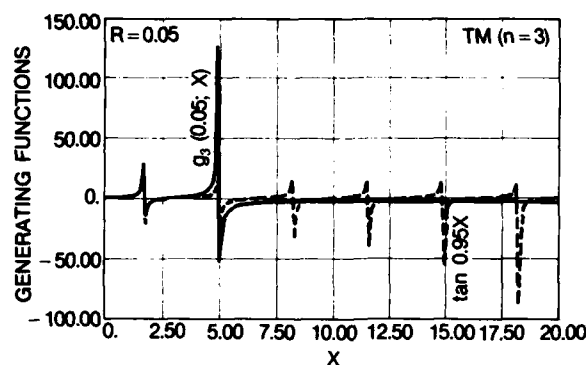


Figure 72. Generating functions for $Y_{3p}^{(2)}$ with $R = 0.05$.

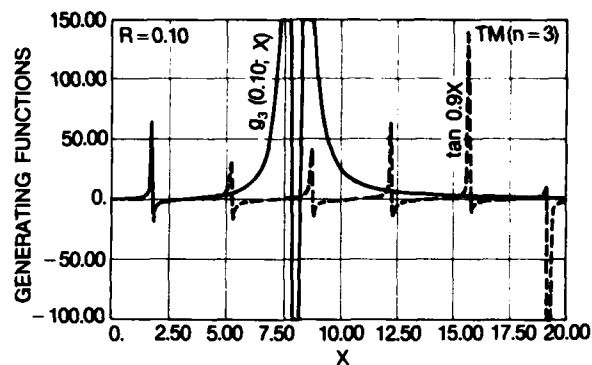


Figure 73. Generating functions for $Y_{3p}^{(2)}$ with $R = 0.10$.

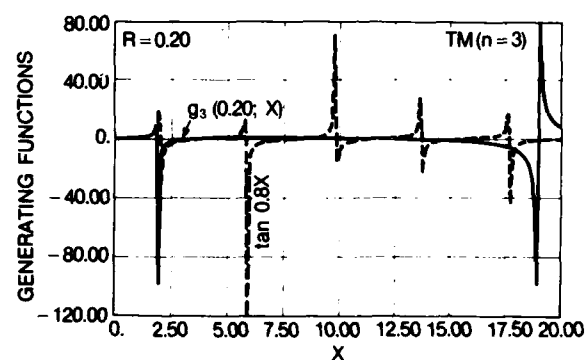


Figure 74. Generating functions for $Y_{3p}^{(2)}$ with $R = 0.20$.

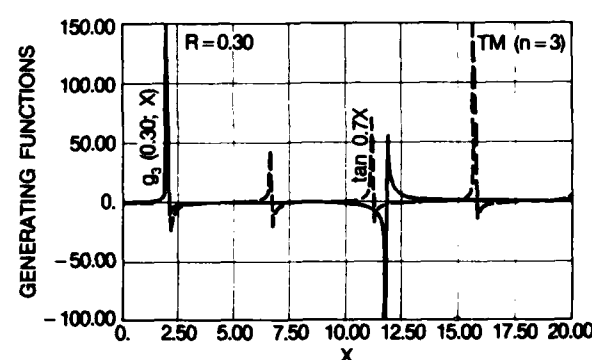


Figure 75. Generating functions for $Y_{3p}^{(2)}$ with $R = 0.30$.

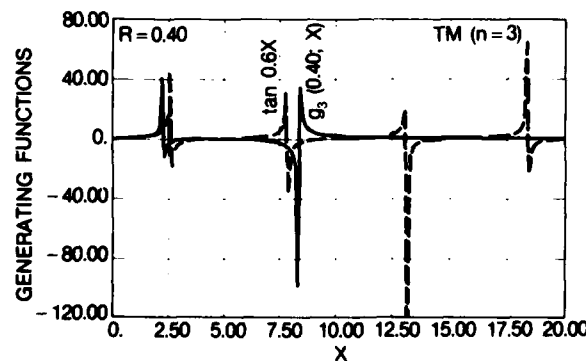


Figure 76. Generating functions for $Y_{3p}^{(2)}$ with $R = 0.40$.

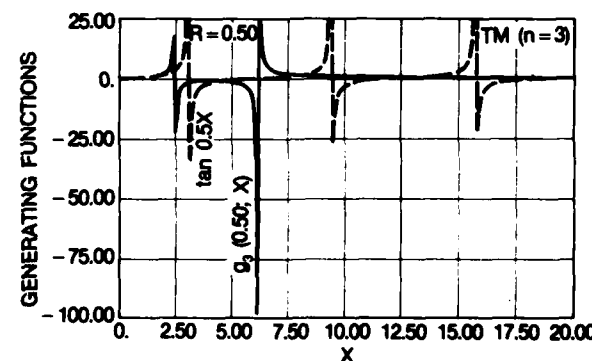


Figure 77. Generating functions for $Y_{3p}^{(2)}$ with $R = 0.50$.

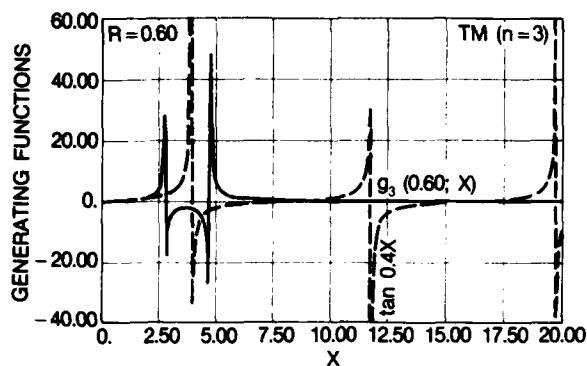


Figure 78. Generating functions for $\gamma_{3p}^{(2)}$ with $R = 0.60$.

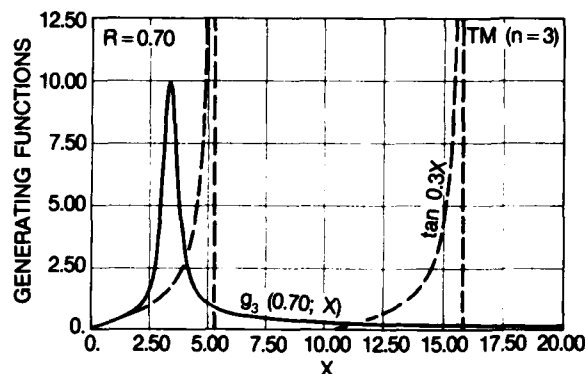


Figure 79. Generating functions for $\gamma_{3p}^{(2)}$ with $R = 0.70$.

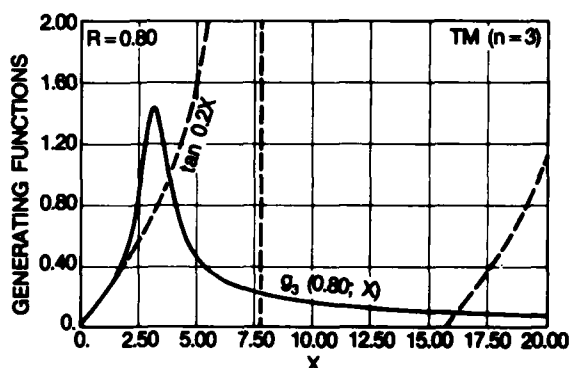


Figure 80. Generating functions for $\gamma_{3p}^{(2)}$ with $R = 0.80$.

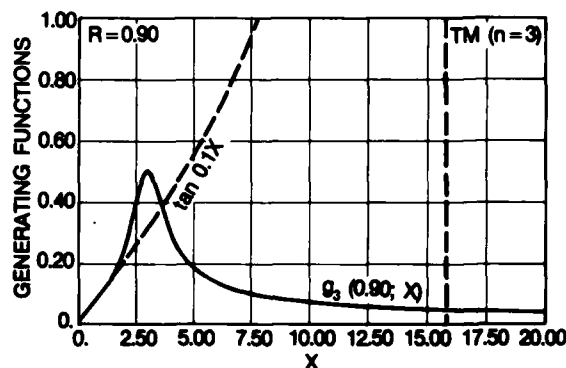


Figure 81. Generating functions for $\gamma_{3p}^{(2)}$ with $R = 0.90$.

Next, we briefly consider the intersections (i.e., the locations of the eigenvalues) of $g_3(R; x)$ and $\tan(1 - R)x$. For small values of R (see fig. 72 for $R = 0.05$), the first two singularities in $g_3(R; x)$ just precede those for $\tan(1 - R)x$. For this situation, the first intersection will occur just beyond $x = 3\pi/2(1 - R)$, i.e., on the negative arcs of both functions. The next few eigenvalues occur between the inner pair of singularities on the negative arcs of the tangent just after the tangent returns from $-\infty$. The bulk of the remaining properties of the locations of the crossings of g_3 with the tangent curve has already been described in the foregoing discussions. These predicted characteristics can be verified if we examine the corresponding TM sets of curves for $n = 3$ in figures 72 through 81.

3.3.4 The $\gamma_{4p}^{(2)}(R)$

Continuing to the next higher order, $n = 4$, we have the two relations

$$\begin{aligned} [\gamma_{ai_4}(\gamma_a)]'_{\gamma_a=jx} &\equiv \left[\frac{420}{(jx)^4} + \frac{55}{(jx)^2} + 1 \right] \cosh(jx) \\ &\quad - \left[\frac{420}{(jx)^5} + \frac{195}{(jx)^3} + \frac{10}{jx} \right] \sinh(jx) \\ &\equiv \left(\frac{420}{x^4} - \frac{55}{x^2} + 1 \right) \cos x - \left(\frac{420}{x^5} - \frac{195}{x^3} + \frac{10}{x} \right) \sin x, \end{aligned} \quad (128)$$

and

$$\begin{aligned} [\gamma_{ak_4}(\gamma_a)]'_{\gamma_a=jx} &\equiv -e^{-(jx)} \left[\frac{420}{(jx)^5} + \frac{420}{(jx)^4} + \frac{195}{(jx)^3} + \frac{55}{(jx)^2} + \frac{10}{jx} + 1 \right] \\ &\equiv - \left\{ \left[\left(\frac{420}{x^4} - \frac{55}{x^2} + 1 \right) \cos x - \left(\frac{420}{x^5} - \frac{195}{x^3} + \frac{10}{x} \right) \sin x \right] \right. \\ &\quad \left. + j \left[\left(\frac{420}{x^5} - \frac{195}{x^3} + \frac{10}{x} \right) \cos x + \left(\frac{420}{x^4} - \frac{55}{x^2} + 1 \right) \sin x \right] \right\}, \end{aligned} \quad (129)$$

which when substituted into equation (116) and rearranged gives us

$$\begin{aligned} 0 &= j \left\{ \left[\left(\frac{420}{x^5} - \frac{195}{x^3} + \frac{10}{x} \right) \left(\frac{420}{y^5} - \frac{195}{y^3} + \frac{10}{y} \right) \right. \right. \\ &\quad + \left. \left(\frac{420}{x^4} - \frac{55}{x^2} + 1 \right) \left(\frac{420}{y^4} - \frac{55}{y^2} + 1 \right) \right] \sin(x-y) - \left[\left(\frac{420}{x^4} - \frac{55}{x^2} + 1 \right) \left(\frac{420}{y^5} - \frac{195}{y^3} + \frac{10}{y} \right) \right. \\ &\quad \left. \left. - \left(\frac{420}{y^4} - \frac{55}{y^2} + 1 \right) \left(\frac{420}{x^5} - \frac{195}{x^3} + \frac{10}{x} \right) \right] \cos(x-y) \right\}, \end{aligned}$$

or, in what we can now call our preferred form, this becomes

$$\begin{aligned} \tan[(1-R)x] &= x \left[(420 - 55x^2 + x^4)(420 - 195R^2x^2 + 10R^4x^4) \right. \\ &\quad \left. - R(420 - 55R^2x^2 + R^4x^4)(420 - 195x^2 + 10x^4) \right] \\ &\quad + [(420 - 195x^2 + 10x^4)(420 - 195R^2x^2 + 10R^4x^4) \\ &\quad + Rx^2(420 - 55x^2 + x^4)(420 - 55R^2x^2 + R^4x^4)] \equiv g_4(R; x). \end{aligned} \quad (130)$$

We note that the denominator of $g_4(R;x)$ is a quintic in x^2 , and the numerator is the product of x and a quartic in x^2 . This is a level of complexity beyond those met thus far, but the general nature of the analysis required is pretty much the same as that we have carried out thus far. Upon examination of the denominator of $g_4(R;x)$, we find that there are in this case at most four positive values of x that are roots. Hence, $g_4(R;x)$ will have at most four singularities for positive x . In fact, this is reflected in the behavior of $g_4(R;x)$ as shown in figures 82 through 84, where we can discern for $R \leq 0.20$ the existence of four singularities. Figure 84 explicitly shows for $R = 0.20$ three of the four. As R increases, we see that the inner pair move together to coalesce and then disappear by the time R attains the value $R = 0.30$ (see fig. 85). With further increase in R , the remaining two singularities repeat this behavior, and by $R = 0.80$ all the singularity in $g_4(R;x)$ ceases. For $R \geq 0.80$, we have the usual well-behaved smooth increase to a maximum, which decreases and moves inward with increasing R . This behavior of $g_4(R;x)$ is easily seen in figures 90 and 91 for $R = 0.80$ and 0.90 , respectively. The numerator of $g_4(R;x)$ is a product of x with a polynomial that is a quartic in x^2 . Examination of this numerator shows that $g_4(R;x)$ will possess a maximum of four roots for positive x . For small R these are located, as we have seen in other cases, as follows: one each between the inner and the outer pairs of singularities and two between the inner pair of singularities. This can be seen in figure 82 for $R = 0.05$. As R increases, the innermost pair of roots move together, then merge, and by $R = 0.10$ (see fig. 83), disappear, leaving g_4 negative between the pair of inner singularities. As R increases further, the two inner singularities disappear, and two roots are present between the remaining pair of singularities (see fig. 85). As R grows larger, these two zeros move towards one another, merge, and disappear. For $R = 0.60$, as can be plainly seen in figure 88, there are no finite positive values of x for which $g_4(R;x)$ vanishes.

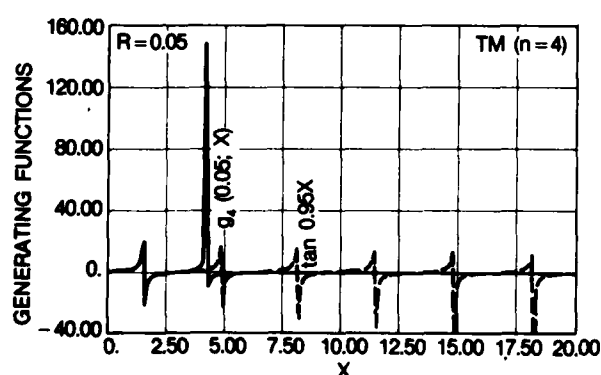


Figure 82. Generating functions for $\gamma_{4p}^{(2)}$ with $R = 0.05$.

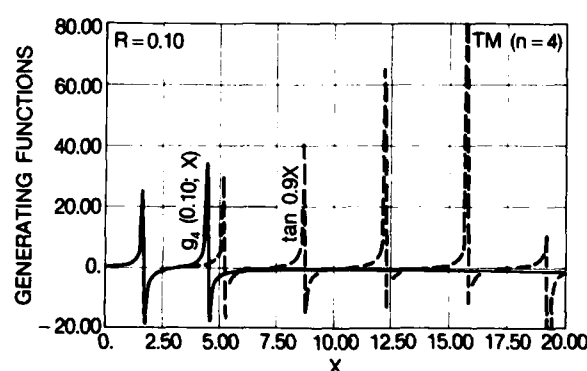


Figure 83. Generating functions for $\gamma_{4p}^{(2)}$ with $R = 0.10$.

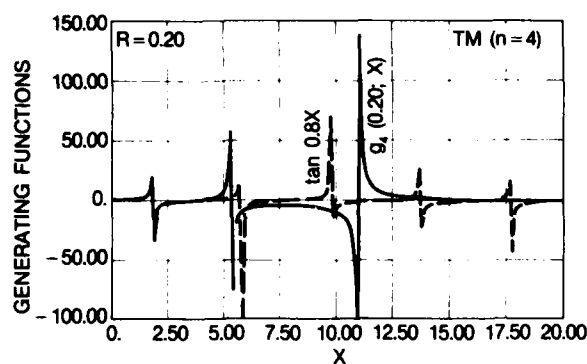


Figure 84. Generating functions for $\gamma_{4p}^{(2)}$ with $R = 0.20$.

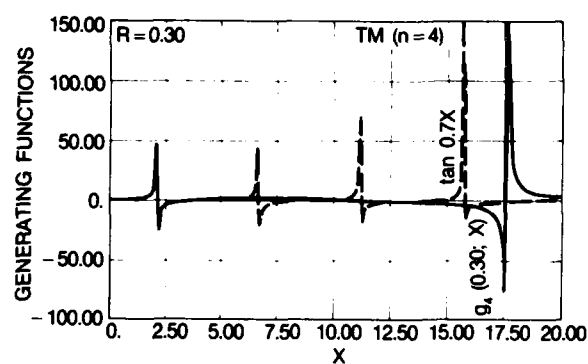


Figure 85. Generating functions for $\gamma_{4p}^{(2)}$ with $R = 0.30$.

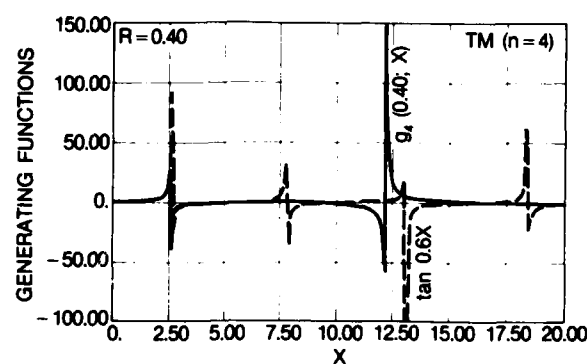


Figure 86. Generating functions for $\gamma_{4p}^{(2)}$ with $R = 0.40$.

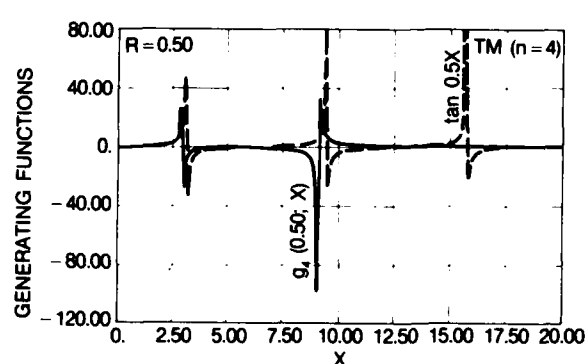


Figure 87. Generating functions for $\gamma_{4p}^{(2)}$ with $R = 0.50$.

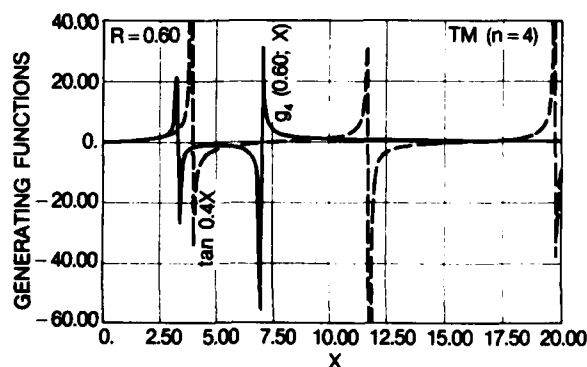


Figure 88. Generating functions for $\gamma_{4p}^{(2)}$ with $R = 0.60$.

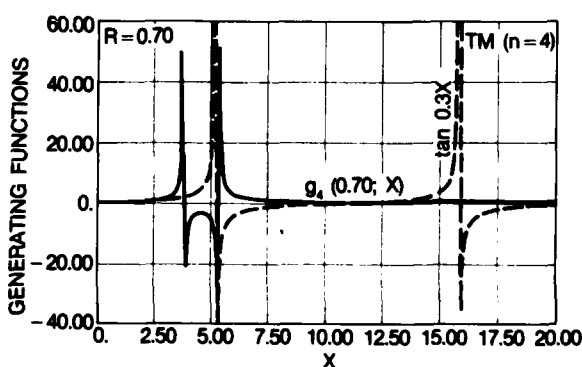


Figure 89. Generating functions for $\gamma_{4p}^{(2)}$ with $R = 0.70$.

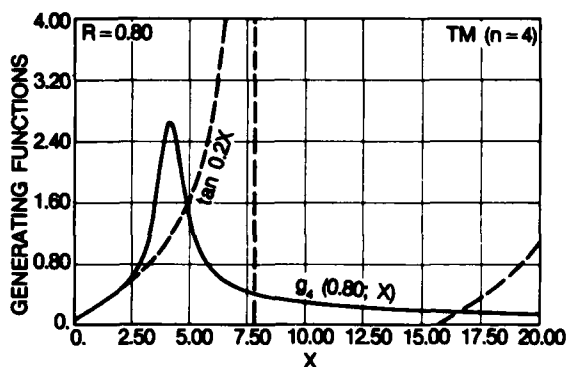


Figure 90. Generating functions for $\gamma_{4p}^{(2)}$ with $R = 0.80$.

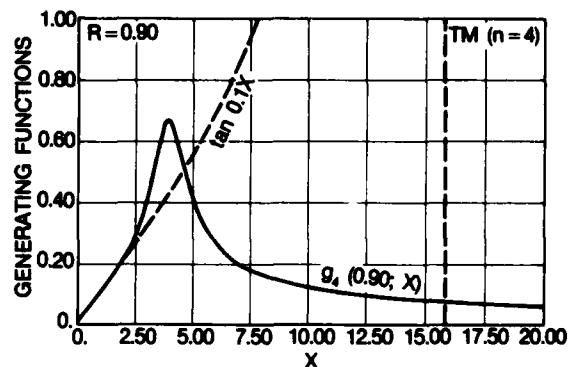


Figure 91. Generating functions for $\gamma_{4p}^{(2)}$ with $R = 0.90$.

For future reference, we write out $g_4(R; x)$ in reduced form:

$$\begin{aligned}
 g_4(R; x) \equiv & (1 - R)x \left[1 - \frac{1}{84}(11 - 28R + 11R^2)x^2 + \frac{1}{35,280}(28 - 252R + 463R^2 - 252R^3 \right. \\
 & + 28R^4)x^4 - 5R^2(39 - 71R + 39R^2)x^6 + 10R^4x^8 \Big] + \left[1 - \frac{1}{28}(13 - 28R + 13R^2)x^2 \right. \\
 & + \frac{1}{2,352}(56 - 308R + 507R^2 - 308R^3 + 56R^4)x^4 \\
 & + \frac{1}{35,280}R(84 - 390R + 605R^2 - 390R^3 + 84R^4)x^6 \\
 & \left. - \frac{R^3}{35,280}(11 - 20R + 11R^2)x^8 + \frac{R^5x^{10}}{176,400} \right] .
 \end{aligned} \tag{131}$$

As can be seen in figures 82 through 85, the two curves lie very close together for an appreciable range of x when $R \lesssim 0.30$. Careful analysis of these expansions shows that $g_4(R; x)$ lies above the $\tan(1 - R)x$. For the small R values, $g_4(R; x)$ attains its first singularity before the tangent function. For larger R this characteristic is plainly seen (fig. 87 through 89 for $R = 0.50$ to 0.70). From the behavior of the two functions for the smaller values of R which correspond to the presence of singularities in $g_4(R; x)$, it is relatively easy to discern the fact that there will be no intersection until at least $x = 6$. However, as R increases beyond $r = 0.40$ (see fig. 86, for example), the first eigenvalue $x_{41}^{(2)}(R)$ occurs at a smaller value of x . All the remaining features of the behavior of the intersection positions have essentially been discussed in the foregoing cases.

3.3.5 The $\gamma_{5p}^{(2)}(R)$

For the final case, we shall present an explicit discussion for TM, $n = 5$. Our two starting relations are

$$\begin{aligned} [\gamma_{a5}(\gamma_a)]'_{\gamma_a=jx} &\equiv \left[\frac{4725}{(jx)^6} + \frac{2205}{(jx)^4} + \frac{120}{(jx)^2} + 1 \right] \sinh(jx) \\ &- \left[\frac{4725}{(jx)^5} + \frac{630}{(jx)^3} + \frac{15}{(jx)} \right] \cosh(jx) \equiv j \left[\left(\frac{4725}{x^5} - \frac{630}{x^3} + \frac{15}{x} \right) \cos x \right. \\ &\left. - \left(\frac{4725}{x^6} - \frac{2205}{x^4} + \frac{120}{x^2} - 1 \right) \sin x \right] , \end{aligned} \quad (132)$$

and

$$\begin{aligned} [\gamma_{ak5}(\gamma_a)]'_{\gamma_a=jx} &\equiv -e^{-jx} \left[\frac{4725}{(jx)^6} + \frac{4725}{(jx)^5} + \frac{2205}{(jx)^4} + \frac{630}{(jx)^3} + \frac{120}{(jx)^2} + \frac{15}{jx} + 1 \right] \\ &\equiv \left\{ \left[\left(\frac{4725}{x^6} - \frac{2205}{x^4} + \frac{120}{x^2} - 1 \right) \cos x + \left(\frac{4725}{x^5} - \frac{630}{x^3} + \frac{15}{x} \right) \sin x \right] \right. \\ &\left. - j \left[\left(\frac{4725}{x^6} - \frac{2205}{x^4} + \frac{120}{x^2} - 1 \right) \sin x - \left(\frac{4725}{x^5} - \frac{630}{x^3} + \frac{15}{x} \right) \cos x \right] \right\} . \end{aligned} \quad (133)$$

Substituting, as usual, these two relations into equation (116) will give us

$$\begin{aligned} 0 &= j \left[\left(\frac{4725}{x^6} - \frac{2205}{x^4} + \frac{120}{x^2} - 1 \right) \left(\frac{4725}{y^6} - \frac{2205}{y^4} + \frac{120}{y^2} - 1 \right) \right. \\ &\quad \left. + \left(\frac{4725}{x^5} - \frac{630}{x^3} + \frac{15}{x} \right) \left(\frac{4725}{y^5} - \frac{630}{y^3} + \frac{15}{y} \right) \right] \sin(x - y) \\ &- \left[\left(\frac{4725}{x^5} - \frac{630}{x^3} + \frac{15}{x} \right) \left(\frac{4725}{y^6} - \frac{2205}{y^4} + \frac{120}{y^2} - 1 \right) \right. \\ &\quad \left. - \left(\frac{4725}{x^6} - \frac{2205}{x^4} + \frac{120}{x^2} - 1 \right) \left(\frac{4725}{y^5} - \frac{630}{y^3} + \frac{15}{y} \right) \right] \cos(x - y) , \end{aligned}$$

which can be manipulated to the relation

$$\tan[(1 - R)x] = 15x \left[\frac{315 - 42x^2 + x^4}{4725 - 2205x^2 + 120x^4 - x^6} - \frac{R(315 - 42R^2x^2 + R^4x^4)}{4725 - 2205R^2x^2 + 120R^4x^4 - R^6x^6} \right] \quad (134)$$

$$+ [1 + 225R^2(315 - 42x^2 + 15x^4)(315 - 42R^2x^2 + 15R^4x^4)]$$

$$+ (4725 - 2205x^2 + 120x^4 - x^6)(4725 - 2205R^2x^2 + 120R^4x^4 - R^6x^6) \equiv g_5(R;x) .$$

As we can anticipate at this stage of the discussion, $g_5(R;x)$ is a ratio of two polynomials. Its denominator is a sixth-degree polynomial in x^2 . It has as its numerator the product of x and a quintic in x^2 . Again it would appear that we have to deal with a higher degree of complexity than experienced earlier in the properties of the two functions that generate the eigenvalues. For reference purposes we give the reduced form of $g_5(R;x)$:

$$\begin{aligned} g_5(R;x) \equiv & (1 - R)x[1,460,025 - 4,725(42 - 5R + 42R^2)x^2 + 945(5 - 35R + 63R^2 \\ & - 35R^3 + 5R^4)x^4 + 15R(25 - 124R + 212R^2 - 124R^3 + 23R^4)x^6 - 6R^3(7 - 13R + 7R^2)x^8 \\ & + R^4x^{10}] + [1,460,025 - 99,225(7 - 15R + 7R^2)x^2 + 945(40 - 210R + 343R^2 - 210R^3 \\ & + 40R^4)x^4 - 305(1 - 225R + 56R^2 - 84R^3 + 56R^4 - 225R^5 + R^6)x^6 + 3R^2(49 - 3,150R \\ & + 320R^2 - 3,150R^3 + 49R^4)x^8 - R^4(8 - 3,375R + 8R^2)x^{10} + R^6x^{12}] . \end{aligned}$$

Again examining the numerator of $g_5(R;x)$, we observe that the maximum number of finite positive roots is four. As usual, g_5 and $\tan(1 - R)x$ and their slopes coincide at the origin. This time, the denominator shows by simple examination that the maximum number of its positive zeros in x^2 is six. However, if we look closely at the coefficient of x^{10} in the denominator, we observe that its sign will be positive if $R > 0.002370$. This corresponds to an extremely small inner sphere. For R values exceeding this ratio just cited, there will be at most four singularities for $g_5(R;x)$ on the positive x -axis. At this time, we choose to ignore the characteristics of the extremely small R case.

Figures 92 through 95, for R from 0.05 to 0.30, display the situation for the range of R where $g_5(R;x)$ possesses four singularities and the number of zeros goes from four to two. Figures 96 through 99 (for $R = 0.40$ to $R = 0.70$) show the characteristics of $g_5(R;x)$ for the range of R where there are only two singularities and the number of positive finite roots goes from two to zero.

The essential behavior of $g_5(R;x)$, $\tan(1 - R)x$, and the eigenvalues is very much like that we have already seen (except for $R < 0.002374$). Figures 100 and 101 for $R = 0.80$ and 0.90 , respectively, are now quite familiar to us for the situation where $g_5(R;x)$ has no singularities.

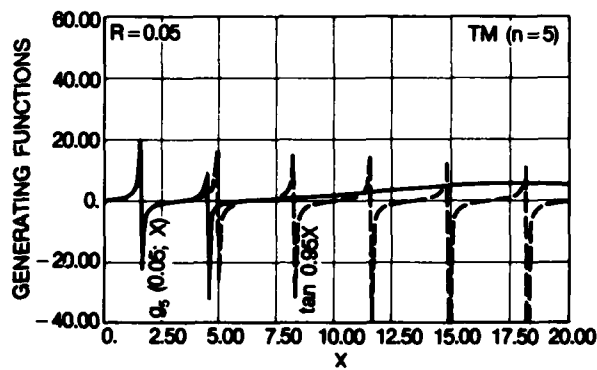


Figure 92. Generating functions for $\gamma_{5p}^{(2)}$ with $R = 0.05$.

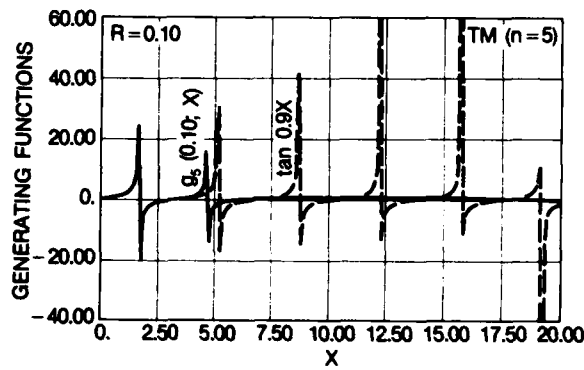


Figure 93. Generating functions for $\gamma_{5p}^{(2)}$ with $R = 0.10$.

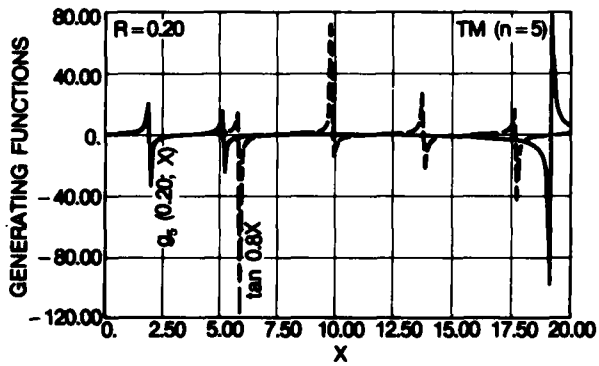


Figure 94. Generating functions for $\gamma_{5p}^{(2)}$ with $R = 0.20$.

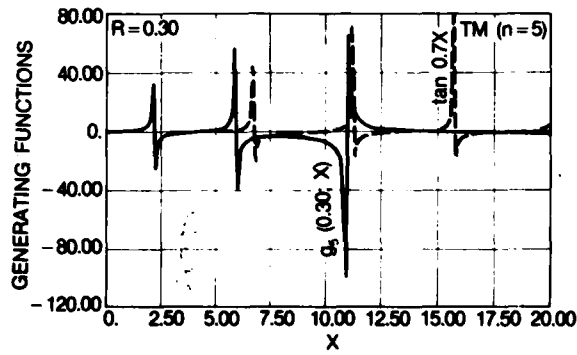


Figure 95. Generating functions for $\gamma_{5p}^{(2)}$ with $R = 0.30$.

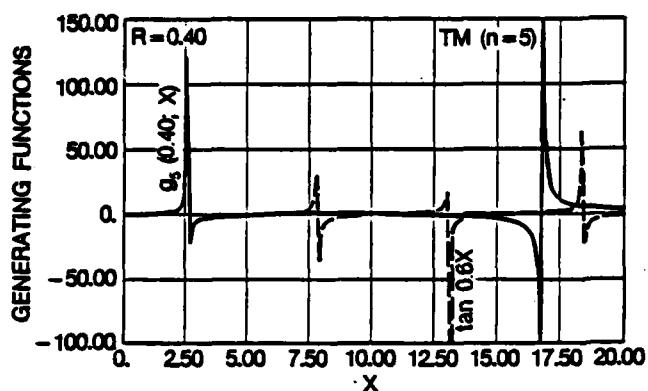


Figure 96. Generating functions for $\gamma_{5p}^{(2)}$ with $R = 0.40$.

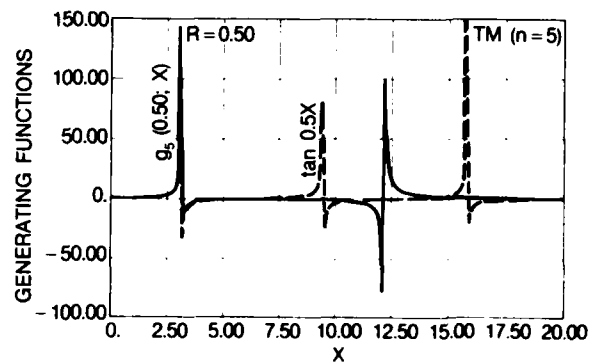


Figure 97. Generating functions for $\gamma_{5p}^{(2)}$ with $R = 0.50$.

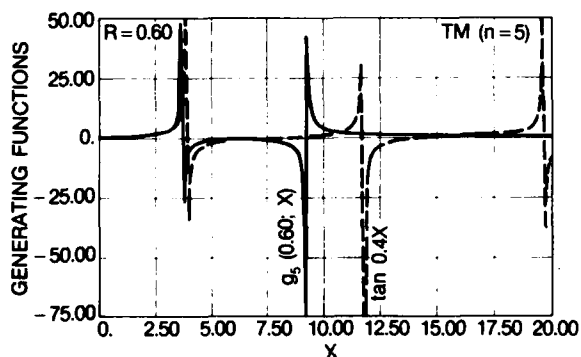


Figure 98. Generating functions for $\gamma_{5p}^{(2)}$ with $R = 0.60$.

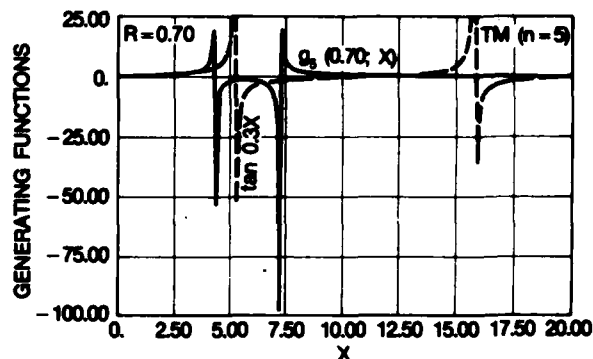


Figure 99. Generating functions for $\gamma_{5p}^{(2)}$ with $R = 0.70$.

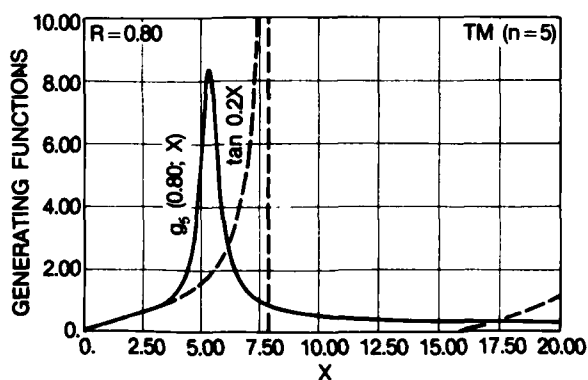


Figure 100. Generating functions for $\gamma_{5p}^{(2)}$ with $R = 0.80$.

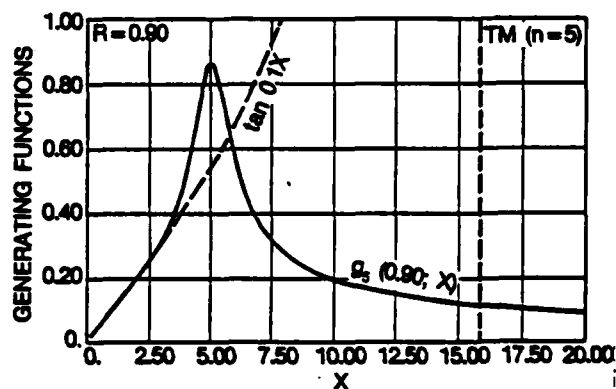


Figure 101. Generating functions for $\gamma_{5p}^{(2)}$ with $R = 0.90$.

3.4 Summary Discussion of Eigenvalues

In the preceding section we presented in various degrees of extensive detail the behavior of the appropriate functions whose intersections yield the eigenvalues for a large number of the lower-lying TE and TM modes. We observe that as the order index n increased, invariably the functions $f_n(R;x)$ and $g_n(R;x)$ became more complex. Where we could, we merely referred to common characteristics that appeared for lower orders, which may seem to imply serious omission of detail in the discussion. Fortunately, the resulting discussion should be quite adequate when one properly carries over the portions of earlier detailed discussions. These discussions of each individual case and the large number of accompanying illustrations should be ample enough resources to establish that the eigenvalues can be determined analytically with an investment of effort of modest difficulty at best. It should be noted, however, that although the functions f_n and g_n may present themselves as somewhat formidable obstacles for determining the eigenvalues, this is certainly not the actual situation, except for a small number of eigenvalues. Even this small set can be made tractable with additional analytic effort. In general, once any eigenvalue, say the p^{th} , $\gamma_{np}^{(j)}$, is found for fixed j and n , good approximate values of the others for that j, n can be readily determined. This is a consequence of the very close approximation to periodicity that the set displays. This property is evident in figures 102 and 103. Figure 102 displays the manner in which the TM eigenvalues $(\gamma_{np}^{(2)})_a$ vary with R , the ratio of inner to outer radii for the non-lossy dielectric, where n goes from 1 to 5. The corresponding situation for the TE eigenvalues $(\gamma_{np}^{(1)})_a$ for n from 1 to 4 is shown in figure 103. In the interest of clarity, these sets of eigenvalues were divided up and displayed as shown in these two figures. Most of the numerical values from which the curves were obtained are given in table 1. In appendix B we present the computer program that generated the curves in the figures and the values in table 1.

We have already mentioned the approximate periodicity with p for given j and n that the eigenvalues display. Next we point out that the proper behavior is displayed by the $\gamma_{np}^{(j)}(R)$ as R decreases; i.e., they go over smoothly to the $R = 0$ or empty spherical cavity modes given, for example, by Harrington.⁴

⁴R. F. Harrington, *Time-Harmonic Electromagnetic Fields*, Tables 6.1 and 6.2, McGraw-Hill Book Co., Inc., NY (1961), 270.

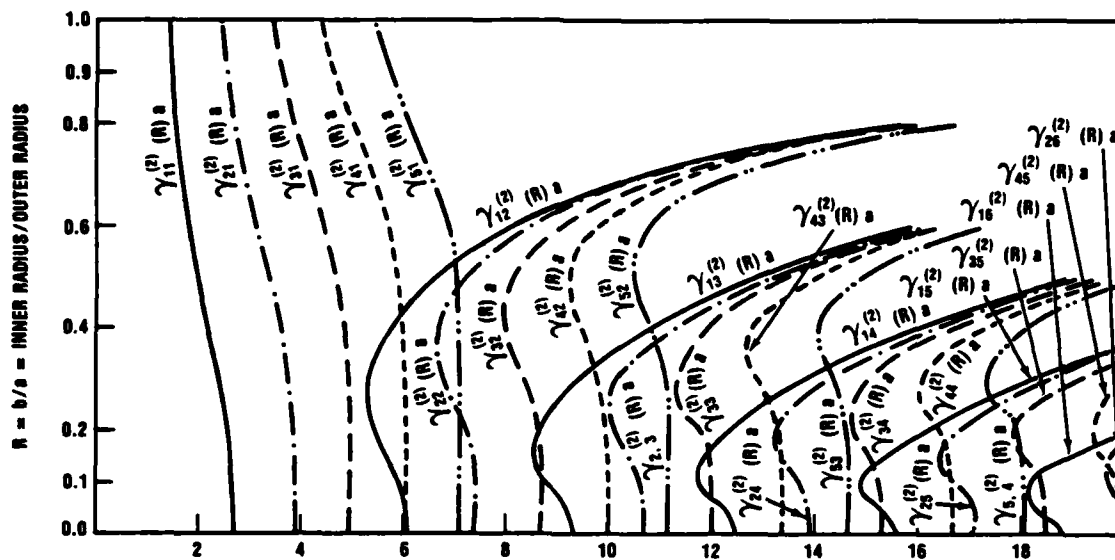


Figure 102. TM modes $\gamma_{np}^{(2)}(R)a$ for non-lossy concentric spherical cavity.

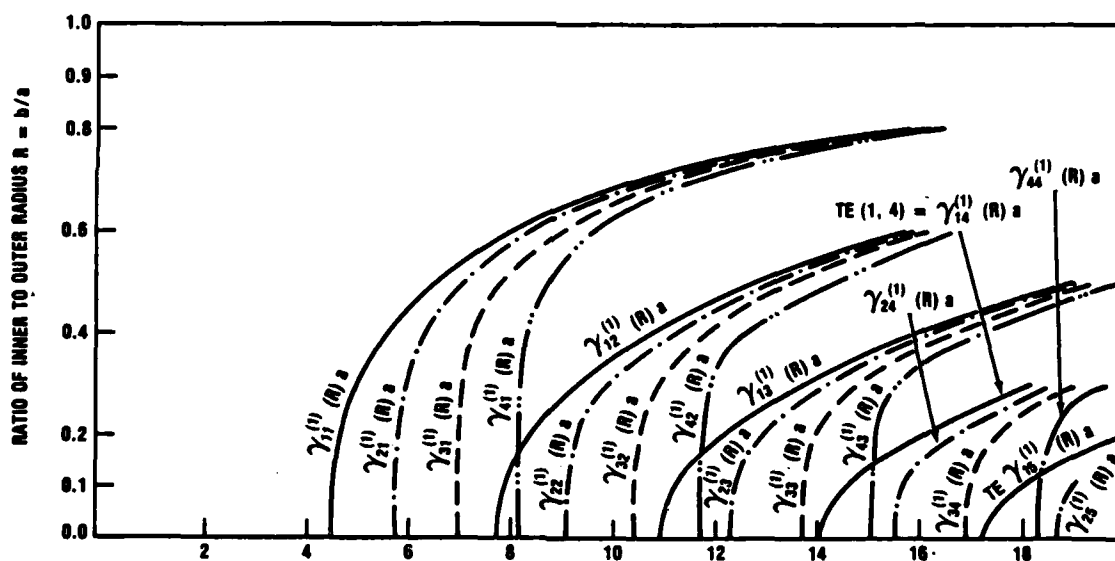


Figure 103. TE modes $\gamma_{np}^{(1)}(R)a$ for non-lossy concentric spherical cavity.

TABLE 1. NUMERICAL VALUES OF THE CONCENTRIC SPHERICAL CAVITY
EIGENVALUES $\gamma_{np}^{(j)}(R) \equiv x_{np}^{(j)}(R)$ (FOR VALUES NOT EXCEEDING 20)

TABLE 1a. THE TE EIGENVALUES $x_{np}^{(1)}(R)$

n = 1	p = 1	p = 2	p = 3	p = 4	p = 5
R = 0.10	4.52229	7.84656	11.18355	14.55528	17.95607
R = 0.20	4.68640	8.37806	12.16588	16.00839	19.88013
R = 0.30	5.04272	9.31415	13.70082	18.13297	
R = 0.40	5.63899	10.69922	15.86357		
R = 0.50	6.57200	12.72134	18.95438		
R = 0.60	8.05525	15.81259			
R = 0.70	10.60490				
R = 0.80	15.78670				

n = 2	p = 1	p = 2	p = 3	p = 4	p = 5
R = 0.05	5.76350	9.09544	12.32478	15.52005	18.70149
R = 0.10	5.76489	9.10671	12.36709	15.62634	18.90949
R = 0.20	5.79965	9.31046	12.90198	16.59799	
R = 0.30	5.96125	9.95545	14.16502	18.49099	
R = 0.40	6.35744	11.14065	16.17099		
R = 0.50	7.11156	13.02612	19.16249		
R = 0.60	8.44278	16.01949			
R = 0.70	10.86580				
R = 0.80	15.94308				

n = 3	p = 1	p = 2	p = 3	p = 4	p = 5
R = 0.05	6.98792	10.41712	13.69806	16.92349	
R = 0.10	6.98800	10.41787	13.70239	16.93949	
R = 0.20	6.99344	10.47287	13.91692	17.45049	
R = 0.30	7.05135	10.83867	14.83834	19.01999	
R = 0.40	7.28038	11.77298	16.62299		
R = 0.50	7.84504	13.47112	19.47099		
R = 0.60	8.99127	16.32599			
R = 0.70	11.24556				
R = 0.80	16.17449				

n = 4	p = 1	p = 2	p = 3	p = 4	p = 5
R = 0.05	8.18256	11.70491	15.03967	18.30099	
R = 0.10	8.18256	11.70495	15.03998	18.30249	
R = 0.20	8.18328	11.71655	15.10656	18.51699	
R = 0.30	8.20089	11.89008	15.69443	19.70949	
R = 0.40	8.31928	12.56665	17.21049		
R = 0.50	8.71681	14.04366	19.87549		
R = 0.60	9.67169	16.72599			
R = 0.70	11.73234				
R = 0.80	16.47849				

TABLE 1. NUMERICAL VALUES OF THE CONCENTRIC SPHERICAL CAVITY EIGENVALUES
 $\gamma_{np}^{(j)}(R) \equiv x_{np}^{(j)}(R)$ (FOR VALUES NOT EXCEEDING 20) (Cont'd)

TABLE 1b. THE TM EIGENVALUES $x_{np}^{(2)}(R)$

n = 1	p = 1	p = 2	p = 3	p = 4	p = 5	p = 6
R = 0.05	2.74162	6.09682	9.24655	12.31915	15.33189	18.31399
R = 0.10	2.72705	5.96203	8.86383	11.77078	14.87325	18.13634
R = 0.15	2.68855	5.69396	8.55252	11.80250	15.28791	18.86890
R = 0.20	2.61986	5.44453	8.60724	12.24786	16.04527	19.89957
R = 0.30	2.41244	5.34975	9.37465	13.72043	18.14151	
R = 0.35	2.29633	5.49884	9.97643	14.70131	19.48265	
R = 0.40	2.18403	5.75930	10.71862	15.86959		
R = 0.50	1.9846	6.6185	12.7281	18.9565		
R = 0.60	1.82158	8.07212	15.81490			
R = 0.70	1.68939	10.61018				
R = 0.80	1.58100	15.78800				
R = 0.90	1.49067					
R = 0.99	1.42100					

n = 2	p = 1	p = 2	p = 3	p = 4	p = 5	p = 6
R = 0.05	3.87022	7.44284	10.71155	13.91527	17.08799	
R = 0.10	3.86985	7.43550	10.67031	13.77915	16.77725	19.73127
R = 0.15	3.86737	7.39009	10.45973	13.35562	16.40299	19.70049
R = 0.20	3.85861	7.25623	10.12745	13.23926	16.74256	
R = 0.30	3.79300	6.82286	10.17676	14.23332	18.51972	
R = 0.40	3.62547	6.73938	11.20525	16.19031		
R = 0.50	3.38587	7.26026	13.04726	19.16882		
R = 0.56	3.23654	7.89972	14.65640			
R = 0.60	3.14079	8.49565	16.02691			
R = 0.70	2.92296	10.88207				
R = 0.80	2.73793	15.94677				
R = 0.90	2.58197					
R = 0.99	2.46150					

n = 3	p = 1	p = 2	p = 3	p = 4	p = 5	p = 6
R = 0.05	4.97340	8.72175	12.06357	15.31344	18.52349	
R = 0.10	4.97341	8.72142	12.06080	15.30030	18.47949	
R = 0.15	4.97327	8.71675	12.02450	15.15368	18.12549	
R = 0.20	4.97235	8.68951	11.85647	14.77432	17.86149	
R = 0.30	4.95761	8.41775	11.37826	15.00803	19.08649	
R = 0.40	4.88138	8.03405	11.92239	16.66549		
R = 0.50	4.68865	8.16066	13.51647	19.48399		
R = 0.60	4.41209	9.10303	16.34049			
R = 0.70	4.12700	11.27912				
R = 0.80	3.87106	16.18199				
R = 0.90	3.65137					
R = 0.99	3.48150					

TABLE 1. NUMERICAL VALUES OF THE CONCENTRIC SPHERICAL CAVITY EIGENVALUES
 $\gamma_{np}^{(j)}(R)a \equiv x_{np}^{(j)}(R)$ (FOR VALUES NOT EXCEEDING 20) (Cont'd)

TABLE 1b. THE TM EIGENVALUES $x_{np}^{(2)}(R)$

n = 4	p = 1	p = 2	p = 3	p = 4	p = 5
R = 0.05	6.06194	9.96754	13.38012	16.67399	19.91499
R = 0.10	6.06194	9.96753	13.37997	16.67299	19.91099
R = 0.20	6.06185	9.96279	13.33330	16.46049	19.40899
R = 0.30	6.05884	9.85890	12.86632	16.05899	19.84549
R = 0.40	6.03032	9.46274	12.86093	17.29099	
R = 0.50	5.90808	9.25947	14.12652	19.89849	
R = 0.60	5.64693	9.86902	16.75099		
R = 0.70	5.31651	11.79056			
R = 0.80	4.99586	16.49099			
R = 0.90	4.71383				
R = 0.99	4.49450				

n = 5	p = 1	p = 2	p = 3	p = 4	p = 5
R = 0.05	7.14022	11.18899	14.67012	18.00849	
R = 0.10	7.14022	11.18898	14.67010	18.00799	
R = 0.20	7.14021	11.18833	14.66128	17.95149	
R = 0.30	7.13963	11.15620	14.40138	17.38199	
R = 0.40	7.12981	10.88525	14.00492	18.06249	
R = 0.50	7.06229	10.49027	14.86804		
R = 0.60	6.84586	10.76781	17.25299		
R = 0.70	6.49409	12.40438			
R = 0.80	6.11614	16.87000			
R = 0.90	5.77313				
R = 0.99	5.50500				

The variation of the eigenvalues with R displays a very rich diversity of characteristics. We shall emphasize only a restricted number of these, which is far from exhaustive. One immediately evident characteristic is the grouping of the eigenvalues into families of the form $\gamma_{np}^{(j)}(R)$ for j and p fixed and the index n varying. If we fix our attention on the spectral group $\gamma_{n1}^{(1)}(R)a$, we observe for these TE eigenvalues that as R increases from zero the eigenvalues vary quite slowly at first. The larger the value of the index n , the greater the range of R with this slow variation. This behavior is repeated for the family belonging to $p = 2$. Now, however, there is a smaller range of R over which the variation in $\gamma_{n2}^{(1)}(R)a$ is slow. As p increases, we observe in figure 103 the continuation of this trend. Immediately following this very slow variation of eigenvalue with increasing R , we find in each case in figure 103 a region we call the "knee" over which this rate of change speeds up from slow to rapid variation with R . Once past the knee of the curve, $\gamma_{np}^{(1)}a$ increases much more slowly as R increases. What we have here is a rough qualitative division of the concentric spherical cavity TE eigenvalues into three regimes corresponding to a small interior sphere, an intermediate sized interior sphere, and lastly a large enclosed sphere. Before looking at figure 102 for the TM eigenvalues, we note that all the $\gamma_{np}^{(1)}(R)$ always increase with R whether variation is rapid or slow.

Now let us examine the manner in which the TM eigenvalues vary as R is varied. The same general characteristics are displayed by the $\gamma_{np}^{(2)}$ for $p \geq 2$, i.e., they form distinct families for each p ; also they indicate that

three eigenvalue regimes can be identified which correspond to small, intermediate, or large inner spheres. Thus we see, for the $p \geq 2$ families, at first a slow change in $\gamma_{np}^{(2)}$ as R increases from zero. The larger n is, the larger is this range of R . This is followed by the intermediate region in which this variation goes from slow to quite rapid and then in turn the final region of rapid variation in $\gamma_{np}^{(2)}$ with R . In the TM case we have a different type of behavior that is quite evident in figure 102. Unlike the simple knee of the TE eigenvalue trajectory, we now have a "nose" in the intermediate TM region. This feature indicates the presence of an interesting property, namely that for $p \geq 2$ as the inner sphere radius grows in size with the outer radius fixed, the TM eigenfrequency decreases initially (for a not insignificant range of R in many cases) and then later increases with R as one would expect. The behavior for large R is that where the inner sphere is quite close to the outer sphere. It would seem to be quite natural in this situation that the eigenfrequencies be such that multiples of half-wavelengths span the gap between inner and outer spheres. For the TE modes (see fig. 103) and for the $p \geq 2$ TM modes (see fig. 102) this is indeed the case.

For R large, the conducting boundary surfaces are close together and parallel. In any small region containing portions of these boundary surfaces, we have what approximately looks like a parallel-plate capacitor system. We should have some natural field distribution that looks like the parallel-plate system. The TE solutions cannot satisfy this. What we do observe is that the TM family of $\gamma_{n1}^{(2)}(R)$ values fills the bill here. Each trajectory in this family starts out at the empty spherical cavity eigenvalue (i.e., for $R = 0$) and then, as R increases, decreases in the familiar manner initially. Now however, $\gamma_{n1}^{(2)}(R)$ continues to decrease as R continues to increase. This behavior is strikingly unlike all the other trajectories of eigenvalues.

Another feature of considerable significance is readily evident in figure 102 for the TM eigenvalues and also in figure 103 for the TE eigenvalues. Whenever the trajectories intersect we have degeneracy present. This degeneracy is present in addition to the usual degeneracy associated with the angular variables θ and ϕ . It should be recalled that this property does not exist for the empty spherical cavity. For the systems that we shall be discussing in subsequent reports, that are derived from the concentric spherical cavity problem, this feature shall play a very important role. Note that for a given value of R we observe at most a double degeneracy occurring.

Some further interesting features that can be extracted from figures 102 and 103 are the ordering of the eigenvalues. Clearly, for very small R values, the ordering is precisely that of the empty spherical cavity. As R increases, we can observe switching of order of pairs of eigenvalues as the trajectories cross. In addition to this rearranging of the ordering of the eigenvalues due to degeneracy, another contributing factor enters. This is the result of the "nose" region in the TM trajectories which move the eigenvalues to lower values with increasing R ; e.g., at $R = 0.3$ the TM value of $\gamma_{12}^{(2)}(0.3)$ lies lower than the TE value of $\gamma_{21}^{(1)}(0.3)$.

Although we have explicitly evaluated a rather large number of eigenvalues $\gamma_{np}^{(1)}(R)$ up to the value 20, we have by no means determined them all. We do have, however, all those for values up to about 6.50. Clearly, the density of eigenvalues increases rather quickly.

Further examination of the eigenvalue trajectories will reveal many other physically important features. Since each of these will be dealt with in subsequent reports, we shall defer any further discussion until they appear.

The cavity field distributions have been obtained for each of the modes in table 1. Discussion in depth of the field details constitutes the next report in the sequence.

APPENDIX A.--ORTHOGONALITY OF THE ELECTRIC FIELD EIGENVECTORS $E_{n\mathbf{p}\mathbf{m}}^{(j, \mathbf{e})}(\mathbf{r})$

APPENDIX A

We shall demonstrate here the orthogonality relation for the electric eigenvector modes. Consider first the TE modes themselves. We have, then, upon integrating over the concentric spherical cavity,

$$\begin{aligned} & \iiint d\tau(\vec{r}) \vec{E}_{n'p'm'}^{(1,0)}(\vec{r}) \cdot \vec{E}_{n'p'm'}^{(1,0)}(\vec{r}) \\ &= \int_a^b dr r^2 \int_0^\pi d\theta \sin \theta \int_0^{2\pi} d\phi [\vec{\nabla} \times (\vec{r} \phi_{n'p'm'}^{(0)})] [\vec{\nabla} \times (\vec{r} \phi_{n'p'm'}^{(0)})] , \end{aligned}$$

which by equation (24) becomes

$$\begin{aligned} &= \int_a^b dr r^2 \int_0^\pi d\theta \sin \theta \int_0^{2\pi} d\phi \\ &\times \left\{ \frac{1}{\sin^2 \theta} \frac{\partial \phi_{n'p'm'}^{(0)}(\vec{r})}{\partial \phi} \frac{\partial \phi_{n'p'm'}^{(0)}(\vec{r})}{\partial \phi} + \frac{\partial \phi_{n'p'm'}^{(0)}(\vec{r})}{\partial \theta} \frac{\partial \phi_{n'p'm'}^{(0)}(\vec{r})}{\partial \theta} \right\} . \end{aligned}$$

Let us focus on the integration over ϕ . We have

$$\begin{aligned} &\frac{1}{\sin^2 \theta} \int_0^{2\pi} d\phi \frac{\partial \phi_{n'p'm'}^{(0)}}{\partial \phi} \frac{\partial \phi_{n'p'm'}^{(0)}}{\partial \phi} = \frac{mm'}{\sin^2 \theta} \int_0^{2\pi} d\phi \phi_{n'p'm'}^{(0)} \phi_{n'p'm'}^{(0)} = \frac{mm'}{\sin^2 \theta} \phi_{np}(\gamma_{np}^{(1)} r) \\ &\times \phi_{n'p'}(\gamma_{n'p'}^{(1)} r) P_{nm}(\cos \theta) P_{n'm'}(\cos \theta) \int_0^{2\pi} d\ell \cos m\ell \cos \ell m' \end{aligned}$$

which becomes

$$= \pi \delta_{mm'} \frac{m^2}{\sin^2 \theta} \phi_{np}(\gamma_{np}^{(1)} r) \phi_{n'p'}(\gamma_{n'p'}^{(1)} r) P_{nm}(\cos \theta) P_{n'm'}(\cos \theta)$$

also

$$\begin{aligned} &\int_0^{2\pi} d\ell \frac{\partial \phi_{n'p'm'}^{(0)}}{\partial \theta} \frac{\partial \phi_{n'p'm'}^{(0)}}{\partial \theta} = \phi_{np}(\gamma_{np}^{(1)} r) \phi_{n'p'}(\gamma_{n'p'}^{(1)} r) \frac{dP_{nm}(\cos \theta)}{d\theta} \frac{dP_{n'm'}(\cos \theta)}{d\theta} \\ &\cdot \int_0^{2\pi} d\ell \sin m\ell \sin m'\ell = \delta_{mm'} \pi \phi_{np}(\gamma_{np}^{(1)} r) \phi_{n'p'}(\gamma_{n'p'}^{(1)} r) \frac{dP_{nm}(\cos \theta)}{d\theta} \frac{dP_{n'm'}(\cos \theta)}{d\theta} \end{aligned}$$

Combining the two pieces we obtain after integrating over ϕ

$$\pi \delta_{mm'} \int_a^b dr r^2 \phi_{np}(\gamma_{np}^{(1)} r) \phi_{n'p'}(\gamma_{n'p'}^{(1)} r) \int_0^\pi d\theta \sin \theta \left\{ \frac{m^2}{\sin^2 \theta} P_{nm}(\cos \theta) P_{n'm'}(\cos \theta) + \frac{dP_{nm}(\cos \theta)}{d\theta} \frac{dP_{n'm'}(\cos \theta)}{d\theta} \right\}.$$

However, the integral over θ is given in Stratton¹ as

$$\delta_{nn'} \frac{2n(n+1)}{2n+1} \frac{(n+m)!}{(n-m)!}.$$

We then have remaining integration over the radius, namely,

$$\pi \delta_{nn'} \delta_{mm'} \frac{2n(n+1)}{2n+1} \frac{(n-m)!}{(n+m)!} \int_a^b dr r^2 \phi_{np}(\gamma_{np}^{(1)} r) \phi_{n'p'}(\gamma_{n'p'}^{(1)} r).$$

Now $\phi_{np}(j\gamma_{np}^{(1)} r)$ satisfies the differential equation

$$0 = (j\gamma_{np}^{(1)} r)^2 \frac{d^2}{d(j\gamma_{np}^{(1)} r)^2} \phi_{np}(j\gamma_{np}^{(1)} r) + 2(j\gamma_{np}^{(1)} r) \frac{d}{d(j\gamma_{np}^{(1)} r)} \phi_{np}(j\gamma_{np}^{(1)} r) - [(j\gamma_{np}^{(1)} r)^2 + n(n+1)] \phi_{np}(j\gamma_{np}^{(1)} r),$$

and $\phi_{n'p'}(j\gamma_{n'p'}^{(1)} r)$ satisfies the equation

$$0 = (j\gamma_{n'p'}^{(1)} r)^2 \frac{d^2}{d(j\gamma_{n'p'}^{(1)} r)^2} \phi_{n'p'}(j\gamma_{n'p'}^{(1)} r) + 2(j\gamma_{n'p'}^{(1)} r) \frac{d}{d(j\gamma_{n'p'}^{(1)} r)} \phi_{n'p'}(j\gamma_{n'p'}^{(1)} r) - [(j\gamma_{n'p'}^{(1)} r)^2 + n'(n'+1)] \phi_{n'p'}(j\gamma_{n'p'}^{(1)} r).$$

Then multiplying the first of these by $\phi_{n'p'}(j\gamma_{n'p'}^{(1)} r)$ and the second by $\phi_{np}(j\gamma_{np}^{(1)} r)$ and subtracting will give us, after some further reduction,

¹J. Stratton, *Electromagnetic Theory*, McGraw-Hill Book Co., Inc., NY (1941), 417.

APPENDIX A

$$\begin{aligned}
 0 = & \phi_{np'}(j\gamma_{np'}^{(1)}r) \frac{d^2\phi_{np}(j\gamma_{np}^{(1)}r)}{dr^2} - \phi_{np}(j\gamma_{np}^{(1)}r) \frac{d^2\phi_{np'}(j\gamma_{np'}^{(1)}r)}{dr^2} \\
 & + \frac{2}{r} \phi_{np'}(j\gamma_{np'}^{(1)}r) \frac{d\phi_{np}(j\gamma_{np}^{(1)}r)}{dr} - \frac{2}{r} \phi_{np}(j\gamma_{np}^{(1)}r) \frac{d\phi_{np'}(j\gamma_{np'}^{(1)}r)}{dr} \\
 & + \phi_{np'}(j\gamma_{np'}^{(1)}r) \phi_{np}(j\gamma_{np}^{(1)}r) [(j\gamma_{np'}^{(1)})^2 - (j\gamma_{np}^{(1)})^2] .
 \end{aligned}$$

Integrating this over r from a to b we have for the first two terms

$$\begin{aligned}
 & \int_a^b dr r^2 \left\{ \phi_{np'}(j\gamma_{np'}^{(1)}r) \frac{d^2\phi_{np}(j\gamma_{np}^{(1)}r)}{dr^2} - \phi_{np}(j\gamma_{np}^{(1)}r) \frac{d^2\phi_{np'}(j\gamma_{np'}^{(1)}r)}{dr^2} \right\} = \\
 & \left\{ r^2 \left[\phi_{np'}(j\gamma_{np'}^{(1)}r) \frac{d\phi_{np}(j\gamma_{np}^{(1)}r)}{dr} - \phi_{np}(j\gamma_{np}^{(1)}r) \frac{d\phi_{np'}(j\gamma_{np'}^{(1)}r)}{dr} \right] \right\}_{r=a}^{r=b} \\
 & - 2 \int_a^b dr r \left\{ \phi_{np'}(j\gamma_{np'}^{(1)}r) \frac{d\phi_{np}(j\gamma_{np}^{(1)}r)}{dr} - \phi_{np}(j\gamma_{np}^{(1)}r) \frac{d\phi_{np'}(j\gamma_{np'}^{(1)}r)}{dr} \right\} .
 \end{aligned}$$

The first term on the right-hand side vanishes since the $\phi_{np}(j\gamma_{np}^{(1)}r)$ vanish at the cavity boundaries. The remaining term cancels the second pair of terms in our original integral over r . Thus, we have left

$$[(j\gamma_{np'}^{(1)})^2 - (j\gamma_{np}^{(1)})^2] \int_a^b dr r^2 \phi_{np'}(j\gamma_{np'}^{(1)}r) \phi_{np}(j\gamma_{np}^{(1)}r) = 0 .$$

For $p' \neq p$ the scalar functions are orthogonal and hence

$$\iiint_{\text{conc spher cavity}} d\tau(\vec{r}) \vec{E}_{npm}^{(1,o)}(\vec{r}) \cdot \vec{E}_{n'p'm}^{(1,o)}(\vec{r}) = [\Omega_{npm}^{(1,o)}]^2 \delta_{nn'} \delta_{pp'} \delta_{mm} .$$

Next we consider the TE even modes. By following the same steps we find

$$\iiint d\tau(\vec{r}) \vec{E}_{npm}^{(1,e)}(\vec{r}) \cdot \vec{E}_{n'p'm}^{(1,e)}(\vec{r}) = [\Omega_{npm}^{(1,e)}]^2 \delta_{nn'} \delta_{pp'} \delta_{mm} .$$

Now for the TM odd eigenvectors:

$$\begin{aligned} & \iiint d\mathbf{r}(\vec{r}) \vec{E}_{\text{npm}}^{(2,0)}(\vec{r}) \cdot \vec{E}_{\text{n}'\text{p}'\text{m}'}^{(2,0)}(\vec{r}) \\ &= \int_a^b dr r^2 \int_0^\pi d\theta \sin \theta \int_0^{2\pi} d\phi \sin \theta \frac{1}{(j\omega\epsilon)^2} \\ &\times [\vec{\nabla} \times \vec{\nabla} \times (\vec{r}\psi_{\text{npm}}^{(0)})] \cdot [\vec{\nabla} \times \vec{\nabla} \times (\vec{r}\psi_{\text{n}'\text{p}'\text{m}'}^{(0)})] . \end{aligned}$$

However, using equation (24) we have

$$\vec{\nabla} \times \vec{\nabla} \times (\vec{r}\psi_{\text{npm}}^{(0)}) = \left(\vec{e}_r \frac{\partial}{\partial r} + \frac{\vec{e}_\theta}{r} \frac{\partial}{\partial \theta} + \frac{\vec{e}_\phi}{r \sin \theta} \frac{\partial}{\partial \phi} \right) \times \left(\frac{\vec{e}_\theta}{\sin \theta} \frac{\partial \psi_{\text{npm}}^{(0)}}{\partial \phi} - \vec{e}_\phi \frac{\partial \psi_{\text{npm}}^{(0)}}{\partial \theta} \right) ,$$

which after some manipulation reduces to

$$\begin{aligned} \vec{\nabla} \times \vec{\nabla} \times (\vec{r}\psi_{\text{npm}}^{(0)}) &= \vec{e}_r \left\{ \frac{\partial^2}{\partial r^2} [\vec{r}\psi_{\text{npm}}^{(0)}] - (\gamma_{\text{np}}^{(2)})^2 [\vec{r}\psi_{\text{npm}}^{(0)}] \right\} \\ &+ \vec{e}_\theta \frac{\partial}{\partial \theta} \left(\frac{1}{r} \frac{\partial}{\partial r} [\vec{r}\psi_{\text{npm}}^{(0)}] \right) + \frac{\vec{e}_\phi}{\sin \theta} \frac{\partial}{\partial \phi} \left(\frac{1}{r} \frac{\partial}{\partial r} [\vec{r}\psi_{\text{npm}}^{(0)}] \right) . \end{aligned}$$

Then we have the relation

$$\begin{aligned} (j\omega\epsilon)^2 \vec{E}_{\text{npm}}^{(2,0)}(\vec{r}) \cdot \vec{E}_{\text{n}'\text{p}'\text{m}'}^{(2,0)}(\vec{r}) &= \left\{ \frac{\partial^2}{\partial r^2} [\vec{r}\psi_{\text{npm}}^{(0)}] - (\gamma_{\text{np}}^{(2)})^2 [\vec{r}\psi_{\text{npm}}^{(0)}] \right\} \\ &\times \left\{ \frac{\partial^2}{\partial r^2} [\vec{r}\psi_{\text{n}'\text{p}'\text{m}'}^{(0)}] - (\gamma_{\text{n}'\text{p}'}^{(2)}) [\vec{r}\psi_{\text{n}'\text{p}'\text{m}'}^{(0)}] \right\} + \left\{ \frac{\partial}{\partial \theta} \left(\frac{1}{r} \frac{\partial}{\partial r} [\vec{r}\psi_{\text{npm}}^{(0)}] \right) \right\} \\ &\times \left\{ \frac{\partial}{\partial \theta} \left(\frac{1}{r} \frac{\partial}{\partial r} [\vec{r}\psi_{\text{n}'\text{p}'\text{m}'}^{(0)}] \right) \right\} + \frac{1}{\sin^2 \theta} \left\{ \frac{\partial}{\partial \phi} \left(\frac{1}{r} \frac{\partial}{\partial r} [\vec{r}\psi_{\text{npm}}^{(0)}] \right) \right\} \\ &\cdot \left\{ \frac{\partial}{\partial \phi} \left(\frac{1}{r} \frac{\partial}{\partial r} [\vec{r}\psi_{\text{n}'\text{p}'\text{m}'}^{(0)}] \right) \right\} \end{aligned}$$

or, more explicitly,

APPENDIX A

$$\begin{aligned}
 & \left\{ \frac{d^2}{dr^2} [r\psi_{np}(j\gamma_{np}^{(2)}r)] - [\gamma_{np}^{(2)}]^2 [r\psi_{np}(j\gamma_{np}^{(2)}r)] \right\} \left\{ \frac{d^2}{dr^2} [r\psi_{n'p'}(j\gamma_{n'p'}^{(2)}r)] \right. \\
 & \left. - [\gamma_{n'p'}^{(2)}]^2 [r\psi_{n'p'}(j\gamma_{n'p'}^{(2)}r)] \right\} \cdot P_{nm}(\cos \theta) P_{n'm'}(\cos \theta) \sin m\phi \sin m'\phi \\
 & + \left\{ \frac{1}{r} \frac{d}{dr} [r\psi_{np}(j\gamma_{np}^{(2)}r)] \right\} \left\{ \frac{1}{r} \frac{d}{dr} [r\psi_{n'p'}(j\gamma_{n'p'}^{(2)}r)] \right\} \cdot \frac{dP_{nm}(\cos \theta)}{d\theta} \\
 & \cdot \frac{dP_{n'm'}(\cos \theta)}{d\theta} \sin m\phi \sin m'\phi + mm' \left\{ \frac{1}{r} \frac{d}{dr} [r\psi_{np}(j\gamma_{np}^{(2)}r)] \right\} \\
 & \cdot \left\{ \frac{1}{r} \frac{d}{dr} [r\psi_{n'p'}(j\gamma_{n'p'}^{(2)}r)] \right\} \cdot P_{nm}(\cos \theta) P_{n'm'}(\cos \theta) \cos m\phi \cos m'\phi .
 \end{aligned}$$

Integration over ϕ gives $\pi\delta_{mm'}$, for each of the first two terms and $\pi m^2\delta_{mm'}$, for the third term. In turn, integration over θ of the sum of the second and third terms gives

$$\frac{2\pi n(n+1)}{2n+1} \frac{(n+m)!}{(n-m)!} \delta_{nn'} \delta_{mm'} ,$$

while integration over θ after ϕ gives

$$\frac{2\pi}{2n+1} \frac{(n+m)!}{(n-m)!} .$$

We have at this stage

$$\begin{aligned}
 (j\omega\epsilon)^2 \iiint d\tau \vec{E}_{n'p'm'}^{(2,0)} \cdot \vec{E}_{np}^{(2,0)} &= \frac{2\pi}{2n+1} \frac{(n+m)!}{(n-m)!} \delta_{nn'} \delta_{mm'} \\
 \times \int_a^b dr r^2 &\left\{ \frac{d^2}{dr^2} [r\psi_{np}(j\gamma_{np}^{(2)}r)] - [\gamma_{np}^{(2)}]^2 [r\psi_{np}(j\gamma_{np}^{(2)}r)] \right\} \\
 &\cdot \left\{ \frac{d^2}{dr^2} [r\psi_{n'p'}(j\gamma_{n'p'}^{(2)}r)] - [\gamma_{n'p'}^{(2)}]^2 [r\psi_{n'p'}(j\gamma_{n'p'}^{(2)}r)] \right\} \\
 + n(n+1) &\left\{ \frac{1}{r} \frac{d}{dr} [r\psi_{np}(j\gamma_{np}^{(2)}r)] \right\} \cdot \left\{ \frac{1}{r} \frac{d}{dr} [r\psi_{n'p'}(j\gamma_{n'p'}^{(2)}r)] \right\} .
 \end{aligned}$$

If we use the differential equation that defines the $\psi_{np}(j\gamma_{np}^{(2)}r)$, namely that of equation (48), we can rewrite the integral on the right-hand side as

$$n(n+1) \int_a^b dr \left\{ n(n+1) \psi_{np}(j\gamma_{np}^{(2)} r) \psi_{np'}(j\gamma_{np'}^{(2)} r) + \frac{d}{dr} [r \psi_{np}(j\gamma_{np}^{(2)} r)] \right. \\ \left. \cdot \frac{d}{dr} [r \psi_{np'}(j\gamma_{np'}^{(2)} r)] \right\}.$$

Consider the integral of the second term which we can evaluate as follows:

$$\int_a^b dr \frac{d}{dr} [r \psi_{np}(j\gamma_{np}^{(2)} r)] \frac{d}{dr} [r \psi_{np'}(j\gamma_{np'}^{(2)} r)] = \\ \left\{ r \psi_{np}(j\gamma_{np}^{(2)} r) \frac{d}{dr} [r \psi_{np'}(j\gamma_{np'}^{(2)} r)] \right\}_{r=a}^{r=b} \\ - \int_a^b dr r \psi_{np}(j\gamma_{np}^{(2)} r) \frac{d^2}{dr^2} [r \psi_{np'}(j\gamma_{np'}^{(2)} r)] = - \int_a^b dr r \psi_{np}(j\gamma_{np}^{(2)} r) \\ \cdot \left\{ [\gamma_{np'}^{(2)}]^2 [r \psi_{np'}(j\gamma_{np'}^{(2)} r)] + \frac{n(n+1)}{r^2} [r \psi_{np'}(j\gamma_{np'}^{(2)} r)] \right\}.$$

Combining the pieces then, we have

$$(j\omega\epsilon)^2 \iiint d\tau \vec{E}_{npm}^{(2,0)}(\vec{r}) \cdot \vec{E}_{n'p'm'}^{(2,0)} = \frac{-2\pi n(n+1)(n+m)!}{(2n+1)(n-m)!} \delta_{nn'} \delta_{mm'} [\gamma_{np'}^{(2)}]^2 \\ \cdot \int_a^b dr r^2 \cdot \psi_{np}(j\gamma_{np}^{(2)} r) \psi_{np'}(j\gamma_{np'}^{(2)} r).$$

Processing this remaining integral exactly as we did the corresponding one for $\phi_{np}\phi_{np'}$, we will find the integral over the radius r from a to b vanishes for $p \neq p'$. Thus, we have

$$\iiint d\tau \vec{E}_{npm}^{(2,0)}(\vec{r}) \cdot \vec{E}_{n'p'm'}^{(2,0)}(\vec{r}) = [\Omega_{npm}^{(2,0)}]^2 \delta_{nn'} \delta_{mm'} \delta_{pp'}.$$

Next we demonstrate orthogonality between the $\vec{E}_{npm}^{(j,0)}$ and the $\vec{E}_{npm}^{(j,e)}$. Thus, consider

$$\iiint d\tau(\vec{r}) \vec{E}_{npm}^{(1,e)}(\vec{r}) \cdot \vec{E}_{n'p'm'}^{(1,0)}(\vec{r}) = \int_a^b dr r^2 \phi_{np}(j\gamma_{np}^{(1)} r) \phi_{n'p'}(j\gamma_{n'p'}^{(1)} r) \int_0^\theta d\theta \sin \theta \\ \cdot \int_a^{2\pi} d\phi \left\{ \frac{-1}{\sin^2 \theta} \cdot m m' P_{nm}(\cos \theta) P_{n'm'}(\cos \theta) \sin m\phi \cos m'\phi \right. \\ \left. + \frac{dP_{nm}(\cos \theta)}{d\theta} \frac{dP_{n'm'}(\cos \theta)}{d\theta} \cos m\phi \sin m'\phi \right\}.$$

APPENDIX A

But

$$\int_0^{2\pi} d\phi \sin m\phi \cos m'\phi = 0 = \int_0^{2\pi} d\phi \cos m\phi \sin m'\phi .$$

A similar result is obtained for $\vec{E}_{npm}^{(2,e)} \cdot \vec{E}_{n'p'm'}^{(2,o)}$. Then we have

$$\iiint d\tau(\vec{r}) \vec{E}_{npm}^{(j,e)}(\vec{r}) \cdot \vec{E}_{n'p'm'}^{(j,o)}(\vec{r}) = 0 , j = 1, 2 .$$

Finally we show orthogonality between the $\vec{E}_{npm}^{(1,)}$ and the $\vec{E}_{npm}^{(2,)}$. Clearly,

$$\iiint d\tau \vec{E}_{npm}^{(1,e)} \cdot \vec{E}_{n'p'm'}^{(2,o)} = 0 = \iiint d\tau \vec{E}_{npm}^{(1,o)} \cdot \vec{E}_{n'p'm'}^{(2,e)} .$$

(This follows immediately from the integration over ϕ .) Continuing,

$$\begin{aligned} \iiint d\tau \vec{E}_{npm}^{(1,o)} \cdot \vec{E}_{n'p'm'}^{(2,o)}(\vec{r}) &= \frac{-1}{j\omega\epsilon} \int_a^b dr r^2 \int_0^\pi d\theta \sin \theta \int_0^{2\pi} d\phi [\vec{\nabla} \times (\vec{r}\phi_{npm}^{(o)})] \\ &\cdot [\vec{\nabla} \times \vec{\nabla} \times (\vec{r}\psi_{n'p'm'}^{(o)})] , \end{aligned}$$

which by equations (24) and (25) in the body of the report becomes

$$\begin{aligned} &= -\frac{1}{j\omega\epsilon} \int_a^b dr r^2 \int_0^\pi d\theta \sin \theta \int_0^{2\pi} d\phi \left\{ \frac{\vec{e}_\theta}{\sin \theta} \frac{\partial \phi_{npm}^{(o)}}{\partial \theta} - \vec{e}_\phi \frac{\partial \phi_{npm}^{(o)}}{\partial \theta} \right\} \\ &\cdot \left\{ -\vec{e}_r \left[\frac{1}{r \sin \theta} \frac{\partial}{\partial \phi} \sin \theta \frac{\partial}{\partial \theta} + \frac{1}{r \sin^2 \theta} \frac{\partial^2}{\partial \phi^2} \right] \psi_{n'p'm'}^{(o)} + \vec{e}_\theta \frac{\partial}{\partial \theta} \frac{1}{r} \right. \\ &\cdot \left. \frac{\partial}{\partial r} [r \psi_{n'p'm'}^{(o)}] + \frac{\vec{e}_\phi}{\sin \theta} \frac{\partial}{\partial \phi} \frac{1}{r} \frac{\partial}{\partial r} [r \psi_{n'p'm'}^{(o)}] \right\} = -\frac{1}{j\omega\epsilon} \int_a^b dr r^2 \int_0^\pi d\theta \\ &\int_0^{2\pi} d\phi \left\{ \frac{\partial \phi_{npm}^{(o)}}{\partial \phi} \frac{1}{r} \frac{\partial}{\partial r} \left[r \frac{\partial \psi_{n'p'm'}^{(o)}}{\partial \theta} \right] - \frac{\partial \phi_{npm}^{(o)}}{\partial \theta} \frac{1}{r} \frac{\partial}{\partial r} \left[r \frac{\partial \psi_{n'p'm'}^{(o)}}{\partial \phi} \right] \right\} . \end{aligned}$$

However, if we note that the integration over ϕ vanishes for all m, m' we have

$$\iiint d\tau(\vec{r}) \vec{E}_{npm}^{(1,o)}(\vec{r}) \cdot \vec{E}_{n'p'm'}^{(2,o)}(\vec{r}) = 0 .$$

For precisely the same reason we obtain

$$\iiint d\tau(\vec{r}) \vec{E}_{npm}^{(1,e)}(\vec{r}) \cdot \vec{E}_{n'p'm'}^{(2,e)}(\vec{r}) = 0.$$

Now consider

$$\begin{aligned} \iiint d\tau \vec{E}_{npm}^{(1,o)} \cdot \vec{E}_{n'p'm'}^{(2,e)} &= -\frac{1}{j\omega\epsilon} \int_a^b dr r^2 \int_0^\pi d\phi \left\{ \frac{1}{\sin\theta} \frac{\partial\phi_{npm}^{(o)}}{\partial\phi} \right. \\ &\cdot \frac{\partial}{\partial\theta} \left(\frac{1}{r} \frac{\partial}{\partial\theta} [r\psi_{n'p'm'}^{(e)}] \right) - \frac{1}{\sin\theta} \frac{\partial\phi_{npm}^{(o)}}{\partial\theta} \cdot \frac{\partial}{\partial\phi} \left(\frac{1}{r} \frac{\partial}{\partial r} [r\psi_{n'p'm'}^{(e)}] \right) = \\ &- \frac{1}{j\omega\epsilon} \int_a^b dr r^2 \int_0^\pi d\theta \int_0^{2\pi} d\phi \left\{ \phi_{np}(j\gamma_{np}^{(1)}r) \frac{1}{r} \frac{d}{dr} [r\psi_{n'p'}(j\gamma_{n'p'}^{(2)}r)] \right\} \\ &\cdot P_{nm}(\cos\theta) \frac{dP_{n'm'}(\cos\theta)}{d\theta} m \cos m\phi \cos m'\phi \\ &+ \frac{dP_{nm}(\cos\theta)}{d\theta} P_{n'm'}(\cos\theta) m' \sin m\phi \sin m'\phi. \end{aligned}$$

But

$$m \int_0^{2\pi} d\phi \cos m\phi \cos m'\phi = m\pi\delta_{mm'},$$

and

$$m' \int_0^{2\pi} d\phi \sin m\phi \sin m'\phi = m'\pi\delta_{mm'}.$$

We thus have

$$\begin{aligned} \iiint d\tau \vec{E}_{npm}^{(1,o)} \cdot \vec{E}_{n'p'm'}^{(2,e)} &= -\frac{m\pi\delta_{mm'}}{j\omega\epsilon} \int_a^b dr \left\{ r\phi_{np}(j\gamma_{np}^{(1)}r) \frac{d}{dr} \right. \\ &\cdot [r\psi_{n'p'}(j\gamma_{n'p'}^{(2)}r)] \left. \right\} \int_0^\pi d\theta \frac{d}{d\theta} P_{nm}P_{n'm'}, \end{aligned}$$

and

$$\int_0^\pi d\theta \frac{d}{d\theta} [P_{nm}(\cos\theta)P_{n'm'}(\cos\theta)] = P_{nm}(\cos\theta)P_{n'm'}(\cos\theta) \Big|_{\theta=0}^{\theta=\pi} \equiv 0.$$

APPENDIX A

Hence we have

$$\iiint d\tau \hat{E}_{n\mathbf{p}\mathbf{m}}^{(1,o)} \cdot \hat{E}_{n'\mathbf{p}'\mathbf{m}'}^{(2,e)} = 0$$

and for the same reasons we obtain the last of the six relations we need:

$$\iiint d\tau \hat{E}_{n\mathbf{p}\mathbf{m}}^{(1,e)} \cdot \hat{E}_{n'\mathbf{p}'\mathbf{m}'}^{(2,o)} = 0 \quad .$$

APPENDIX B.--COMPUTER PROGRAM FOR THE EIGENVALUES AND THEIR GENERATING
FUNCTIONS

APPENDIX B

```

C   TEM
      COMMON R,TEXT
      INTEGER TEXT(2),T(2),T1(2)
      DIMENSION X(200),Y(200),RTAN(200),X1I(10),X1F(10),XCROSS(10)
      DIMENSION IFLAG(15)
      DATA IMARK/' */
10  WRITE (1,20)
20  FORMAT (///'ENTER TYPE OF RUN'/
- 'TM1/TM2/TM3/TM4/TM5/TE1/TE2/TE3/TE4')
      WRITE (1,30) T(1),T(2)
30  FORMAT ('PREVIOUS RUN WAS: ',2A2///
- '(OR ENTER "Q" TO QUIT)')
      READ (1,40) (T1(I),I=1,2)
40  FORMAT (2A2)
      IF (T1(1).EQ.'Q ') GO TO 1000
      IF (T1(1).NE.' ') GO TO 50
          T1(1)=T(1)
          T1(2)=T(2)
50  T(1)=T1(1)
      T(2)=T1(2)
      TEXT(1)=T1(1)
      TEXT(2)=T1(2)
      IF ((T(1).EQ.'TM').AND.(T(2).EQ.'1 ')) ICALL=1
      IF ((T(1).EQ.'TM').AND.(T(2).EQ.'2 ')) ICALL=2
      IF ((T(1).EQ.'TM').AND.(T(2).EQ.'3 ')) ICALL=3
      IF ((T(1).EQ.'TM').AND.(T(2).EQ.'4 ')) ICALL=4
      IF ((T(1).EQ.'TM').AND.(T(2).EQ.'5 ')) ICALL=5
      IF ((T(1).EQ.'TE').AND.(T(2).EQ.'1 ')) ICALL=6
      IF ((T(1).EQ.'TE').AND.(T(2).EQ.'2 ')) ICALL=7
      IF ((T(1).EQ.'TE').AND.(T(2).EQ.'3 ')) ICALL=8
      IF ((T(1).EQ.'TE').AND.(T(2).EQ.'4 ')) ICALL=9
60  WRITE (1,70) R
70  FORMAT ('ENTER R (PREVIOUS VALUE WAS ',F7.5,' )')
      READ (1,80) R1
80  FORMAT (F10.8)
      IF (R1.GE.1.) GO TO 60
      IF (R1.EQ.0.) R1=R
      R=R1
      NPNTS=200
      DELX=.1
      K=0
      L=0
      M=0
      KEND=0
      DO 90 I=1,15
          IFLAG(I)=0
90  CONTINUE
100 IF (L.NE.1) GO TO 110
      DO 220 M=1,10
          IF (M.GE.10) GO TO 430
110 IF (L.NE.0) DELX=(XF-XI)/NPNTS
      DO 210 I=0,NPNTS
          X(I)=FLOAT(I)/10.
          IF (L.NE.0) X(I)=XI+FLOAT(I)*DELX
          XT=X(I)
          CALL FNCTN (ICALL,XT,YT)
          Y(I)=YT
          A=(1.-R)*X(I)
          S=SIN(A)
          C=COS(A)

```

```

      RTAN(I)=S/C
      ICROSS=0
      DIFF=YT-RTAN(I)
      IF (DIFF.LE.0) ND=0
      IF (DIFF.GT.0) ND=1
      IF (I.EQ.0) ND1=ND
      IF (ND.NE.ND1) ICROSS=1
      IF((RTAN(I).LT.0.).AND.(RTAN(I-1).GT.0.)) ICROSS=0
      IF((RTAN(I).LT.0.).AND.(RTAN(I-1).GT.0.).AND.(RTAN(I-1).LT.
-Y(I-1))) ICROSS=1
      IF (I.EQ.0) ICROSS=0
      ND1=ND
      IF (L.NE.0) GO TO 120
        IF (ICROSS.EQ.1) K=K+1
        IF((K.EQ.1).AND.(ABS(DIFF).LT.0.00001)) K=0
        IF (K.EQ.0) ICROSS=0
        IF (ICROSS.EQ.1) X1I(K)=X(I)-DELX
120    IF (L.NE.1) GO TO 130
        IF ((ICROSS.EQ.1).AND.(ABS(DIFF).GT.10.)) IFLAG(K)=1
130    IF ((I.EQ.0).AND.(ICROSS.EQ.1)) IFLAG(K)=1
        IF ((L.EQ.1).AND.(IFLAG(K).EQ.1)) GO TO 150
        IF (ICROSS.EQ.1) WRITE (1,140)
140    FORMAT ('*')
        IF (Y(I)*RTAN(I).LT.0.) GO TO 150
        IF (L.EQ.2) GO TO 170
        IF (ABS(DIFF).LE.0.00001) X1F(K)=X(I)
        IF (L.EQ.0) GO TO 150
        IF (K.EQ.0) GO TO 150
        IF (ABS(Y(I)-RTAN(I)).LE.0.00001) GO TO 320
        IF (ABS(X(I)-X(I-1)).LE.0.000001) GO TO 320
150    IF (ICROSS.EQ.1) X1I(K)=X(I)-DELX
160    IF ((L.EQ.1).AND.(ICROSS.EQ.1)) X1F(K)=X(I)
        IF ((L.EQ.0).AND.(ICROSS.EQ.1)) X1F(K)=X(I)
        IF ((L.EQ.1).AND.(ICROSS.EQ.1))GO TO 170
        IF (L.NE.0) X1F(K)=X(I)
170    IF (L.EQ.1) GO TO 200
        IF (ICROSS.NE.1) WRITE (1,180) X(I),Y(I),RTAN(I)
        IF (ICROSS.EQ.1) WRITE (1,190) X(I),Y(I),RTAN(I)
180    FORMAT (F12.5,5X,2F12.5)
190    FORMAT (F12.5,5X,2F12.5,5X,'*')
200    IF ((L.EQ.1).AND.(ICROSS.EQ.1)) XI=X1I(K)
        IF ((L.EQ.1).AND.(ICROSS.EQ.1)) XF=X1F(K)
        IF ((L.EQ.1).AND.(ICROSS.EQ.1)) GO TO 100
        IF (L.EQ.0) KEND=K
210    CONTINUE
        IF (L.NE.1) GO TO 230
220    CONTINUE
230    IF (L.EQ.1) GO TO 310
        IF (L.EQ.2) GO TO 350
240    NFLAG=0
        DO 250 K=1,KEND
            NFLAG=NFLAG+IFLAG(K)
250    CONTINUE
        K1=KEND-NFLAG
        WRITE (1,260) T(1),T(2),R
260    FORMAT (//13X,2A2,'ROOTS FOR R=',F7.5//
-10X,'K',13X,'XI',10X,'XF'/)
        DO 290 K=1,KEND
            IF (IFLAG(K).EQ.0) WRITE (1,270) K,X1I(K),X1F(K)
            IF (IFLAG(K).EQ.1) WRITE (1,280) K,X1I(K),X1F(K)

```

APPENDIX B

```

270     FORMAT (10X,I1,5X,2F12.5)
280     FORMAT (10X,I1,5X,2F12.5,5X,'#')
290 CONTINUE
      WRITE (1,300) K1
300     FORMAT(// 'THERE ARE ',I2,' CROSSTERS'/
      - 'ENTER # OF CROSSTER TO EXPAND'/
      - 'OR RETURN TO CONTINUE')
      READ (1,370) K
      IF (K.EQ.0) GO TO 350
310     XI=X1I(K)
      XF=X1F(K)
      L=1
      M=0
      IFLAG(K)=0
      GO TO 100
320     WRITE (1,330) K
330     FORMAT (///I1,' CROSSTER OCCURS AT')
      WRITE (1,190) X(I),Y(I),RTAN(I)
      WRITE (1,340)
340     FORMAT (///)
      GO TO 240
350     WRITE (1,360)
360     FORMAT (// 'ENTER 1 TO START OVER'/
      - ' 2 FOR EXPANDED SCALE'/
      - 'OTHERWISE RETURN FOR GRAF')
      READ (1,370) IGRAF
370     FORMAT (I3)
      L=1
      M=0
      IF (IGRAF.EQ.1) GO TO 10
      IF (IGRAF.EQ.2) GO TO 380
      CALL GRAF (NPNTS,X,Y,RTAN)
      GO TO 240
380     WRITE (1,390)
390     FORMAT ('ENTER K')
      READ (1,370) K
      WRITE (1,400)
400     FORMAT ('ENTER INITIAL AND FINAL VALUES OF X')
      READ (1,410) XI,XF
410     FORMAT (2F9.5)
      IF ((XI.NE.0.).AND.(XF.NE.0.)) GO TO 420
      XI=X1I(K)
      XF=X1F(K)
420     L=2
      M=0
      GO TO 100
430     WRITE (1,440)
440     FORMAT ('NOT A REAL CROSSTER')
      M=0
      IFLAG(K)=1
      GO TO 240
1000 STOP
      END
C
C
C
C
      SUBROUTINE FNCTN (ICALL,XT,YT)
      COMMON R
      XSQ=XT*XT

```

```

RSQ=R*R
IF (ICALL.EQ.1) GO TO 10
IF (ICALL.EQ.2) GO TO 20
IF (ICALL.EQ.3) GO TO 30
IF (ICALL.EQ.4) GO TO 40
IF (ICALL.EQ.5) GO TO 50
IF (ICALL.EQ.6) GO TO 60
IF (ICALL.EQ.7) GO TO 70
IF (ICALL.EQ.8) GO TO 80
IF (ICALL.EQ.9) GO TO 90
10  TM1N=(1.-R)*XT*(1.+R*XSQ)
    TM1D=RSQ*XT**4-(1.-R+RSQ)*XSQ+1.
    YT=TM1N/TM1D
    GO TO 100
20  TM2N=3*(1.-R)*XT*(RSQ*XSQ**2-2*(1.-R)**2*XSQ+12.)
    TM2D=(R*XSQ)**3-3*R*(2*RSQ-3*R+2.)*XSQ**2-18*(RSQ-2*R+1.)*XSQ
    -+36.
    YT=TM2N/TM2D
    GO TO 100
30  A=15.-2*XSQ
    B=15.-2*XSQ*RSQ
    C=XSQ**2-21*XSQ+45.
    D=(XSQ*RSQ)**2-21*XSQ*RSQ+45.
    TM3N=3*XT*(A/C-R*B/D)
    TM3D=1.+9*R*XSQ*A*B/(C*D)
    YT=TM3N/TM3D
    GO TO 100
40  A=420.-55*XSQ+XSQ**2
    B=420.-55*XSQ*RSQ+(RSQ*XSQ)**2
    C=420.-195*XSQ+10*XSQ**2
    D=420.-195*XSQ*RSQ+10*(XSQ*RSQ)**2
    TM4N=XT*(A/C-R*B/D)
    TM4D=1.+R*XSQ*(A*B)/(C*D)
    YT=TM4N/TM4D
    GO TO 100
50  A=4725.-630*XSQ+15*XSQ**2
    B=4725.-630*RSQ*XSQ+15*(RSQ*XSQ)**2
    C=4725.-2205*XSQ+120*XSQ**2-XSQ**3
    D=4725.-2205*RSQ*XSQ+120*(RSQ*XSQ)**2-(RSQ*XSQ)**3
    TM5N=XT*(A/C-R*B/D)
    TM5D=1.+R*XSQ*A*B/(C*D)
    YT=TM5N/TM5D
    GO TO 100
60  TE1N=(1.-R)*XT
    TE1D=1.+R*XSQ
    YT=TE1N/TE1D
    GO TO 100
70  TE2N=(1.-R)*(1.+(1./3.)*R*XSQ)*XT
    TE2D=1.-(1.-3*R+RSQ)*XSQ/3+RSQ*XSQ*XSQ/9
    YT=TE2N/TE2D
    GO TO 100
80  A=15.-XSQ
    B=15.-RSQ*XSQ
    C=5.-2*XSQ
    D=5.-2*RSQ*XSQ
    TE3N=XT*(A/C-R*B/D)
    TE3D=3.+R*XSQ*A*B/(3*C*D)
    YT=TE3N/TE3D
    GO TO 100
90  Y=XT*R

```

APPENDIX B

```

      Y2=Y*Y
      Y3=Y2*Y
      Y4=Y3*Y
      Y5=Y4*Y
      X2=XSQ
      X3=X2*XT
      X4=X3*XT
      X5=X4*XT
      A=105*XT-10*X3
      B=105-45*Y2+Y4
      C=105-45*X2+X4
      D=105*Y-10*Y3
      TE4N=A*B-C*D
      TE4D=C*B+A*D
      YT=TE4N/TE4D
100  RETURN
      END
C
C
C
      SUBROUTINE GRAF (NPNTS,X,Y1,Y2)
      COMMON R,TEXT
      INTEGER TEXT(2)
      INTEGER RTEXT(3)
      DIMENSION X(200),Y1(200),Y2(200)
      ENCODE(6,5,RTEXT)R
5     FORMAT ('R=',F3.2)
      CALL MINMAX (Y1,NPNTS,1,Y1MIN,Y1MAX)
      IF (Y1MAX.GT.150.) Y1MAX=150.
      IF (Y1MIN.LT.-99.) Y1MIN=-99.
      DO 10 I=1,NPNTS
        X(I)=X(I)
        IF (Y1(I).GT.150.) Y1(I)=150.
        IF (Y1(I).LT.-99.) Y1(I)=-99.
10     CONTINUE
      CALL SETPDQ
      CALL SCREEN
      CALL INIT (1.5,1.5)
      CALL SCALE (X,NPNTS,8.,1,0)
      CALL SCALE (Y1,NPNTS,5.,1,1)
      CALL ENTGRA
      CALL XAXIS ('X',1,8.)
      CALL YAXIS ('FUNCTIONS FOR R',15,5.)
      CALL DATAQ (X,Y1,NPNTS,1,1)
      L=3
      DO 20 I=1,NPNTS
        CALL DRAWC (X(I),Y2(I),L,4)
        L=4
20    CONTINUE
      CALL GRID (8.,5.,1.,1.,4,0)
      CALL ABSVEC (1.7,6.,0)
      CALL SYMBOQ (6,RTEXT,7)
      CALL ABSVEC (8.6,6.7,0)
      CALL SYMBOQ (4,TEXT,7)
      CALL EXITGR
      CALL WAIT
      CALL SCREEN
      RETURN
      END

```

DISTRIBUTION

ADMINISTRATOR
DEFENSE TECHNICAL INFORMATION CENTER
ATTN DTIC-DDA (12 COPIES)
CAMERON STATION
ALEXANDRIA, VA 22314

COMMANDER
US ARMY MATERIEL DEVELOPMENT & READINESS
COMMAND
5001 EISENHOWER AVENUE
ALEXANDRIA, VA 22333

DIRECTOR
US ARMY BALLISTIC RESEARCH LABORATORY
ATTN DRSAR-TSB-S (STINFO)
ABERDEEN PROVING GROUND, MD 21005

US ARMY ELECTRONICS TECHNOLOGY & DEVICES
LABORATORY
ATTN DELET-DD
FT MONMOUTH, NJ 07703

MATERIALS TESTING DIRECTORATE
ARMY PULSE RADIATION DIV
ATTN CRAIG R. HAMBACH
ABERDEEN PROVING GROUND, MD 21005

DIRECTOR
US ARMY MATERIEL SYSTEMS ANALYSIS
ACTIVITY
ATTN DRXSY-MP
ABERDEEN PROVING GROUND, MD 21005

COMMANDER
US ARMY MISSILE & MUNITIONS CENTER
& SCHOOL
ATTN ATSK-CTD-F
REDSTONE ARSENAL, AL 35809

US ARMY RESEARCH OFFICE
ATTN DR. JAMES MINK
ATTN DR. HORST GERLACH
PO BOX 12211
RESEARCH TRIANGLE, NC 27709

COMMANDER
US ARMY RSCH & STDY GP (EUR)
ATTN CHIEF, PHYSICS & MATH BRANCH
FPO, NY 09510

COMMANDER
U.S. ARMY WATERVLIET ARSENAL
AMCCOM
SOLID STATE RESEARCH LAB
ATTN MR. CLARK HOMAN
WATERVLIET, NY 12189

HQ, USAF
WASHINGTON, DC 20330

RADC/RBCT
ATTN DR. ROY F. STRATTON
GRIFFISS AFB, NY 13441

UNIVERSITY OF ARIZONA
ELECTRICAL ENGINEERING DEPT
ATTN PROF. CONSTANTINE BALANIS
ATTN PROF. DONALD DUDLEY
TUCSON, AZ 85721

UNIVERSITY OF CALIFORNIA
LAWRENCE LIVERMORE NATIONAL LABS
ATTN L-156, DR. KARL KUNZ
PO BOX 808
LIVERMORE, CA 94550

ELECTRONICS RESEARCH LAB
COLLEGE OF ENGINEERING
UNIVERSITY OF CALIFORNIA
ATTN PROF. KEN MEI
BERKELEY, CA 94720

UNIV OF CALIFORNIA AT LOS ANGELES
ELECTRICAL ENGINEERING DEPT
ATTN PROF. CAVOUR YEH
LOS ANGELES, CA 90024

ENGINEERING SOCIETIES LIBRARY
ATTN ACQUISITIONS DEPT
345 EAST 47TH ST
NEW YORK, NY 10017

UNIVERSITY OF FLORIDA
PHYSICS DEPT
ATTN PROF. ALEX GREEN
GAINESVILLE, FL 32601

UNIV OF FLORIDA
SPACE ASTRONOMY LAB
ATTN RU T. WANG
GAINESVILLE, FL 32601

GENERAL RESEARCH CORP
ADVANCED TECHNOLOGIES DIVISION
ATTN DR. MICHAEL VON BLARICUM
5383 HOLLISTER AVENUE
SANTA BARBARA, CA 93111

UNIVERSITY OF HOUSTON
DEPT OF ELECTRICAL ENGINEERING
ATTN PROF. CHALMERS BUTLER
HOUSTON, TX 77004

JAYCOR
ATTN DR. KENDALL CASEY
39510 PASCO PADRE PKWY
SUITE 300
FREMONT, CA 94538

DISTRIBUTION (Cont'd)

MASSACHUSETTS INSTITUTE OF TECHNOLOGY
DEPT OF ELECTRICAL ENGINEERING &
COMPUTER SCIENCE
ATTN PROF. J. A. KONG
CAMBRIDGE, MA 02139

UNIVERSITY OF MASSACHUSETTS
DEPT OF ELECTRICAL & COMPUTER
ENGINEERING
ATTN PROF. DANIEL SCHAUBERT
AMHERST, MA 01003

UNIVERSITY OF MICHIGAN
DEPT OF ELECTRICAL & COMPUTER
ENGINEERING
ATTN PROF. VAL LIEPA
ANN ARBOR, MI 48109

UNIVERSITY OF MISSISSIPPI
DEPT OF ELECTRICAL ENGINEERING
ATTN PROF. WILSON PEARSON
UNIVERSITY, MS 38677

STATE UNIV OF NEW YORK
DEPT OF PHYSICS
ATTN PROF. JACK SMITH
1400 WASHINGTON AVE
ALBANY, NY 12222

PANAMETRICS INC
ATTN DR. NORMAN PEDERSEN
221 CRESCENT STREET
WALTHAM, MA 02254

RENSSELAER POLYTECHNIC INSTITUTE
PHYSICS DEPT
ATTN PROF. ROLAND LICHTENSTEIN
TROY, NY 12181

ROCHESTER INSTITUTE OF TECHNOLOGY
DEPT OF ELECTRICAL ENGINEERING
ATTN PROF. TAPAN K. SANKAR
PO BOX 9887
ROCHESTER, NY 14623

SANDIA NATIONAL LABORATORIES
ATTN DR. MARVIN E. MORRIS
PO BOX 5800
ALBUQUERQUE, NM 87185

SYRACUSE RESEARCH CORP
ATTN DR. DAVID AUCKLAND
MERRILL LANE
SYRACUSE, NY 13210

SYRACUSE UNIVERSITY
ELECTRICAL ENGINEERING DEPT
ATTN PROF. ROGER HARRINGTON
SYRACUSE, NY 13210

US ARMY ELECTRONICS RESEARCH &
DEVELOPMENT COMMAND
ATTN COMMANDER, DRDEL-CG
ATTN TECHNICAL DIRECTOR,
DRDEL-CT
ATTN PUBLIC AFFAIRS OFFICE, DRDEL-IN

HARRY DIAMOND LABORATORIES
ATTN D/TSO/DIVISION DIRECTORS
ATTN RECORD COPY, 81200
ATTN HDL LIBRARY, 81100 (3 COPIES)
ATTN HDL LIBRARY, 81100 (WOODBIDGE)
ATTN TECHNICAL REPORTS BRANCH, 81300
ATTN LEGAL OFFICE, 97000
ATTN ZABLUDOWSKI, B., 47400 (GIDEP)
ATTN FARRAR, F., 11200
ATTN JOHNSON, T., 11200
ATTN PISANE, G., 21100
ATTN SINDORIS, A., 21100
ATTN LIBELO, L., 11200 (25 COPIES)

END

FILMED

DTIC